Delft University of Technology

Department of Precision and Microsystems Engineering

Modelling hydroplaning using Modified Reynolds equation

Name: H.J. Wapstra

Report no: EM 10.003
Coach: Dr. Ir. R.A.J. van Ostayen
Professor: Prof. Dr. Ir. D.J. Rixen
Specialisation: Engineering Dynamics
Type of report: MSc. Thesis
Date: 22-01-2010

ἄνδρα μοι ἔννεπε, μοῦσα, πολύτροπον, ὃς μάλα πολλὰ
πλάγχθη, ἐπεὶ Τροίης ἱερὸν πτολίεθρον ἔπερσεν·
πολλῶν δ᾽ ἀνθρώπων ἴδεν ἄστεα καὶ νόον ἔγνω,
πολλὰ δ᾽ ὅ γ᾽ ἐν πόντῳ πάθεν ἄλγεα ὃν κατὰ θυμόν,
ἀρνύμενος ἥν τε ψυχὴν καὶ νόστον ἑταίρων.
ἀλλ᾽ οὐδ᾽ ὣς ἑτάρους ἐρρύσατο, ἱέμενός περ·
αὐτῶν γὰρ σφετέρῃσιν ἀτασθαλίῃσιν ὄλοντο,
νήπιοι, οἳ κατὰ βοῦς Ὑπερίονος Ἠελίοιο
ἤσθιον· αὐτὰρ ὁ τοῖσιν ἀφείλετο νόστιμον ἦμαρ.
τῶν ἁμόθεν γε, θεά, θύγατερ Διός, εἰπὲ καὶ ἡμῖν.

Homer, the odyssey 800BC

TELL ME, O MUSE, of that ingenious hero who travelled far and wide after he had sacked the famous town of Troy. Many cities did he visit, and many were the nations with whose manners and customs he was acquainted; moreover he suffered much by sea while trying to save his own life and bring his men safely home; but do what he might he could not save his men, for they perished through their own sheer folly in eating the cattle of the Sun-god Hyperion; so the god prevented them from ever reaching home. Tell me, too, about all these things, O daughter of Jove, from whatsoever source you may know them.

Translation by: Samuel Butler, 1900

To Martina Fantini, my muse

Preface

This is the MSc. thesis report for the master programme Mechanical Engineering, Variant Solid and Fluid mechanics, specialization Engineering Dynamics at the TU Delft. Part of the project was carried out at Goodyear Innovation Centre in Colmar Berg, Luxembourg. The aim of this thesis is to apply a modified Reynolds equation to model the hydroplaning phenomenon, with sufficient accuracy and with short computational time so it can be used as a design tool.

For the realization of this thesis I would like to thank my supervisors, Ron van Ostayen and Daniel Rixen from the TU Delft and Vincent Decouvreur and Didier Quorin from Goodyear for their feedback and inspiration.

Summary

Hydroplaning occurs when a layer of water builds between the rubber tires of the vehicle and the road surface, leading to the loss of traction and thus preventing the vehicle from responding to control inputs such as steering, braking or accelerating. Current hydroplaning analysis requires combining visco-elastic tire models and intricate fluid dynamics models, which require tremendous computational effort. It is of interest to model hydroplaning fast, such that the modelling can be used in the tire design process.

To obtain a fast modelling process the Reynolds equations is used, which is a simplification from the Navier-Stokes equations as a result of the thin film conditions, resulting in dominant behavior of the viscous terms. The current study investigates the direct application of the Reynolds equation, adds an inertia correction, both to the inlet condition and to the full film area. The unknown wetted length of the inlet is solved by the introduction of a fill rate model based on cavitation.

Tire modelling is done with an elastic half space as well as with hyperelastic models made in a finite element program, ABAQUS.

In this case fluid structure interaction is very important due to the strong coupling between the incompressible fluid and the highly elastic structure. The models developed start with a classical staggering for the elastic half space model. This can be diverging or at best slowly converging, therefore an interface quasi Newton method recently published is applied which takes into account the response of the structure in previous iterations. Finally a coupling between the fluid code in Matlab and the structural model in ABAQUS is outlined to benchmark the potential of the method.

Some first results obtained using the methods presented in this research indicate that the use of a modified Reynolds equation in modelling of hydroplaning shows promise, both in accuracy and in computational effort.

Introduction

This is a report on the application of lubrication theory for hydroplaning prediction. The hydroplaning phenomenon, described in section I together with the different modeling approaches, occurs when a layer of water builds between the rubber tires of the vehicle and the road surface, leading to the loss of traction and thus preventing the vehicle from responding to control inputs such as steering, braking or accelerating. Current hydroplaning modelling techniques are generally slow and therefore expensive to run. It is of interest to model hydroplaning fast, say in the order of a couple of hours, such that the modelling can be used in the tire design process, where comparison of multiple designs is desirable.

Section II outlines the fluid dynamics, in this case the lubrication theory. The lubrication theory consists of the Reynolds equation developed by Osborne Reynolds in 1888. The main aspect of this theory is the thin film assumption which results in the dominant behavior of the viscous terms in the Navier-Stokes equations, therefore the inertia terms are neglected, resulting in a constant pressure over the film thickness. The current study investigates the direct application of the Reynolds equation, adds an inertia correction, both to the inlet condition as well as in the full film area. The inertia correction to the inlet is furthermore corrected by an energy correction and a momentum correction. The unknown wetted length of the inlet is solved by the introduction of a fill rate model. The different models are solved with a finite element model developed in Matlab.

Section III describes the structural mechanics, the different tire models that are applied. First an elastic half space model is described, developed in Matlab, then several hyper-elastic models are outlined, which are made in a finite element program, Abaqus. Two basic different geometries have been implemented, a so-called Grosch wheel which is a small scale solid wheel and a more realistic full scale tire model with three grooves and a cavity.

Section IV describes the Fluid-Structure Interaction models that have been used. In this case fluid structure interaction is very important due to the strong coupling between the incompressible fluid and the highly elastic structure. The models developed start with a classical staggering in Matlab for the elastic half space model. This can be diverging or at best slowly converging, therefore an interface quasi Newton method is explained which takes into account the response of the structure in previous iterations. Finally a coupling between the fluid code in Matlab and the structural model in ABAQUS is described to lead to section V where the results are presented and discussed.

Contents

Section I
Hydroplaning

1. Hydroplaning

Hydroplaning (Greek: ‘$\upsilon\delta\rho\omega$ - water) or sometimes also called aquaplaning (Latin: aqua - water) is the phenomenon of the loss of traction of a rubber tire due to presence of a water layer between the tire and the road surface. The loss of traction makes the vehicle insensitive to control inputs such as steering, braking and accelerating. It is therefore of interest to model hydroplaning to be able to develop tires that perform well under wet conditions and for a modelling approach to be useful in the design process it is also of interest that the model performs fast, typically in the order of several hours.

Several observations with regard to hydroplaning have been made and in general three different kinds of hydroplaning are distinguished, i.e. viscous hydroplaning, dynamic hydroplaning and inverted rubber hydroplaning, which will be explained in the next sections. After listing the observations made with regard to hydroplaning the current modelling techniques are reviewed.

1.1. Definition of hydroplaning speed

Tire hydroplaning speed is defined by the speed at which the hydrodynamic lift acting on the tire is equal to the weight of the vehicle supported by that tire.

$$F_{v,s} = F_v$$

Where F_v indicates the weight of the vehicle and $F_{v,s}$ indicates the lift force generated by the fluid at hydroplaning speed.

1.2. Observations

First observations of aquaplaning were made in the late 50’s as a result of military airplanes overrunning a wet runway and large airplanes experiencing reduced tire to surface friction during wheel spin-up in a landing procedure. This led to a treadmill study in 1957 [1]. In this study a pneumatic tire under free rolling conditions on a belt covered with water was observed to spin-down to a complete stop at a certain belt speed. This is one of eight manifestations that were observed, others are detachment of the tire footprint, hydrodynamic ground pressure, suppression of tire bow wave, scouring action of escaping fluid in tire-ground footprint, loss in braking traction and loss of tire directional stability [2]. The next sections give a summary of the observations made by Horn and Dreher.

1.2.1. Detachment of tire footprint

The first explanation given of hydroplaning assumes that if ground speed increases a wedge of fluid progressively penetrates the footprint and hydrodynamic pressure is developed between tire and ground. The resultant hydrodynamic lift causes the footprint to detach from the surface. This is illustrated in figure 1.1 and 1.2, that were obtained during a hydroplaning study at the NASA Langley landing loads track.

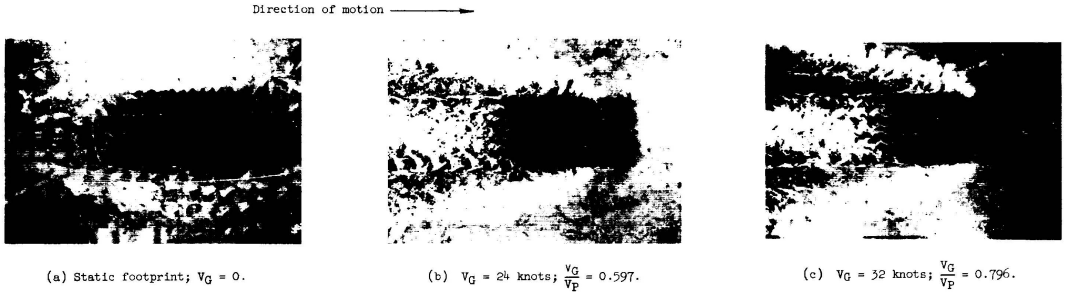

Figure 1.1: Footprint detachment, partial hydroplaning. 5.60-13 tire on a glass runway, vertical load 2225 N, tire pressure 1,38 bar , water depth 12,70 mm [2]

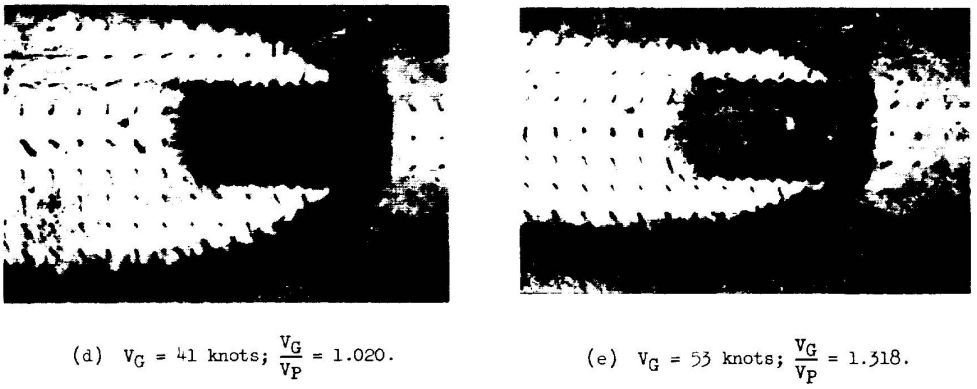

Figure 1.2: Footprint detachment, full hydroplaning. 5.60-13 tire on a glass runway, vertical load 2225 N, tire pressure 1,38 bar, water depth 12,70 mm [2]

From these pictures can be noted that the portion of the footprint that is last to detach from the surface, as ground speed increases, is the portion under the sidewall of the tire, an effect which is not observed in aircraft tires. This indicates that higher contact pressure exists under the sidewall compared to the rest of the footprint.

1.2.2. Hydrodynamic ground pressure

Measurements of the hydrodynamic pressure on the wetted surface remains a challenge but successful measurements have been done of the hydrodynamic pressure acting on the ground surface under the tire. These measurements were done using a flush-diaphragm-type pressure gage installed below the surface at the centerline of the tire. A flush diaphragm pressure gage is a gage where the diaphragm is placed flush to the surface therefore eliminating any cavity that could collect fluid from the process. Typical pressure profiles are shown in figure 1.3 and figure 1.4.

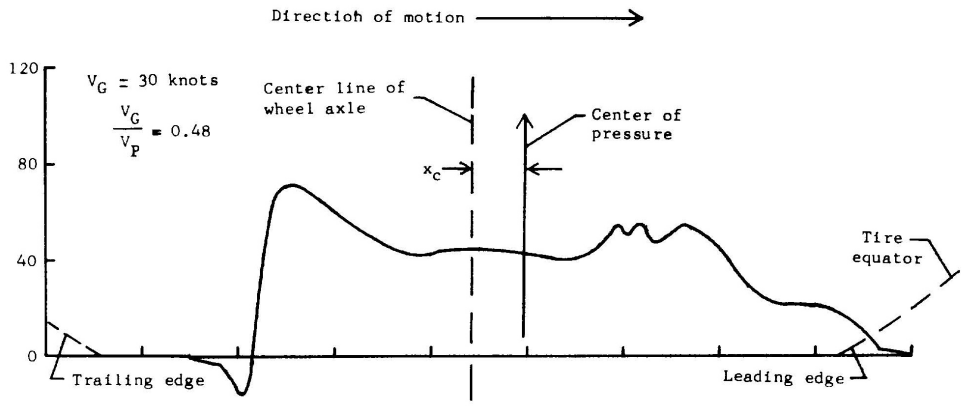

Figure 1.3: Hydrodynamic ground pressure $\frac{lb}{in^2}$, Vertical load per tire approximately 24919 N, tire pressure 3.44 bar, water depth 12,70 mm [2]

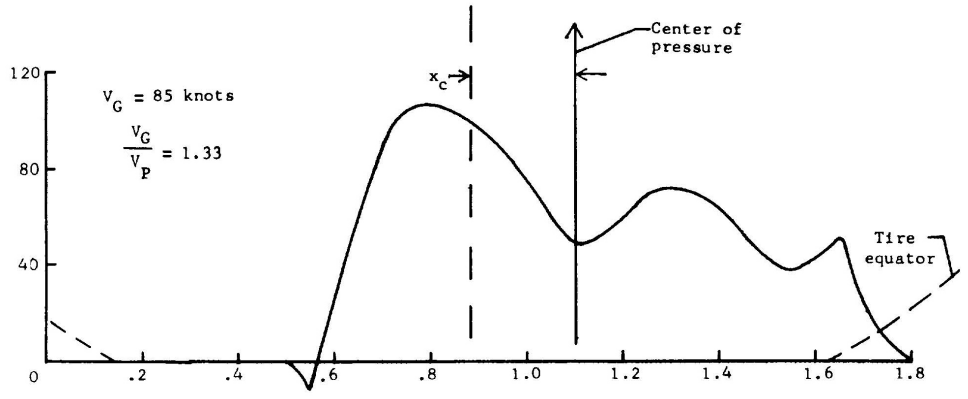

Figure 1.4: Hydrodynamic ground pressure $\frac{lb}{in^2}$, Vertical load per tire approximately 24919 N, tire pressure 3,44 bar, water depth 12,70 mm [2]

From this data some interesting observations can be made:

- The ground hydrodynamic pressure develops ahead of the initial tire ground contact point, due to the tire bow wave.
- The peak ground hydrodynamic pressure is larger than the tire inflation pressure, in case of the 85 knot ground speed.
- Negligible hydrodynamic ground pressure is developed in the rear of the footprint.

The second point indicates that either local inward buckling or deformation of the tire occurs under this high hydrodynamic pressure. The exact reason for point 3 is explained by Horne and Dreher as inertia of the tire preventing the tire inflation pressure from restoring the tire to its undeflected radius.

1.2.3. Spin-down of unbraked wheel

As a tire enters the hydroplaning condition spin-down of the unbraked, free rolling wheel is observed meaning that the wheel slows down or comes to a complete stop. Two effects are accounted to this observation:

- With increasing speed the hydrodynamic pressure build-up causes footprint detachment and therefore reduces tire spin-up moment towards zero.
- Next to that the center of pressure and thus resulting lift shifts increasingly forward with increasing speed. See figure 1.3 and figure 1.4.

1.2.4. Suppression of tire bow wave

For all speeds below the hydroplaning speed a bow wave in front of the tire is observed. With increasing ground speed the angle of the bow wave with respect to the road reduces progressively until the full hydroplaning speed is reached the bow wave completely disappears. See figure 1.5.

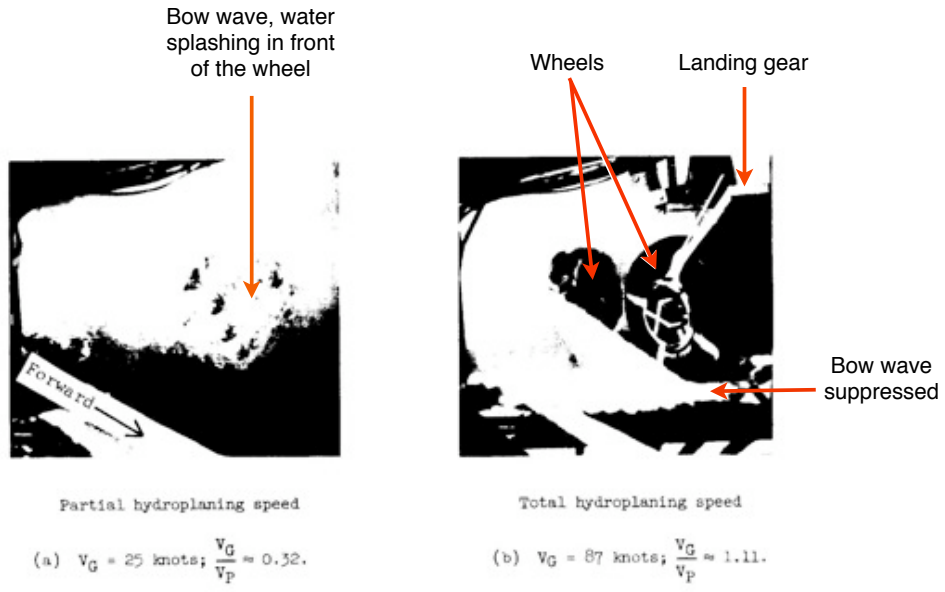

Figure 1.5: Four wheel bogie in partial and full hydroplaning, tire pressure 5,17 bar, vertical load 99229 N, water depth 50 mm. [2]

1.2.5. Scouring action of escaping fluid in tire-ground footprint region

Locked wheels during braking on a dry pavement results in large amounts of molten tread rubber to be deposited on the pavement. Under full hydroplaning conditions this is not observed, on the contrary, escaping fluids under the hydrodynamic pressure result in white streaks formed by the tires on the pavement. This can be seen as a cleaning effect of the pavement. Observations of this effect have also been made at speeds below full hydroplaning speed, attributed to the viscous effect als resulting in high hydrodynamic pressures.

1.2.6. Peaking of fluid displacement drag

Figure 1.6 shows that fluid drag is reduced at speeds above the full hydroplaning speed. This can be accounted for by the tires lifted of the road and therefore are displacing less fluid from the leading edge.

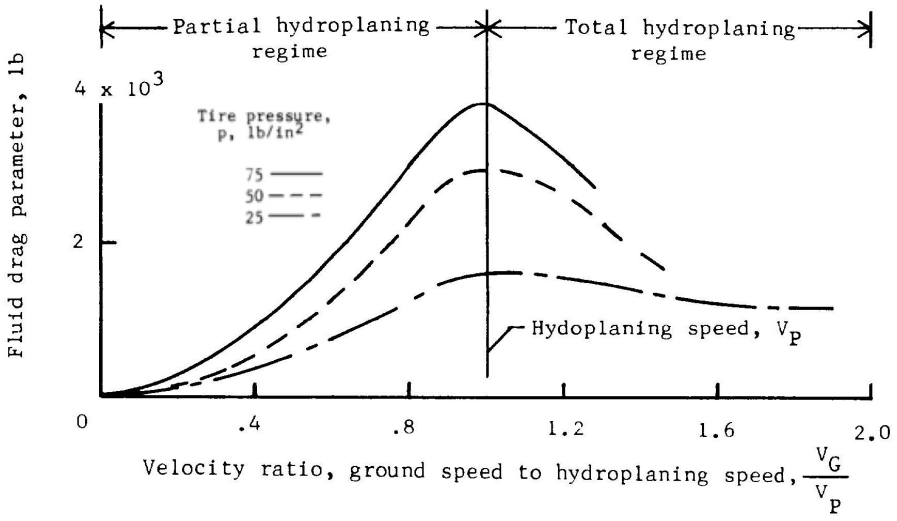

Figure 1.6: Fluid drag at partial and full hydroplaning speed. Vertical load 99229 N, water depth 25,4 mm. [2]

1.2.7. Loss in braking traction

Braking of tires on wet surfaces already experiences a reduced friction coefficient as can been seen in figure 1.7 [3].

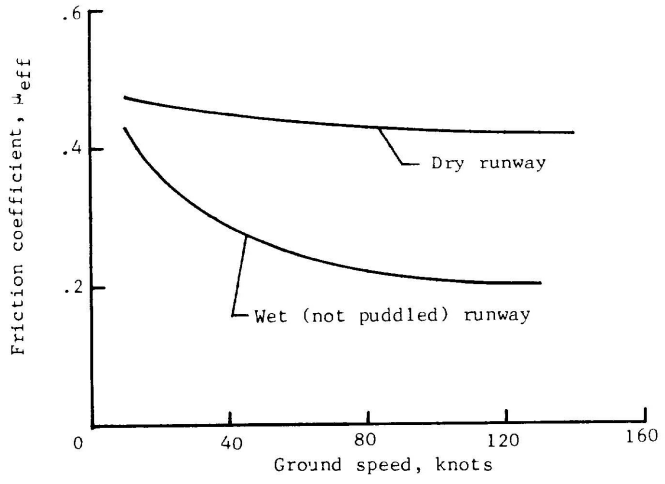

Figure 1.7: 880 jet transport aircraft on a concrete runway, tire pressure 10,34 bar, weight 667460 N, rib tread [2]

When conditions are sufficient to induce full hydroplaning, a catastrophic loss in friction is observed, see figure 1.8, with friction coefficients approaching those of free rolling.

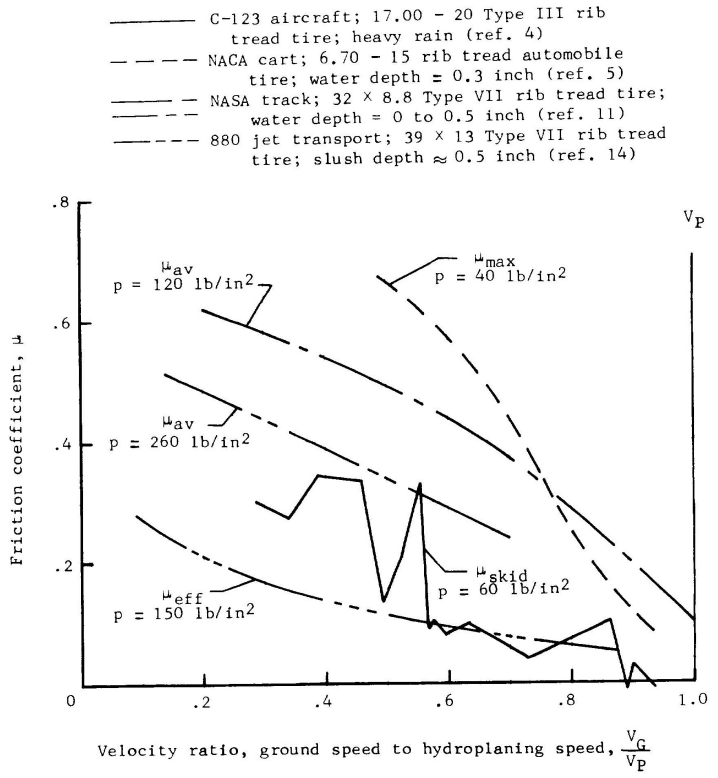

Figure 1.8: [2]

1.2.8. Loss of directional stability

In accordance with the reduction of friction in the longitudinal direction under braking one can also expect to experience reduced friction in lateral direction. A study by the Federal Aviation Agency [3],[4] done with speeds above the predicted hydroplaning speed with a side wind present resulting in the plane to yaw and drift laterally.

1.3. Significant parameters to hydroplaning

From the observations done by Horne and Dreher the following parameters have been deemed significant to contribute to the hydroplaning phenomenon:

- Fluid parameters
  - Depth of fluid
  - Density of fluid
- Tire parameters
  - Inflation pressure

  - Tire tread design
- Vehicle parameters
  - Vehicle weight
- Surface parameters
  - Pavement crown
  - Surface texture
  - Pavement grooves
  - Pavement unevenness

It is interesting to note that Horne and Dreher did not deem the fluid viscosity as a relevant parameter, although, especially after a long dry period, the rainfall mixes with the oil, dust, rubber debris and other contaminations on the road surface resulting in a mixture with a higher viscosity than pure water and therefore very good lubrication properties increasing the risk of hydroplaning.

2. Modelling of hydroplaning

With the different parameters and observations clear it is possible to attempt to model the hydroplaning phenomenon. To model the phenomena involved in hydroplaning, three different kinds of hydroplaning are commonly distinguished [5]; viscous hydroplaning, dynamic hydroplaning and inverted rubber hydroplaning. Several modeling approaches have been applied to the problem, of which an overview is given.

2.1. Hydroplaning distinctions

In literature commonly the following distinctions are made:

- *Viscous hydroplaning*
  Viscous hydroplaning is a classification made by Moore [6] where the phenomena are attributed to lubrication on the asperities of the road. The driving force in the lubrication is the local slip that occurs in a tire during braking or acceleration.

- *Dynamic hydroplaning*
  Dynamic hydroplaning is commonly referred to as due to thick layers of water forming a penetrating wedge in the leading edge of the tire resulting in partial or full hydroplaning

- *Inverted rubber hydroplaning*
  Inverted rubber hydroplaning is attributed to the phenomenon where due to locked wheels the rubber melts and forms a lubricating film that causes a hydroplaning effect. Although very interesting it is beyond the scope of this research and further investigation of it is left for future research.

Apart from reverted rubber hydroplaning the distinction between viscous and dynamic hydroplaning is not well defined, the next section will show different modelling approaches of which models based on dynamic hydroplaning generally overestimate the hydroplaning speed and attribute this to viscous effects without any calculation. At the same time the viscous hydroplaning models are also overestimating the hydroplaning speeds and this is attributed to inertia effects, again without further calculation. The challenge is to model hydroplaning using lubrication theory in combination with contact and at the same time taking into account inertia effects either in the full film or in the inlet.

2.2. Modelling approaches

The modelling approaches to hydroplaning can be divided into many different categories. Here an overview is given of some interesting approaches: models coupling a FEM model to a FVM model, models using only a CFD code, models based on lubrication theory.

FEM coupled to FVM Several authors published on the coupled method, for example Nakajima [7], who implemented the explicit code from MSC.Dytran. This couples a Lagrangian tire model with an Eulerian fluid model through coupling elements. The analysis is done with a water layer of 10 mm so inertia effects are deemed dominant. The model focuses on tread design. The results are that the lift force is proportional to the square of the velocity.

Another model is proposed by Cho et. al. [8] where the viscosity is neglected. The model is also using a 10 mm water layer, a P205/60R15 tire with the non-symmetric tread pattern. The tire is inflated at 2 bar and has a vertical load of 4.2 kN. The resulting lift force is seen in the next figure:

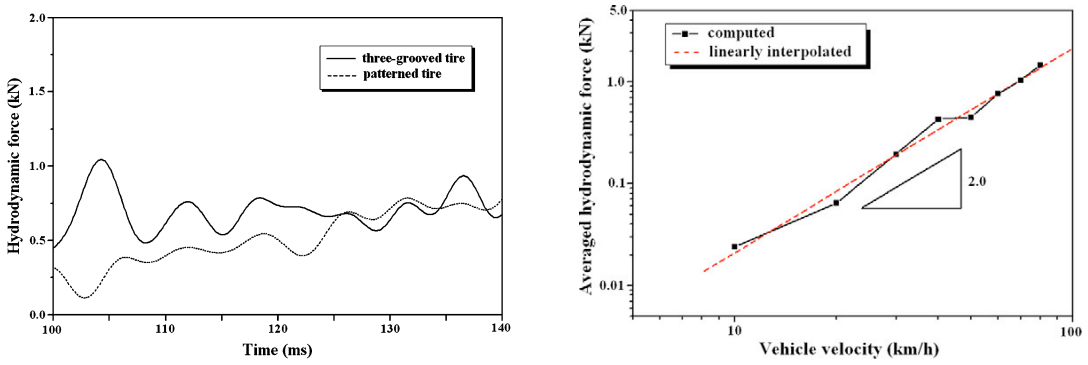

Fig. 11. Hydrodynamic force. (a) Time history (60 km/h), (b) velocity dependence.

Figure 2.1: Lift force [8]

Cho et.al. also conclude a lift force proportional to the square of the velocity.

Other authors on numerical models in hydroplaning are for example Zmindak [1997] [9]

CFD models Ong and Fwa [10] made a Fluent model with the geometry of Browne [11] . Their results match the experiments of Browne and the formula proposed by Nasa. Main limitation of only using a CFD code is off course the fact that a deformed tire shape has to be assumed, where in the case of hydroplaning it is the fluid structure interaction that is interesting due to the strong coupling because of the incompressible fluid and the highly elastic structure.

Lubrication theory: D.F. Moore Moore [6] applied the lubrication theory on the hydroplaning phenomenon, based on the longitudinal slip occurring during braking and acceleration over a sinusoidal asperity on the road surface. See figure:

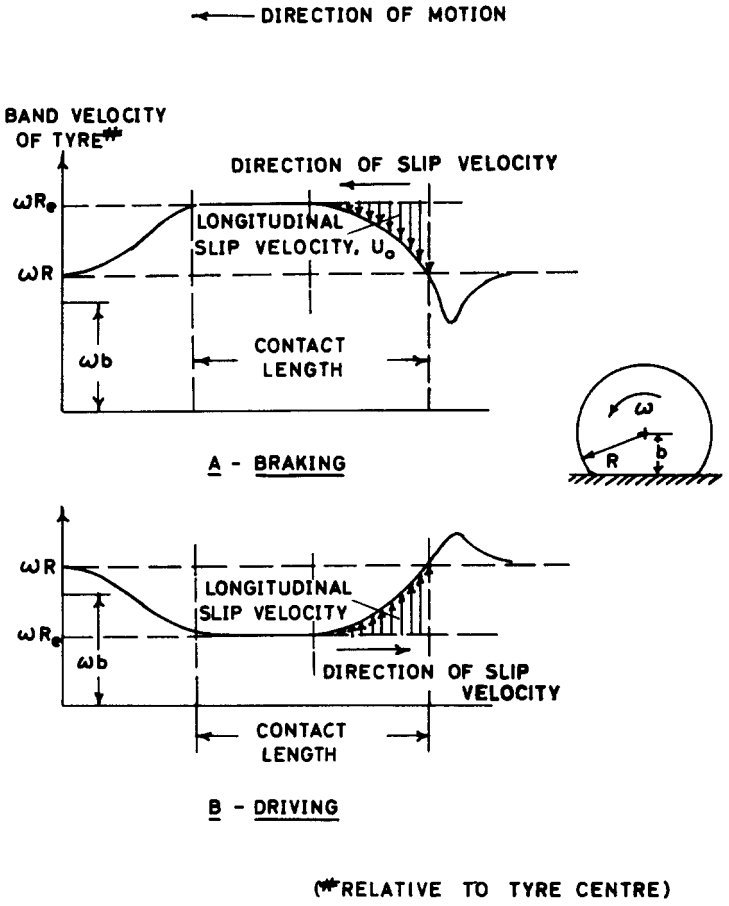

FIG. 1. Band velocity for a rolling pneumatic tyre when braked or driven, showing longitudinal slip velocity at rear of contact length.

Figure 2.2: Longitudinal slip [6]

The assumed asperity of the road has the following shape:

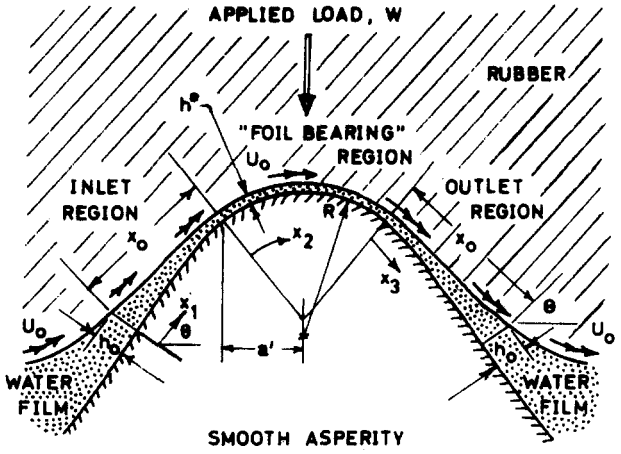

FIG. 2. The three characteristic regions for the case of rubber sliding on a smooth, sinusoidal asperity covered with a thin water-film.

Figure 2.3: Sinusoidal asperity [6]

The resulting pressure profile is:

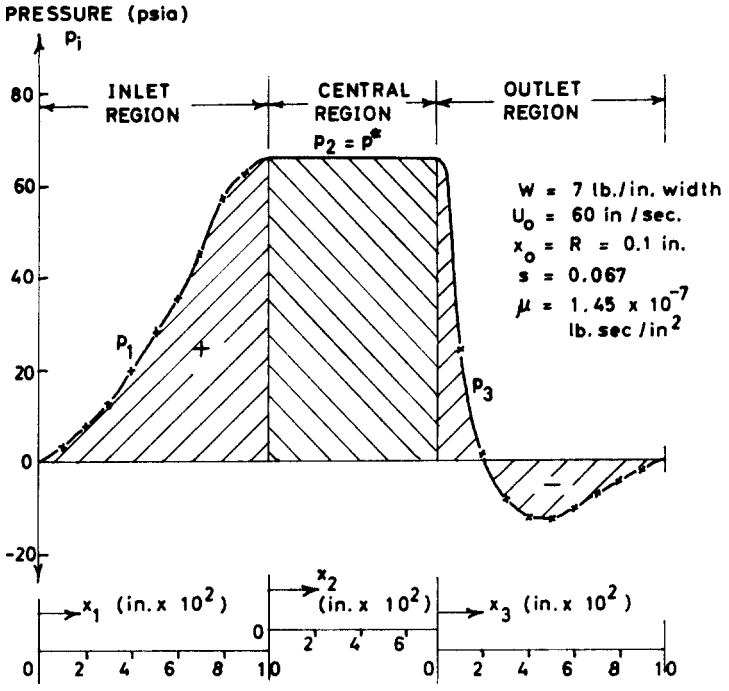

FIG. 3. The generation of hydrodynamic pressures in the inlet, central and outlet regions.

Figure 2.4: Pressure distribution [6]

These values in SI units are shown in table 2.2:
The fractional slip is indicated with s and is defined as:

$$s = \frac{\omega_{\text{driving}} - \omega_{\text{rolling}}}{\omega_{\text{rolling}}} \tag{2.1}$$

Load	W	7 lb/in	1.23 N/mm
Velocity	U_0	60 in/sec	1.52400 m/s
Radius of asperity	R	0.1 in	2,54 mm
Viscosity	μ	1.45 e-7 $lbsec/in^2$	1e-3 Pa s

Table 1: Conversion table

One can see that the order of magnitude of the pressure is around 70 psi or 482 kPa.

Lubrication theory: Do, Marsac and Mosset Do, Marsace and Mosset [12] present a model based on the Stribeck curve, determining the resultant friction on wet pavement, depending on the speed. The new model called "modified exponential model" requires 4 constants. Based on existing data from VERT and HERMES European projects, it is possible to relate three of them to measurable parameters such as road surface macro- and microtexture, wheel slip, tire tread depth and water layer thickness. Further analyses are needed for the fourth parameter, which describes a viscous effect of friction.

Lubrication theory: Andren & Jolkin Another attempt to apply the Reynolds equation to the hydroplaning phenomenon was done by Adren and Jolkin [13], a research for the Swedish government. This research applies the Reynolds equation in a finite difference scheme and models the tire in two different ways, first as a solid, linear elastic half space and second as a P.I.A.R.C test tire in the finite element programme, ABAQUS. The results show that the hydroplaning speed is only reached at 1600 m/s. One major limitation of the research is the Green function approach, assuming local linearity with which the tire model has been condensed to a influence matrix rather than having an full FSI model. Since the leading edge has a steeply diverging shape the estimation for the central film thickness is of huge influence on the results from the Reynolds equation. Next to that the deformation of the tire is critical in the leading edge as the formation of a pocket is of huge influence on the Reynolds equation and is perhaps not accurately represented by the Green function approach.

2.3. experimental results

Horne & Dreher [2] were among the earliest to document tests on the hydroplaning phenomenon and their observations have been described in section I.

Browne, Cheng and Kistler [11] made an theoretical model based on inertia, viscosity and possible turbulence and did experimental verification of the models. The models include two different inlet conditions, a pressure equal to zero or a pressure equal to the stagnation pressure. The experimental setup consists of two aluminium plates, milled to a convex shape which is assumed for the tire. The results are in agreement with the work of Horne & Joyner [2]

Ervin and Balderas [14] did a hydroplaning study for lightly loaded truck tires for the University of Michigan Transportation Research Institute, comparing the influence

of velocity, rib and lug tires, tire configuration as seen on trucks, inflation pressure, treadwear and swapping of the tires.

2.4. Further literature

Several different modelling and testing approaches have been applied to the hydroplaning phenomenon of which a few have been highlighted, the interested reader can find even more, similar modelling approaches in for example: Padovan [2007] [15], Hays and Browne [1974] [16], Meyer and Walter [17], Claeys [2001] [18], Zmindak [1997] [9]. In general, pavement design for hydroplaning is a good starting point to search for literature as from this side the largest amount of publications have been done, usually driven by government, road or transportation institutes.

3. Summary

This section has shown the early observations regarding hydroplaning, which is defined as the phenomenon of the loss of traction of a rubber tire due to presence of a water layer between the tire and the road surface. The loss of traction makes the vehicle insensitive to control inputs such as steering, braking and accelerating. The main observations regarding hydroplaning are the spin-down of the tire to a complete stop at a certain speed, detachment of the tire footprint, hydrodynamic ground pressure increase, suppression of tire bow wave, scouring action of escaping fluid in tire-ground footprint all resulting in loss in braking traction and loss of tire directional stability.

To model hydroplaning the distinction is made between dynamic, viscous and inverted rubber hydroplaning. The distinction between viscous and dynamic hydroplaning is not well defined, models based on dynamic hydroplaning generally overestimate the hydroplaning speed and attribute this to viscous effects without any calculation. At the same time the viscous hydroplaning models are also overestimating the hydroplaning speeds and this is attributed to inertia effects, again without further calculation. The challenge is to model hydroplaning using lubrication theory in combination with contact and at the same time taking into account inertia effects either in the full film or in the inlet. These are therefore the main topics for the next section that describes the fluid models applied. Furthermore, several other modelling approaches have been listed, from analytical to a full CFD model. The general limitation of these modelling approaches is the computational time and it is therefore interesting to investigate the (modified) lubrication theory as an approach to model hydroplaning. If computational time can be reduced to several hours the modelling approach becomes interesting as a design tool.

3.1. Overview section II - IV

Now that the overview of hydroplaning is clear the three major aspects of modelling hydroplaning, i.e. the fluid, the solid and the solid fluid interaction, are described. It starts with zooming in on the fluid modelling (section II), then the tire modelling is dealt with (section III) and finally the fluid structure interaction is described (section IV). The fluid modelling starts with the derivation of the Navier Stokes equation from which the Reynolds equation is derived under the thin film assumption. For this equation the inertia effects in the fluid film and in the inlet are investigated. Then cavitation is taken into account resulting in a fill rate model where also starved lubrication can be modelled. The tire modelling starts with a linear elastic model developed in Matlab and then a hyperelastic model developed in ABAQUS. The fluid structure interaction starts with classical staggering and then an interface method is introduced to speed up the convergence of the model.

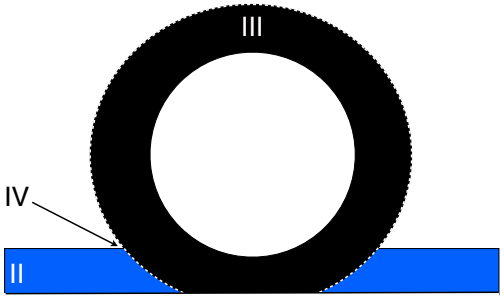

- Section II: Fluid dynamics: Lubrication theory
  - Navier Stokes
  - Reynolds
    - Inertia in the fluid film
    - Inertia in the inlet
    - Fill rate
- Section III: Solid Mechanics: Tire modelling
  - Linear elastic half space model
  - Hyper elastic finite element model
- Section IV: Fluid Structure Interaction
  - Classical staggering
  - Interface Quasi Newton method
  - Coupling ABAQUS to Matlab

Section II
Fluid dynamics: Lubrication theory

This section describes the modeling of a fluid using lubrication theory, to begin with the momentum balance for a fluid, the Navier Stokes equations for an incompressible Newtonian fluid is derived and from there theory of lubrication developed by Osborne Reynolds is derived. In this derivation the thin film assumption is explained and implemented resulting in neglecting the inertia terms in the Navier Stokes equations. To verify this an inertia correction is set-up for the fluid film. Next to that the inertia effects in the inlet are investigated, an approximation is made by assuming a stagnation pressure and an iterative energy and momentum correction is made to this approximation. Finally a cavitation model is extended to function as a fill rate model such that the location of the inlet, which is a priori unknown, can be determined.

4. Navier Stokes equations

The Navier Stokes equations are applicable to the fluid modelling of the hydroplaning problem.

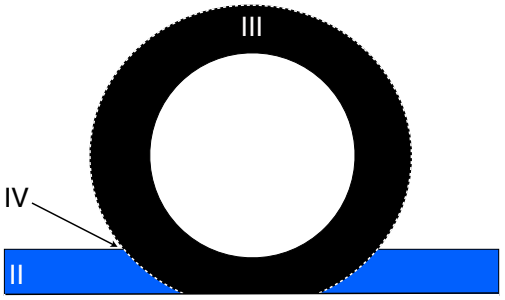

- Section II: Fluid dynamics: Lubrication theory
  - **Navier Stokes**
  - Reynolds
    - Inertia in the fluid film
    - Inertia in the inlet
    - Fill rate
- Section III: Solid Mechanics: Tire modelling
  - Linear elastic half space model
  - Hyper elastic finite element model
- Section IV: Fluid Structure Interaction
  - Classical staggering
  - Interface Quasi Newton method
  - Coupling ABAQUS to Matlab

The complete derivation of the Navier Stokes equations can be found in appendix A, a summary of the assumptions and the resulting equation is given here. Starting with four assumptions:

Assumption 1. ***Continuum****, The fluid is a continuous substance*

Assumption 2. ***Differentiable****, The fluid parameters are, at least weakly, differentiable*

Assumption 3. ***Newtonian fluid***

- *The stress tensor is a linear function of the strain rates.*
- *The fluid is isotropic.*
- *For a fluid at rest, the deviatoric stress must be zero (so that hydrostatic pressure results)*

Assumption 4. *Incompressibility*

$$\frac{D\rho}{Dt} = 0 \tag{4.1}$$

Where ρ indicates the density and t the time. With this the conservation of momentum becomes:

$$\rho\left(\frac{\partial \mathbf{v}}{\partial t} + \mathbf{v}\cdot\nabla\mathbf{v}\right) = -\nabla p + \mu\nabla^2\mathbf{v} + \mathbf{f} \tag{4.2}$$

Where $\mathbf{v}$ indicates the velocity vector, p the pressure, mu the viscosity and $\mathbf{f}$ the body forces such as gravity.

And conservation of mass:

$$\nabla\cdot\mathbf{v} = 0 \tag{4.3}$$

5. Reynolds equation

In this section the Reynolds equation is explained which is used in the area where the thin film assumption, which will be explained later, holds. See figure

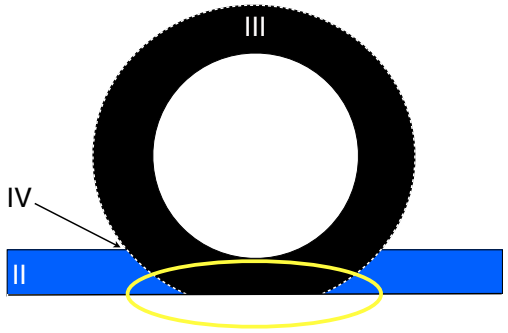

- Section II: Fluid dynamics: Lubrication theory
  - Navier Stokes
  - **Reynolds**
    - Inertia in the fluid film
    - Inertia in the inlet
    - Fill rate
- Section III: Solid Mechanics: Tire modelling
  - Linear elastic half space model
  - Hyper elastic finite element model
- Section IV: Fluid Structure Interaction
  - Classical staggering
  - Interface Quasi Newton method
  - Coupling ABAQUS to Matlab

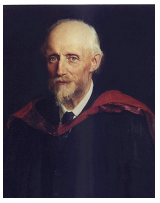

Figure 5.1: O. Reynolds

In 1886 Osborne Reynolds wrote his famous work "On the theory of lubrication and its application to Mr. B. Towers experiments, including an experimental determination of the viscosity of olive oil [19]" The experiment of Beauchamp Towers [20] investigated the influence of lubrication on friction at high sliding velocities. Towers found that friction varied strongly with load and velocity, contrary to Coulomb's formulation, where friction is independent of the sliding velocity.
Inspired by this work Reynolds developed a partial differential equation to describe the the pressure distribution in a thin film between two moving surfaces. Reynolds starts with the expressing the conservation of momentum using the expression for the stress in a viscous fluid as described by Stokes [21]. To see how Stokes arrives at his expression start with the Navier-Stokes equations for an incompressible Newtonian fluid:

$$\rho\left(\frac{\partial \mathbf{v}}{\partial t} + \mathbf{v}\cdot\nabla\mathbf{v}\right) = -\nabla p + \mu\nabla^2\mathbf{v} + \mathbf{f} \tag{5.1}$$

Furthermore the following approach is taken:

Assumption 5. *Thin film approach: the characteristic height, h_0 is much smaller than the characteristic length, l_0 and characteristic width b_0.*

Which results in, according to Osborne Reynolds formulation: "The fluid film is thin therefore the flow is free of eddies (laminar flow) and the forces arising from weight and inertia are small compared to the viscous stresses. The inertia terms in the Navier Stokes equations are ignored." [19]. The thin film assumption and its consequences is most clear when a dimensional analysis is applied to the Navier Stokes equations. Start with the first term of the Navier Stokes equations:

$$\rho\left(\frac{\partial u}{\partial t}+u\frac{\partial u}{\partial x}+v\frac{\partial u}{\partial y}+w\frac{\partial u}{\partial z}\right)=-\frac{\partial p}{\partial x}+\mu\left(\frac{\partial^2 u}{\partial x^2}+\frac{\partial^2 u}{\partial y^2}+\frac{\partial^2 u}{\partial z^2}\right) \tag{5.2}$$

Now define the following dimensionless quantities, indicated with an overbar:

$$\begin{array}{l}\bar{x}=\frac{x}{l_0},\bar{y}=\frac{y}{b_0},\bar{z}=\frac{z}{h_0}\\ \bar{u}=\frac{u}{u_0},\bar{v}=\frac{v}{v_0},\bar{w}=\frac{w}{w_0}\\ \bar{t}=\frac{tu_0}{l_0},\bar{p}=\frac{h_0^2 p}{\mu u_0 l_0}\end{array} \tag{5.3}$$

Where l_0 the characteristic length in x-direction, b_0 the characteristic length in y-direction and h_0 the characteristic length in z-direction, i.e. the film thickness. In the same manner u_0, v_0 and w_0 are the characteristic velocities in x, y, and z-direction. Substitute to obtain:

$$\begin{array}{l}\frac{\rho u_0 l_0}{\mu}\left(\frac{\partial \bar{u}}{\partial \bar{t}}+\bar{u}\frac{\partial \bar{u}}{\partial \bar{x}}+\frac{l_0}{b_0}\frac{v_0}{u_0}\bar{v}\frac{\partial \bar{u}}{\partial \bar{y}}+\frac{l_0}{h_0}\frac{w_0}{u_0}\bar{w}\frac{\partial \bar{u}}{\partial \bar{z}}\right)=\\ -\left(\frac{l_0}{h_0}\right)^2\frac{\partial \bar{p}}{\partial \bar{x}}+\frac{\partial^2 \bar{u}}{\partial \bar{x}^2}+\left(\frac{l_0}{b_0}\right)^2\frac{\partial^2 \bar{u}}{\partial \bar{y}^2}+\left(\frac{l_0}{h_0}\right)^2\frac{\partial^2 \bar{u}}{\partial \bar{z}^2}\end{array} \tag{5.4}$$

Here one recognizes the inverse of the Reynolds number as seen often in fluid mechanics:

$$\mathrm{Re}=\frac{\rho u_0 l_0}{\mu} \tag{5.5}$$

However as already seen in 5.4 the term $\frac{\partial^2 \bar{u}}{\partial \bar{z}^2}$ is dominant due to the thin film assumption and a modified Reynolds number is introduced for x, y and z-direction:

$$\mathrm{Re}_x=\frac{\rho u_0 h_0^2}{\mu l_0},\mathrm{Re}_y=\frac{\rho v_0 h_0^2}{\mu b_0},\mathrm{Re}_z=\frac{\rho w_0 h_0}{\mu} \tag{5.6}$$

It is now clear that under a thin film assumption $h_0 \ll l_0$ and $h_0 \ll b_0$ and with the squeeze velocity small the inertia terms can be neglected and that the $\frac{\partial^2 \bar{u}}{\partial \bar{z}^2}$ viscosity term is dominant. The resulting equation is:

$$\frac{\partial \bar{p}}{\partial \bar{x}}=\mu\frac{\partial^2 \bar{u}}{\partial \bar{z}^2} \tag{5.7}$$

The same reasoning can be used in y and z direction. For y direction this is trivial but for z direction we see the following:

$$\begin{array}{l}\frac{\rho}{\mu}\left(\frac{u_0}{w_0}\frac{h_0^2}{l_0}\frac{\partial \bar{w}}{\partial \bar{t}}+\frac{u_0}{w_0}\frac{h_0^2}{l_0}\bar{u}\frac{\partial \bar{w}}{\partial \bar{x}}+\frac{v_0}{w_0}\frac{h_0^2}{b_0}\bar{v}\frac{\partial \bar{w}}{\partial \bar{y}}+h_0\frac{\partial \bar{w}}{\partial \bar{z}}\right)=\\ -\frac{u_0 l_0}{h_0}\frac{\partial \bar{p}}{\partial \bar{z}}+\left(\frac{h_0}{l_0}\right)^2\frac{\partial \bar{w}}{\partial \bar{x}}+\left(\frac{h_0}{b_0}\right)^2\frac{\partial \bar{w}}{\partial \bar{y}}+\frac{\partial \bar{w}}{\partial \bar{z}}\end{array} \tag{5.8}$$

From this it is clear that:

$$\frac{\partial p}{\partial z}=0 \tag{5.9}$$

In other words, the pressure does not vary over the height of the film. In the further equations the terms are no longer dimensionless. Finally the assumption that is used, which is not strictly necessary but makes further calculations simpler:

Assumption 6. *Constant viscosity in time*

To end up with the following equations:

$$\begin{aligned} \frac{\partial p}{\partial x} &= \mu \frac{\partial^2 u}{\partial^2 z} \\ \frac{\partial p}{\partial y} &= \mu \frac{\partial^2 v}{\partial^2 z} \\ \frac{\partial p}{\partial z} &= 0 \\ 0 &= \frac{\partial u}{\partial x} + \frac{\partial v}{\partial y} + \frac{\partial w}{\partial z} \end{aligned} \tag{5.10}$$

It is interesting to note that several authors, see for example [22], that start with the thin film assumption and derive the Reynolds equation from there. Looking at equation A.26 one can immediately drop the terms involving velocity gradients in x and y direction and also cancel the terms with w to directly obtain equation 5.10 without having to introduce the assumption of incompressibility as Reynolds does.

To solve these equations boundary conditions are necessary, these are determined with the assumption:

Assumption 7. *No slip condition*

To have the following boundary conditions, assuming $\frac{\partial h}{\partial x}$ and $\frac{\partial h}{\partial y}$ are small:

$$\begin{aligned} u\left(z=0\right) &= U_1 \\ v\left(z=0\right) &= V_1 \\ u\left(z=h\right) &= U_2 \\ v\left(z=h\right) &= V_2 \\ w\left(z=h\right) &= \frac{dh}{dt} \\ w\left(z=0\right) &= 0 \end{aligned} \tag{5.11}$$

Two integrations of equation 5.10 results in:

$$\begin{aligned} \frac{\partial p}{\partial x}\frac{1}{2}z^2 &= \mu u + C_1 z + C_2 \\ \frac{\partial p}{\partial y}\frac{1}{2}z^2 &= \mu v + C_3 z + C_4 \end{aligned} \tag{5.12}$$

Apply boundary conditions:

$$
\begin{aligned}
u\left(x,z\right) &= \frac{1}{2\mu}\frac{\partial p}{\partial x}\left(z^2 - hz\right) + \frac{U_2 - U_1}{h}z + U_1 \\
v\left(x,z\right) &= \frac{1}{2\mu}\frac{\partial p}{\partial y}\left(z^2 - hz\right) + \frac{V_2 - V_1}{h}z + V_1
\end{aligned}
\tag{5.13}
$$

Substitute in equation 4.3 to obtain:

$$
\begin{aligned}
&\frac{\partial w}{\partial z} = -\frac{1}{2\mu}\left[\frac{\partial}{\partial x}\left\{\frac{\partial p}{\partial x}\left(z^2 - hz\right)\right\} + \frac{\partial}{\partial y}\left\{\frac{\partial p}{\partial y}\left(z^2 - hz\right)\right\}\right] \\
&-\frac{\partial}{\partial x}\left[\frac{U_2 - U_1}{h}z + U_1\right] - \frac{\partial}{\partial y}\left[\frac{V_2 - V_1}{h}z + V_1\right]
\end{aligned}
\tag{5.14}
$$

Apply integration from $z = 0$ to $z = h$ to obtain the 2D Reynolds equation

$$
\begin{aligned}
&\frac{\partial}{\partial x}\left(\frac{h^3}{12\mu}\frac{\partial p}{\partial x}\right) + \frac{\partial}{\partial y}\left(\frac{h^3}{12\mu}\frac{\partial p}{\partial y}\right) = \frac{U_1 + U_2}{2}\frac{\partial h}{\partial x} + \frac{V_1 + V_2}{2}\frac{\partial h}{\partial y} + \\
&\frac{h}{2}\frac{\partial}{\partial x}\left(U_1 + U_2\right) + \frac{h}{2}\frac{\partial}{\partial y}\left(V_1 + V_2\right) + \frac{\partial h}{\partial t}
\end{aligned}
\tag{5.15}
$$

The right hand side terms are often described as the wedge effect $\frac{\partial h}{\partial x}$, the stretch effect $\frac{\partial U}{\partial x}$ and the squeeze effect $\frac{\partial h}{\partial t}$.

The wedge effect describes the sliding motion of a fluid in a converging or diverging channel, the stretch effect captures the phenomenon of the change of length of the surface as is the case with rubber and elastomer components. Finally the squeeze effect is due to vertical motion of the surfaces. Introducing the vector U the surface velocities are written as:

$$
U = \begin{bmatrix} U_1 + U_2 \\ V_1 + V_2 \end{bmatrix}
\tag{5.16}
$$

The Reynolds equation is sometimes also written as:

$$
\nabla\left(-\frac{h^3}{12\mu}\nabla p + \frac{1}{2}Uh\right) + \frac{\partial h}{\partial t} = 0
\tag{5.17}
$$

This form shows the conservation of mass and is also the basis for the derivation of the cavitation algorithm which will be described later.

5.1. Inertia correction

The inertia effects in the fluid film are studied in this section, see figure:

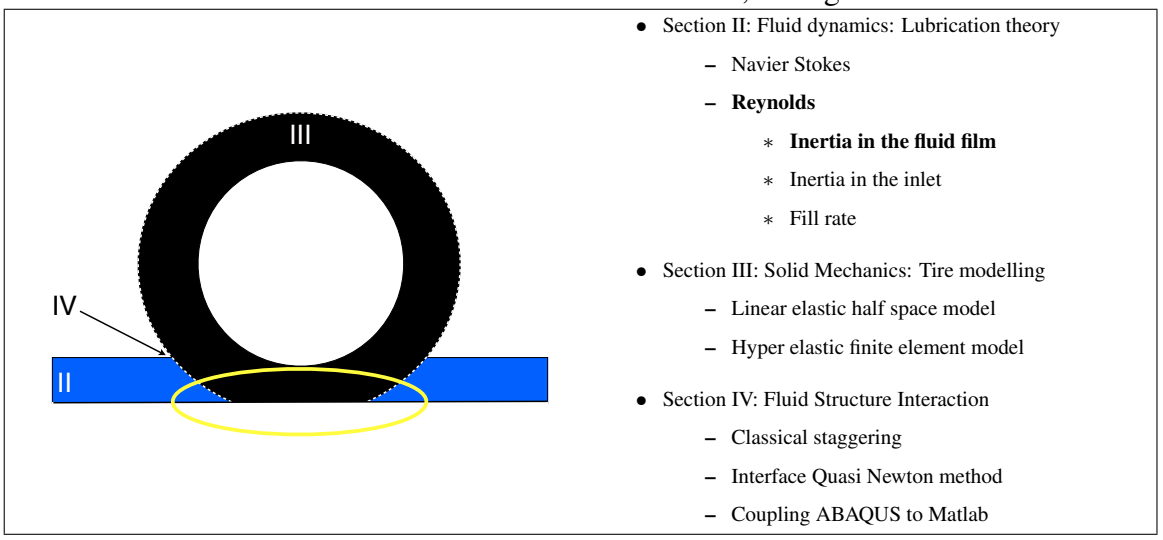

There is no general approach to include inertia effects in the Reynolds equation, in this section inertia effects are studied in two separate cases, first in squeeze and then in sliding. In sliding two different methods are shown in 1D which are then combined and expanded to a 2D model.

5.1.1. Squeeze of a circular disc

The inertia correction is often seen in squeeze problem where the Reynolds equation is applied. First an example of a circular disc in squeeze is given to show the method and the potential of the inertia correction. The circular disc on a flat surface has the following geometry:

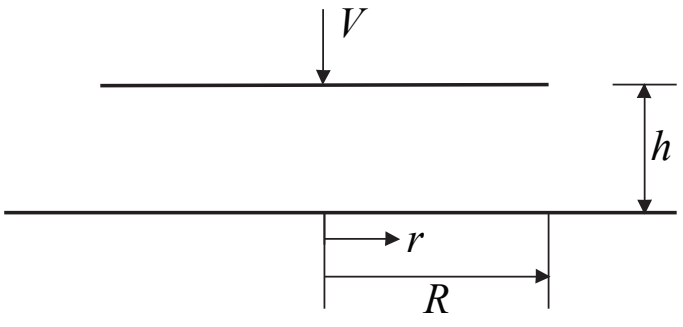

Figure 5.2: Circular disc on flat

Apply the Navier-Stokes equations for an incompressible Newtonian fluid in cylindrical coordinates:

$$\begin{aligned}
&\rho\left(\frac{\partial u_r}{\partial t}+u_r\frac{\partial u_r}{\partial r}+\frac{u_\theta}{r}\frac{\partial u_r}{\partial \theta}+u_z\frac{\partial u_r}{\partial z}-\frac{u_\theta^2}{r}\right)=-\frac{\partial p}{\partial r}+\\
&\quad\mu\left[\frac{1}{r}\frac{\partial}{\partial r}\left(\frac{1}{r}\frac{\partial u_r}{\partial r}\right)+\frac{1}{r^2}\frac{\partial^2 u_r}{\partial \theta^2}+\frac{\partial^2 u_r}{\partial z^2}-\frac{u_r}{r^2}-\frac{2}{r^2}\frac{\partial u_\theta}{\partial \theta}\right]+\rho g_r\\
&\rho\left(\frac{\partial u_\theta}{\partial t}+u_r\frac{\partial u_\theta}{\partial r}+\frac{u_\theta}{r}\frac{\partial u_\theta}{\partial \theta}+u_z\frac{\partial u_\theta}{\partial z}-\frac{u_r u_\theta}{r}\right)=-\frac{1}{r}\frac{\partial p}{\partial \theta}+\\
&\quad\mu\left[\frac{1}{r}\frac{\partial}{\partial r}\left(\frac{1}{r}\frac{\partial u_\theta}{\partial r}\right)+\frac{1}{r^2}\frac{\partial^2 u_\theta}{\partial \theta^2}+\frac{\partial^2 u_\theta}{\partial z^2}+\frac{2}{r^2}\frac{\partial u_r}{\partial \theta}-\frac{u_\theta}{r^2}\right]+\rho g_\theta\\
&\rho\left(\frac{\partial u_z}{\partial t}+u_r\frac{\partial u_z}{\partial r}+\frac{u_\theta}{r}\frac{\partial u_z}{\partial \theta}+u_z\frac{\partial u_z}{\partial z}\right)=-\frac{\partial p}{\partial z}+\\
&\quad\mu\left[\frac{1}{r}\frac{\partial}{\partial r}\left(\frac{1}{r}\frac{\partial u_z}{\partial r}\right)+\frac{1}{r^2}\frac{\partial^2 u_z}{\partial \theta^2}+\frac{\partial^2 u_z}{\partial z^2}\right]+\rho g_z
\end{aligned}\tag{5.18}$$

With the continuity equation:

$$\frac{1}{r}\frac{\partial}{\partial r}\left(r u_r\right)+\frac{1}{r}\frac{\partial u_\theta}{\partial \theta}+\frac{\partial u_z}{\partial z}=0\tag{5.19}$$

In case of axi-symmetric flow and the disc not rotating this can be reduced to:

$$\begin{aligned}
&\rho\left(\frac{\partial u_r}{\partial t}+u_r\frac{\partial u_r}{\partial r}+u_z\frac{\partial u_r}{\partial z}\right)=-\frac{\partial p}{\partial r}+\\
&\quad\mu\left[\frac{1}{r}\frac{\partial}{\partial r}\left(\frac{1}{r}\frac{\partial u_r}{\partial r}\right)+\frac{\partial^2 u_r}{\partial z^2}-\frac{u_r}{r^2}\right]+\rho g_r\\
&\rho\left(\frac{\partial u_z}{\partial t}+u_r\frac{\partial u_z}{\partial r}+u_z\frac{\partial u_z}{\partial z}\right)=-\frac{\partial p}{\partial z}+\\
&\quad\mu\left[\frac{1}{r}\frac{\partial}{\partial r}\left(\frac{1}{r}\frac{\partial u_z}{\partial r}\right)+\frac{\partial^2 u_z}{\partial z^2}\right]+\rho g_z
\end{aligned}\tag{5.20}$$

With the continuity equation:

$$\frac{1}{r}\frac{\partial}{\partial r}\left(r u_r\right)+\frac{\partial u_z}{\partial z}=0\tag{5.21}$$

Again, with assumption 5 the squeeze film thickness is much smaller than the radius of the squeeze surface thus:

$$\begin{aligned}
&h\ll r\\
&\frac{\partial p}{\partial z}\ll\frac{\partial p}{\partial r}
\end{aligned}\tag{5.22}$$

Then, the Navier-Stokes equations can be reduced to:

$$\rho\left(\frac{\partial u_r}{\partial t}+u_r\frac{\partial u_r}{\partial r}+u_z\frac{\partial u_r}{\partial z}\right)=-\frac{\partial p}{\partial r}+\mu\left[\frac{\partial^2 u_r}{\partial z^2}\right]\tag{5.23}$$

In line with the thin film assumption, if $Re^*\ll 1$, where:

$$\mathrm{Re}^* = \frac{\rho U l}{\mu}\left(\frac{h}{l}\right)^2 \tag{5.24}$$

The inertia of the flow can be neglected, reducing to the simple equation:

$$\frac{\partial p}{\partial r} = \mu\left[\frac{\partial^2 u_r}{\partial z^2}\right] \tag{5.25}$$

To solve this differential equation apply assumption 7, resulting in boundary conditions:

$$\begin{aligned} u_r\left(z=0\right) &= 0 \\ u_r\left(z=h\right) &= 0 \end{aligned} \tag{5.26}$$

Integrate twice to obtain:

$$u_r = \frac{1}{2\mu}\frac{\partial p}{\partial r}\left(z^2 - hz\right) \tag{5.27}$$

Substitute the velocity profile in the continuity equation:

$$\frac{1}{r}\frac{\partial}{\partial r}\left(r\frac{1}{2\mu}\frac{\partial p}{\partial r}\left(z^2-hz\right)\right) + \frac{\partial u_z}{\partial z} = 0 \tag{5.28}$$

Integrate with respect to z with boundary conditions, with for convenience:

$$\frac{dh}{dt} = \dot{h} \tag{5.29}$$

$$\begin{aligned} u_z\left(z=0\right) &= 0 \\ u_z\left(z=h\right) &= \dot{h} \end{aligned} \tag{5.30}$$

To obtain:

$$\begin{aligned} &\int_0^h \left\{\frac{1}{r}\frac{\partial}{\partial r}\left(r\frac{1}{2\mu}\frac{\partial p}{\partial r}\left(z^2-hz\right)\right) + \frac{\partial u_z}{\partial z}\right\} dz = 0 \\ &\int_0^h \frac{\partial}{\partial r}\left(r\frac{1}{2\mu}\frac{\partial p}{\partial r}\left(z^2-hz\right)\right)dz = r\int_0^h \frac{\partial u_z}{\partial z}dz \\ &\frac{\partial}{\partial r}\left(r\frac{1}{2\mu}\frac{\partial p}{\partial r}\left(\frac{z^3}{3}-\frac{hz^2}{2}\right)\right)\Bigg|_0^h = r\dot{h} \end{aligned} \tag{5.31}$$

Such that the Reynolds equation in pure squeeze in cylindrical coordinates becomes:

$$\frac{\partial}{\partial r}\left(rh^3\frac{\partial p}{\partial r}\right) = 12\mu r\dot{h} \tag{5.32}$$

The boundary conditions on the pressure are:

$$p\left(r=R\right) = 0 \tag{5.33}$$

And from axial symmetry:

$$\frac{\partial p}{\partial r}\left(r=0\right)=0 \tag{5.34}$$

Resulting in:

$$p=-\frac{3\mu\dot{h}}{h^3}\left(R^2-r^2\right) \tag{5.35}$$

Now take for the circular disc the following geometry and operating conditions:

- R = 25 mm
- $\dot{h}$ = -7.84428 $\frac{km}{h}$
- h_0 = 3 mm
- the fluid is water
  - $\rho = 1 \cdot 10^3 \frac{kg}{m^3}$
  - $\mu = 1 \cdot 10^{-3} Pas$

The resulting lift force is:

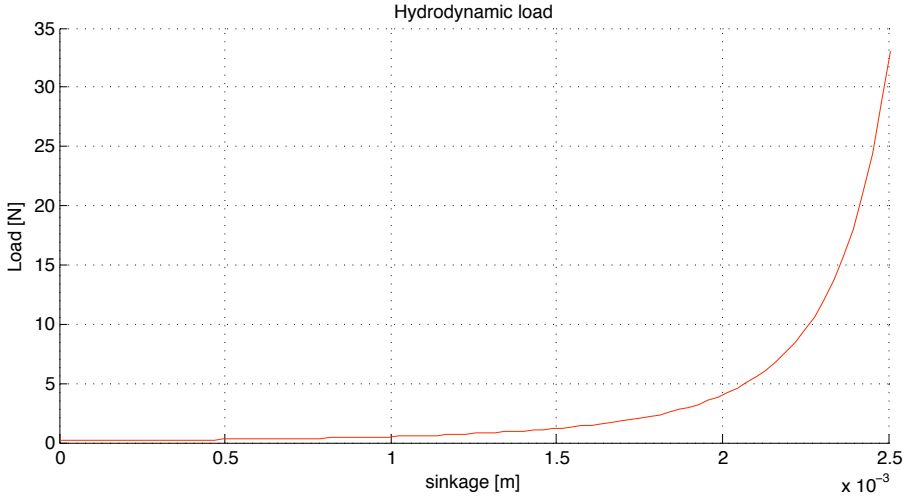

Figure 5.3: Squeeze of a circular disc, pure viscous solution

A solution of a circular disc with the same conditions as in as listed is done with a several CFD codes (ABAQUS CEL, FlowVision) as well as an analytical solution. The resulting lift forces are:

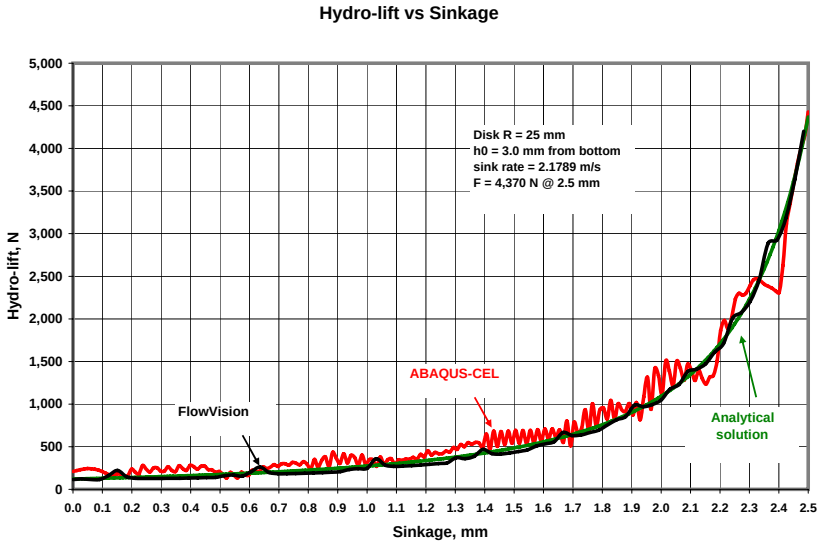

Figure 5.4: Circular disc

One can see the resulting lift force is much higher than seen before, due to the inertia effects dominating in this problem. This can be dealt with by correcting the Reynolds equations for the inertia, first take the obtained velocity profile in radial direction 5.27:

$$u_r = \frac{1}{2\mu}\frac{\partial p}{\partial r}\left(z^2 - hz\right) \tag{5.36}$$

Substitute in the continuity equation 5.21 and take the following boundary conditions:

$$\begin{aligned} u_z\left(z=0\right) &= 0 \\ u_z\left(z=h\right) &= \frac{dh}{dt} \end{aligned} \tag{5.37}$$

To obtain for vertical direction:

$$u_z = -\frac{\dot{h}}{h^3}\left(2z^3 - 3hz^2\right) \tag{5.38}$$

Now, while retaining the thin film assumption but taking into account inertia recall equation 5.23:

$$\rho\left(\frac{\partial u_r}{\partial t} + u_r\frac{\partial u_r}{\partial r} + u_z\frac{\partial u_r}{\partial z}\right) = -\frac{\partial p}{\partial r} + \mu\left[\frac{\partial^2 u_r^*}{\partial z^2}\right] \tag{5.39}$$

Where u_r^* the velocity profile is with the inertia correction included. Notice that this is a fixed point iteration procedure and convergence is not guaranteed. Now, with:

$$\begin{aligned} u_r &= \frac{3r\dot{h}}{h^3}\left(z^2 - hz\right) \\ u_z &= -\frac{\dot{h}}{h^3}\left(2z^3 - 3hz^2\right) \end{aligned} \tag{5.40}$$

One can obtain:

$$\begin{aligned} \frac{\partial u_r}{\partial t} &= \frac{3r}{h^3}\left(z^2 - hz\right)\ddot{h} + \frac{3r\dot{h}^2}{h^4}\left(-3z^2 + 2zh\right) \\ \frac{\partial u_r}{\partial r} &= \frac{3\dot{h}}{h^3}\left(z^2 - hz\right) \\ \frac{\partial u_r}{\partial z} &= \frac{3r\dot{h}}{h^3}\left(2z - h\right) \end{aligned} \tag{5.41}$$

And:

$$\begin{aligned} u_r\frac{\partial u_r}{\partial r} &= \frac{3r\dot{h}}{h^3}\left(z^2 - hz\right)\frac{3\dot{h}}{h^3}\left(z^2 - hz\right) = \frac{9r\dot{h}^2}{h^6}\left(z^4 - 2hz^3 + h^2z^2\right) \\ u_z\frac{\partial u_r}{\partial z} &= -\frac{\dot{h}}{h^3}\left(2z^3 - 3hz^2\right)\frac{3r\dot{h}}{h^3}\left(2z - h\right) = \frac{-3r\dot{h}^2}{h^6}\left(4z^4 - 8hz^3 + 3h^2z^2\right) \end{aligned} \tag{5.42}$$

Substitute in the inertia terms:

$$\begin{aligned} &\frac{\partial u_r}{\partial t} + u_r\frac{\partial u_r}{\partial r} + u_z\frac{\partial u_r}{\partial z} = \\ &\qquad \frac{3r}{h^3}\left(z^2 - hz\right)\ddot{h} + \frac{3r\dot{h}^2}{h^4}\left(-3z^2 + 2zh\right) + \\ &\quad \frac{9r\dot{h}^2}{h^6}\left(z^4 - 2hz^3 + h^2z^2\right) + \frac{-3r\dot{h}^2}{h^6}\left(4z^4 - 8hz^3 + 3h^2z^2\right) = \\ &\frac{3r}{h^3}\left(z^2 - hz\right)\ddot{h} + r\dot{h}^2\left[\frac{-9z^2}{h^4} + \frac{6z}{h^3} + \frac{9z^4}{h^6} - \frac{18z^3}{h^5} + \frac{9z^2}{h^4} - \frac{12z^4}{h^6} + \frac{24z^3}{h^5} - \frac{9z^2}{h^4}\right] = \\ &\frac{3r}{h^3}\left(z^2 - hz\right)\ddot{h} + r\dot{h}^2\left[-\frac{3z^4}{h^6} + \frac{6z^3}{h^5} - \frac{9z^2}{h^4} + \frac{6z}{h^3}\right] \end{aligned} \tag{5.43}$$

So that equation 5.23 becomes:

$$\rho\left\{\frac{3r}{h^3}\left(z^2 - hz\right)\ddot{h} + r\dot{h}^2\left[-\frac{3z^4}{h^6} + \frac{6z^3}{h^5} - \frac{9z^2}{h^4} + \frac{6z}{h^3}\right]\right\} = -\frac{\partial p}{\partial r} + \mu\frac{\partial^2 u_r^*}{\partial z^2} \tag{5.44}$$

So the velocity u_r^* can be obtained from:

$$\frac{\partial^2 u_r^*}{\partial z^2} = \frac{1}{\mu}\left\{\frac{\partial p}{\partial r} + \rho\left\{\frac{3r}{h^3}\left(z^2 - hz\right)\ddot{h} + r\dot{h}^2\left[-\frac{3z^4}{h^6} + \frac{6z^3}{h^5} - \frac{9z^2}{h^4} + \frac{6z}{h^3}\right]\right\}\right\} \tag{5.45}$$

Or:

$$\begin{aligned}\frac{\partial u_r^*}{\partial z} = \frac{1}{\mu}\frac{\partial p}{\partial r}z + \frac{\rho}{\mu}\left\{\frac{3r}{h^3}\left(\frac{z^3}{3} - \frac{hz^2}{2}\right)\ddot{h} + \right. \\ \left. r\dot{h}^2\left[-\frac{3z^5}{5h^6} + \frac{6z^4}{4h^5} - \frac{9z^3}{3h^4} + \frac{6z^2}{2h^3}\right] + C_1\end{aligned} \tag{5.46}$$

Or:

$$\begin{aligned}u_r^* = \frac{1}{2\mu}\frac{\partial p}{\partial r}z^2 + \frac{\rho}{\mu}\left\{\frac{3r}{h^3}\left(\frac{z^4}{12} - \frac{hz^3}{6}\right)\ddot{h} + \right. \\ \left. r\dot{h}^2\left[-\frac{3z^6}{30h^6} + \frac{6z^5}{20h^5} - \frac{9z^4}{12h^4} + \frac{6z^3}{6h^3}\right] + C_1 z + C_2\end{aligned} \tag{5.47}$$

Integrate twice with the same boundary conditions as before to obtain the velocity:

$$\begin{aligned}&u_r^*(z=0) = 0 \\ &C_2 = 0 \\ &u_r^*(z=h) = 0 \\ &C_1 h = -\frac{1}{2\mu}\frac{\partial p}{\partial r}h^2 - \frac{\rho}{\mu}\left\{3r\left(\frac{h}{12} - \frac{h}{6}\right)\ddot{h} + r\dot{h}^2\left[-\frac{3}{30} + \frac{6}{20} - \frac{9}{12} + \frac{6}{6}\right]\right\} \\ &C_1 = -\frac{1}{2\mu}\frac{\partial p}{\partial r}h - \frac{\rho}{\mu}\left\{-\frac{1}{4}r\ddot{h} + \frac{9}{20h}r\dot{h}^2\right\}\end{aligned} \tag{5.48}$$

So the velocity is:

$$\begin{aligned}u_r^* = \\ \frac{1}{2\mu}\frac{\partial p}{\partial r}\left(z^2 - hz\right) + \\ \frac{\rho}{\mu}\left\{\frac{3r}{h^3}\left(\frac{z^4}{12} - \frac{hz^3}{6} + \frac{h^3 z}{12}\right)\ddot{h} + r\dot{h}^2\left[-\frac{3z^6}{30h^6} + \frac{6z^5}{20h^5} - \frac{9z^4}{12h^4} + \frac{6z^3}{6h^3} - \frac{9z}{20h}\right]\right\}\end{aligned} \tag{5.49}$$

Combine the continuity:

$$\frac{1}{r}\frac{\partial}{\partial r}\left(ru_r\right) + \frac{\partial u_z}{\partial z} = 0 \tag{5.50}$$

Integrate with respect to z knowing that:

$$\begin{aligned}u_z(z=0) = 0 \\ u_z(z=h) = \dot{h}\end{aligned} \tag{5.51}$$

To obtain:

$$\int_0^h \frac{\partial}{\partial r}\left(ru_r\right)dz = r\dot{h} \tag{5.52}$$

Where the left hand term can be expanded to:

$$\int_0^h \frac{\partial}{\partial r}\left(r\left[\frac{1}{2\mu}\frac{\partial p}{\partial r}\left(z^2-hz\right)+\frac{\rho}{\mu}\left\{\begin{array}{l}\frac{3r}{h^3}\left(\frac{z^4}{12}-\frac{hz^3}{6}+\frac{h^3z}{12}\right)\ddot{h}+\\ r\dot{h}^2\left[-\frac{3z^6}{30h^6}+\frac{6z^5}{20h^5}-\frac{9z^4}{12h^4}+\frac{6z^3}{6h^3}-\frac{9z}{20h}\right]\end{array}\right\}\right]\right)dz$$
$$\frac{\partial}{\partial r}\left(r\left[\frac{1}{2\mu}\frac{\partial p}{\partial r}\left(\frac{z^3}{3}-\frac{hz^2}{2}\right)+\frac{\rho}{\mu}\left\{\begin{array}{l}\frac{3r}{h^3}\left(\frac{z^5}{60}-\frac{hz^4}{24}+\frac{h^3z^2}{24}\right)\ddot{h}+\\ r\dot{h}^2\left[-\frac{3z^7}{210h^6}+\frac{6z^6}{120h^5}-\frac{9z^5}{60h^4}+\frac{6z^4}{24h^3}-\frac{9z^2}{40h}\right]\end{array}\right\}\right]\right)_0^h \tag{5.53}$$

So the continuity becomes:

$$\frac{\partial}{\partial r}\left(r\left[\frac{1}{12\mu}\frac{\partial p}{\partial r}h^3+\frac{\rho}{\mu}\left\{\frac{rh^2\ddot{h}}{20}-\frac{5rh\dot{h}^2}{56}\right\}\right]\right)=r\dot{h} \tag{5.54}$$

Or:

$$r\left[\frac{1}{12\mu}\frac{\partial p}{\partial r}h^3+\frac{\rho}{\mu}\left\{\frac{rh^2\ddot{h}}{20}-\frac{5rh\dot{h}^2}{56}\right\}\right]=\frac{r^2\dot{h}}{2} \tag{5.55}$$

And for the pressure gradient one can see that:

$$\frac{\partial p}{\partial r}=\frac{6\mu r\dot{h}}{h^3}-\rho\left\{\frac{12r\ddot{h}}{20h}-\frac{60r\dot{h}^2}{56h^2}\right\} \tag{5.56}$$

So the pressure is given by:

$$p=\frac{3\mu r^2\dot{h}}{h^3}-\rho\left\{\frac{6r^2\ddot{h}}{20h}-\frac{30r^2\dot{h}^2}{56h^2}\right\}+C_1r+C_2 \tag{5.57}$$

With the boundary conditions:

$$\begin{array}{l}\frac{\partial p}{\partial r}\left(r=0\right)=0\\ p\left(r=R\right)=0\end{array} \tag{5.58}$$

To obtain the pressure:

$$p=\left(\frac{3\mu\dot{h}}{h^3}+\rho\left\{\frac{3\ddot{h}}{10h}-\frac{15\dot{h}^2}{28h^2}\right\}\right)\left(R^2-r^2\right) \tag{5.59}$$

The presence of inertia effects are clear. Integration of the pressure over the area yields the resulting force:

$$F=\left(\frac{3\mu\dot{h}}{h^3}+\rho\left\{\frac{3\ddot{h}}{10h}-\frac{15\dot{h}^2}{28h^2}\right\}\right)2\pi\frac{R^4}{4} \tag{5.60}$$

Compare the results of the corrected model with the Reynolds equation and the FlowVision simulation:

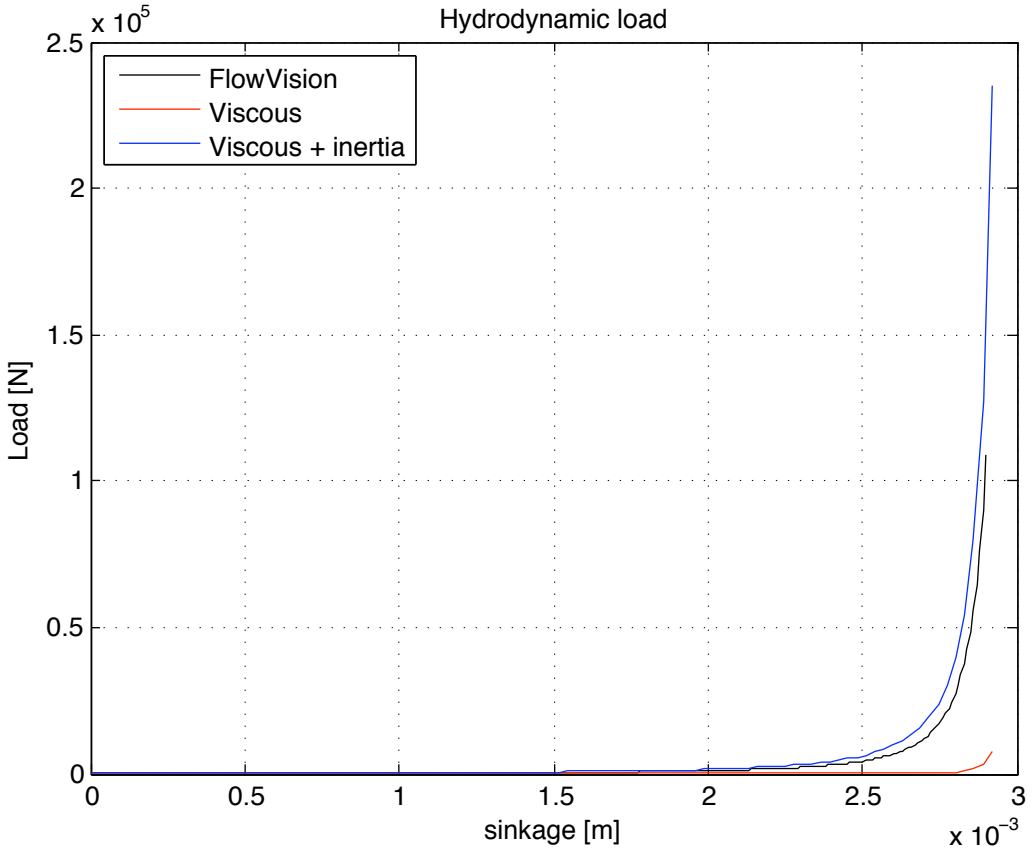

Figure 5.5: Comparison of FlowVision, Reynolds and corrected Reynolds

Clearly already a single update of the pressure profile yields a more accurate solution and can be a good strategy when inertia has substantial influence.

5.1.2. sliding or rolling problems

In the previous section we have seen a pure squeeze problem where inertia was playing an important role and how it was taken into account by an iterative method. However in rolling and sliding problems inertia effects can also be taken into account. To take the inertial effects into account generally 2 approaches are used: the iterative method and the average method. Examples are found in Pinkus and Sternlicht [23] for 1D. This is expanded to a 2D approach where a combination of iterative and averaged is used.

1D iterative method The iterative method for sliding or rolling in 1D is similar to what has been done for squeeze, start with the regular solution of the Reynolds equation:

$$0 = -\frac{\partial p_v}{\partial x} + \mu \frac{\partial^2 u_v}{\partial z^2} \tag{5.61}$$

Where p_v and u_v are the solutions of the pure viscous equations. From continuity it's easily possible to determine w_v since for 1D problems this is reduced to:

$$\frac{\partial u}{\partial x} + \frac{\partial w}{\partial z} = 0 \tag{5.62}$$

Now re-insert the viscous solution in the Navier Stokes equations including the inertia terms:

$$\rho \left(u_v \frac{\partial u_v}{\partial x} + w_v \frac{\partial u_v}{\partial z} \right) = -\frac{\partial p_c}{\partial x} + \mu \frac{\partial^2 u_c}{\partial z^2} \tag{5.63}$$

Where p_c and u_c are the solutions of the inertia corrected equations, which can be explicitly evaluated for given boundary conditions.

1D averaged method The average method, again in 1D, assumes that due to the thin film the inertia cannot vary a lot across the film thickness so the Reynolds equation can be written as:

$$\rho \left(\frac{1}{h} \int_0^h \left(u \frac{\partial u}{\partial x} + w \frac{\partial u}{\partial z} \right) dz \right) = -\frac{\partial p}{\partial x} + \mu \frac{\partial^2 u}{\partial z^2} \tag{5.64}$$

The left hand side of equation 5.64 after integration is a function of x alone and the expression can be integrated with respect to z as before. Such that the velocity profile becomes:

$$u = \frac{1}{2} f(x) z^2 + C_1(x) z + C_2(x) \tag{5.65}$$

From continuity in 1D 5.62:

$$w = -\int \frac{\partial u}{\partial x} dz \tag{5.66}$$

or:

$$w = -\left[\frac{1}{6} \frac{df(x)}{dx} z^3 + \frac{dC_1(x)}{dx} \frac{z^2}{2} + \frac{dC_2(x)}{dx} z \right] + C_3(x) \tag{5.67}$$

For example, take as boundary conditions:

$$\begin{aligned} u(z=0) &= 0 \\ w(z=0) &= 0 \\ u(z=h) &= U \\ w(z=h) &= W \end{aligned} \tag{5.68}$$

Using the first three conditions one can obtain:

$$\begin{aligned} u &= \tfrac{1}{2} f(x) (z^2 - hz) + \tfrac{Uz}{h} \\ w &= -\left\{ \tfrac{1}{6} \tfrac{df(x)}{dx} z^3 + \tfrac{d}{dx} \left[\tfrac{U}{h} - \tfrac{1}{2} f(x) h \right] \tfrac{z^2}{2} \right\} \end{aligned} \tag{5.69}$$

The last boundary conditions allows one to solve for $f(x)$:

$$f(x) = \frac{12}{h^3}\int W dx + \frac{6}{h^3}\int h^2 d\left(\frac{U}{h}\right) + \frac{C_4}{h^3} \tag{5.70}$$

To end up with $\frac{dp}{dx}$:

$$\frac{dp}{dx} = \mu f(x) + \rho\left[\begin{array}{l} -\frac{1}{6}U\frac{dU}{dx} - \frac{1}{5}hf(x)W + \frac{1}{6}\frac{U^2}{h}\frac{dh}{dx} - \frac{1}{60}f(x)\frac{dU}{dx}h^2 \\ +\frac{1}{10}f(x)Uh\frac{dh}{dx} + \frac{1}{120}f^2(x)h^3\frac{dh}{dx} \end{array}\right] \tag{5.71}$$

Which can be evaluated if U, W and h are known. As trivial as this is in 1D, in 2D a more complicated approach is needed, which is explained in the next section.

2D inertia correction In the case of the 2D Reynolds equation there is not a direct substitution possible via the continuity equation to directly determine the pressure with an inertia correction, it is however possible to apply both methods simultaneously, i.e. to iterate and to average, to obtain a correction on the pressure and velocity profile. While retaining the thin film assumption the set of equations to solve starts with the Reynolds equation as seen before:

$$\begin{aligned} 0 &= -\frac{\partial p}{\partial x} + \mu\frac{\partial^2 u}{\partial x^2} \\ 0 &= -\frac{\partial p}{\partial y} + \mu\frac{\partial^2 v}{\partial y^2} \\ \frac{\partial p}{\partial z} &= 0 \end{aligned} \tag{5.72}$$

The pressure profile can now be determined, as well as the velocity profile 5.13, and the new velocity profile can be obtained from:

$$\begin{aligned} \rho\left(\frac{1}{h}\int_0^h \frac{Du}{Dt}dz\right) &= -\frac{\partial p}{\partial x} + \mu\frac{\partial^2 u^*}{\partial x^2} \\ \rho\left(\frac{1}{h}\int_0^h \frac{Dv}{Dt}dz\right) &= -\frac{\partial p}{\partial y} + \mu\frac{\partial^2 v^*}{\partial y^2} \\ \frac{\partial p}{\partial z} &= 0 \end{aligned} \tag{5.73}$$

The new velocity profiles then take the following form:

$$\begin{aligned} u^* &= \frac{1}{2\mu}\left[\rho\left(\frac{1}{h}\int_0^h \frac{Du}{Dt}dz\right) + \frac{\partial p}{\partial x}\right]\left(z^2 - hz\right) + \frac{U_2 - U_1}{h}z + U_1 \\ v^* &= \frac{1}{2\mu}\left[\rho\left(\frac{1}{h}\int_0^h \frac{Dv}{Dt}dz\right) + \frac{\partial p}{\partial y}\right]\left(z^2 - hz\right) + \frac{V_2 - V_1}{h}z + V_1 \end{aligned} \tag{5.74}$$

The volume flow is given by:

$$\begin{aligned} q_x &= \int_0^h u^* dz \\ q_y &= \int_0^h v^* dz \end{aligned} \tag{5.75}$$

From continuity one can obtain the Reynolds equation in 2D with an inertia correction:

$$\frac{\partial q_x}{\partial x} + \frac{\partial q_y}{\partial y} + \frac{\partial h}{\partial t} = 0 \tag{5.76}$$

The updated Reynolds equation can be written as:

$$\begin{aligned} &\frac{\partial}{\partial x}\left(\frac{h^3}{12\mu}\frac{\partial p}{\partial x}\right) + \frac{\partial}{\partial y}\left(\frac{h^3}{12\mu}\frac{\partial p}{\partial y}\right) = -\frac{\partial}{\partial x}\left(\frac{\rho h^2}{12\mu}\int_0^h \frac{Du}{Dt}dz\right) - \frac{\partial}{\partial y}\left(\frac{\rho h^2}{12\mu}\int_0^h \frac{Dv}{Dt}dz\right) \\ &+\frac{U_1+U_2}{2}\frac{\partial h}{\partial x} + +\frac{V_1+V_2}{2}\frac{\partial h}{\partial y} + \frac{h}{2}\frac{\partial}{\partial x}\left(U_1+U_2\right) + \frac{h}{2}\frac{\partial}{\partial y}\left(V_1+V_2\right) + \frac{\partial h}{\partial t} \end{aligned} \tag{5.77}$$

Next step is to evaluate the integrals:

$$\int_0^h \frac{Du}{Dt}dz = \int_0^h \left\{\frac{\partial u}{\partial t} + u\frac{\partial u}{\partial x} + v\frac{\partial u}{\partial y} + w\frac{\partial u}{\partial z}\right\} dz \tag{5.78}$$

In steady state the time derivatives drop out, evaluating the other terms one by one, using the velocity profile from 5.13:

$$\begin{aligned} &\int_0^h u\frac{\partial u}{\partial x}dz = \frac{\frac{\partial p}{\partial x}\frac{\partial^2 p}{\partial x^2}h^5}{120\mu^2} + \frac{\left(\frac{\partial p}{\partial x}\right)^2\frac{\partial h}{\partial x}h^4}{48\mu^2} - \frac{\frac{\partial^2 p}{\partial x^2}\left(3U_1+U_2\right)h^3}{24\mu} - \\ &\frac{\frac{\partial p}{\partial x}\frac{\partial h}{\partial x}\left(3U_1+U_2\right)h^2}{8\mu} - \frac{\partial h}{\partial x}\left(\frac{5}{6}U_1^2 + \frac{7}{6}U_1U_2 + \frac{1}{3}U_2^2\right) \end{aligned} \tag{5.79}$$

And:

$$\begin{aligned} &\int_0^h v\frac{\partial u}{\partial y}dz = \frac{\frac{\partial p}{\partial y}\frac{\partial^2 p}{\partial y^2}h^5}{120\mu^2} + \frac{\frac{\partial p}{\partial y}\frac{\partial p}{\partial x}\frac{\partial h}{\partial y}h^4}{48\mu^2} - \frac{\frac{\partial^2 p}{\partial y \partial x}\left(3V_1+V_2\right)h^3}{24\mu} + \\ &\frac{\frac{\partial p}{\partial y}\frac{\partial h}{\partial y}\left(V_1+V_2\right)h^2}{24\mu} - \frac{\frac{\partial p}{\partial x}\frac{\partial h}{\partial y}\left(5V_1+2V_2\right)h^2}{12\mu} + \\ &\frac{\partial h}{\partial y}\left(-\frac{5}{6}V_1U_1 - \frac{5}{6}V_1U_2 - \frac{1}{3}V_2U_1 - \frac{1}{2}V_2U_2\right) \end{aligned} \tag{5.80}$$

And:

$$\begin{aligned}\int_0^h w\frac{\partial u}{\partial z}dz = [w\cdot u]_0^h - \int_0^h \frac{\partial w}{\partial z}udz = \\ -\int_0^h \left[-\frac{\partial u}{\partial x} - \frac{\partial v}{\partial y}\right]udz = \int_0^h u\frac{\partial u}{\partial x}dz + \int_0^h u\frac{\partial v}{\partial y}dz\end{aligned} \tag{5.81}$$

Where the first term matches with what we have seen before and the second term can be developed into:

$$\begin{aligned}\int_0^h u\frac{\partial v}{\partial y}dz = \frac{\frac{\partial p}{\partial x}\frac{\partial^2 p}{\partial y^2}h^5}{120\mu^2} + \frac{\frac{\partial p}{\partial x}\frac{\partial p}{\partial y}\frac{\partial h}{\partial y}h^4}{48\mu^2} - \frac{\frac{\partial^2 p}{\partial y^2}\left(3U_1+U_2\right)h^3}{24\mu} + \frac{\frac{\partial p}{\partial x}\frac{\partial h}{\partial y}\left(V_1+V_2\right)h^2}{24\mu} \\ -\frac{\frac{\partial p}{\partial y}\frac{\partial h}{\partial y}\left(5U_1+2U_2\right)}{12\mu} + \frac{\partial h}{\partial y}\left(-\frac{5}{6}U_1V_1 - \frac{5}{6}U_1V_2 - \frac{1}{3}U_2V_1 - \frac{1}{3}U_2V_2\right)\end{aligned} \tag{5.82}$$

In a similar manner for the update of velocity v:

$$\int_0^h \frac{Dv}{Dt}dz = \int_0^h \left[\frac{\partial v}{\partial t} + u\frac{\partial v}{\partial x} + v\frac{\partial v}{\partial y} + w\frac{\partial v}{\partial z}\right]dz \tag{5.83}$$

In steady state the time derivatives drop out, evaluating the other terms one by one:

$$\begin{aligned}\int_0^h u\frac{\partial v}{\partial x}dz = \frac{\frac{\partial p}{\partial x}\frac{\partial^2 p}{\partial y\partial x}h^5}{120\mu^2} + \frac{\frac{\partial p}{\partial x}\frac{\partial p}{\partial y}\frac{\partial h}{\partial x}h^4}{48\mu^2} - \frac{\frac{\partial^2 p}{\partial y\partial x}\left(3U_1+U_2\right)h^3}{24\mu} + \\ \frac{\frac{\partial p}{\partial x}\frac{\partial h}{\partial x}\left(V_1+V_2\right)h^2}{24\mu} - \frac{\frac{\partial p}{\partial y}\frac{\partial h}{\partial x}\left(5U_1+2U_2\right)h^2}{24\mu} + \frac{\partial h}{\partial x}\left(-\frac{5}{6}U_1V_1 - \frac{5}{6}U_1V_2 - \frac{1}{3}U_2V_1 - \frac{1}{3}U_2V_2\right)\end{aligned} \tag{5.84}$$

And:

$$\begin{aligned}\int_0^h v\frac{\partial v}{\partial y}dz = \frac{\frac{\partial p}{\partial y}\frac{\partial^2 p}{\partial y^2}h^5}{120\mu^2} + \frac{\left(\frac{\partial p}{\partial y}\right)^2\frac{\partial h}{\partial y}h^4}{48\mu^2} - \frac{\frac{\partial^2 p}{\partial y^2}\left(3V_1+V_2\right)h^3}{24\mu} + \\ \frac{\frac{\partial p}{\partial y}\frac{\partial h}{\partial y}\left(3V_1+V_2\right)h^2}{8\mu} - \frac{\partial h}{\partial y}\left(\frac{5}{6}V_1^2 + \frac{7}{6}V_1V_2 + \frac{1}{2}V_2^2\right)\end{aligned} \tag{5.85}$$

And:

$$\int_0^h w\frac{\partial v}{\partial z}dz = [w\cdot v]_0^h - \int_0^h \frac{\partial w}{\partial z}vdz = -\int_0^h \left(-\frac{\partial u}{\partial x} - \frac{\partial v}{\partial y}\right)vdz \tag{5.86}$$

Where the first term matches with what we have seen before and the second term can be developed into:

$$\int_0^h \left(\frac{\partial u}{\partial x}\right) v dz = \frac{\frac{\partial p}{\partial y}\frac{\partial^2 p}{\partial x^2}h^5}{120\mu^2} + \frac{\frac{\partial p}{\partial y}\frac{\partial p}{\partial x}\frac{\partial h}{\partial x}h^4}{48\mu^2} - \frac{\frac{\partial^2 p}{\partial x^2}\left(3V_1+V_2\right)h^3}{24\mu} + \frac{\frac{\partial p}{\partial y}\frac{\partial h}{\partial x}\left(U_1+U_2\right)h^2}{24\mu} - \frac{\frac{\partial p}{\partial x}\frac{\partial h}{\partial x}\left(5V_1+2V_2\right)h^2}{24\mu} + \frac{\partial h}{\partial x}\left(-\frac{5}{6}V_1U_1 - \frac{5}{6}V_1U_2 - \frac{1}{3}V_2U_1 - \frac{1}{3}V_2U_2\right) \tag{5.87}$$

So now an inertia correction is possible in 2D sliding or rolling problems. The scheme is as follows:

- Solve the Reynolds equation 5.72
- Determine the velocity profile 5.74
- Add the average inertia terms to the Reynolds equation 5.77
- Solve the modified Reynolds equation 5.77

As seen before the inertia effects are not present in the Reynolds equation, it is however possible to include them in an iterative method in squeeze. In a 1D sliding or rolling situation an iterative and averaged method is a possibility to incorporate inertia effects. In 2D rolling or sliding it is less trivial but a novel method using an iteration and an averaging step has been introduced and inertia effects can be taken into account. The next step is to look at the effects in the inlet which will be examined in the next section.

5.2. Inlet condition

In case of a wheel rolling on a surface, with the effects of a bow wave occurring an inlet condition have to be taken into account. See figure for what is seen as the inlet, indicated with the yellow circle:

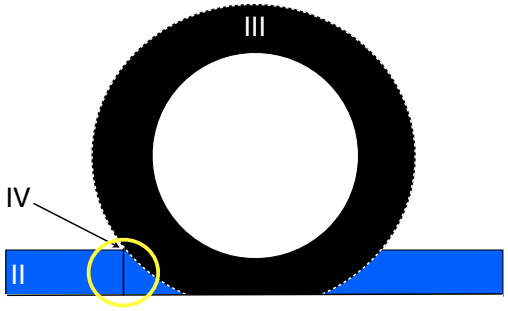

- Section II: Fluid dynamics: Lubrication theory
  - Navier Stokes
  - **Reynolds**
    - Inertia in the fluid film
    - **Inertia in the inlet**
    - Fill rate
- Section III: Solid Mechanics: Tire modelling
  - Linear elastic half space model
  - Hyper elastic finite element model
- Section IV: Fluid Structure Interaction
  - Classical staggering
  - Interface Quasi Newton method
  - Coupling ABAQUS to Matlab

Here three different models have been developed, a simple stagnation pressure at the inlet, a stagnation pressure with an iterative momentum correction and a stagnation pressure with an energy correction. These models will be described in the subsequent sections.

5.2.1. Inlet condition with stagnation pressure

The inlet condition with stagnation pressure is simply putting the pressure at the inlet equal to the dynamic pressure for the Bernoulli equation:

$$p = \frac{1}{2}\rho v^2 \tag{5.88}$$

The point of application of the inlet pressure is a priori unknown as the wetted length of the tire is unknown. As a first assumption the point of application is chosen at the contact between tire and the water layer thickness. It is to be expected that this approximation of the inlet condition gives an overestimation of the pressure as it is assumed that the fluid velocity is zero where in fact there is fluid the flowing in the direction of the footprint, to the sides and possibly upwards as a bow wave. Therefore subsequent methods have been developed to deal with the fact that this approximation is adding energy and/or momentum.

5.2.2. Inlet condition with energy correction

An iterative scheme using the Bernoulli equation and the energy equation is used to determine the inlet pressure. Next to that, as before, the point of application of the inlet pressure is a priori unknown as the wetted length of the tire is unknown. As a first

assumption the point of application is chosen at the contact between tire and the water layer thickness.

The scheme to determine the inlet pressure profile is:

- Solve Bernoulli for first approximation of pressure
- Determine velocity profile from given inlet pressure
- Update the pressure

Which in practice goes as follows, starting with Bernoulli:

$$p + \frac{1}{2}\rho v^2 + gz = constant \tag{5.89}$$

Next, neglect the gravity as the water layer is very thin and assume the pressure in the far flow to be zero. So the inlet pressure becomes:

$$p = \frac{1}{2}\rho v^2 \tag{5.90}$$

Where the velocity is equal to the vehicle velocity. Next, solve the Reynolds equation to determine the pressure distribution in the leading edge of the wheel and consequently the velocity profile. The velocity profile is given by:

$$u = \frac{1}{2\eta}\frac{\partial p}{\partial x}\left(z^2 - hz\right) + \frac{U_2 - U_1}{h}z + U_1 \tag{5.91}$$

Next the energy equation comes into play, start with the first law of thermodynamics:

$$\frac{dQ}{dt} - \frac{dW}{dt} = \frac{dE}{dt} \tag{5.92}$$

Where W is work done by the system, Q is heat added to the system and E denotes the energy. Next, apply Reynolds' transport theorem to write for a fixed control volume Ω:

$$\frac{DE}{Dt} = \frac{\partial}{\partial t}\left(\int_{\Omega} e\rho dV\right) + \int_{d\Omega} e\rho\left(\mathbf{V}\cdot\mathbf{n}\right)dA \tag{5.93}$$

The energy per unit mass (e) consists of: internal energy, kinetic energy, potential energy and other energy sources such as chemical energy, electrostatic or magnetic field effects. For this application the other sources are neglected. The internal, kinetic and potential energy are the written as:

$$e = \hat{u} + \frac{1}{2}v^2 + gz \tag{5.94}$$

The work terms can be written as: shaft work ($\dot{W}_s$), viscous work ($\dot{W}_v$) and pressure work $\dot{W}_p$). $The pressure work occurs only on the control surface and is equal to the pressure on a surface e$

$$\dot{W}_p = \int_{d\Omega} p\left(\mathbf{V}\cdot\mathbf{n}\right)dA \tag{5.95}$$

The work done by the viscous stresses at the control surface is the inner product of the stresses and the velocity.

$$\dot{W}_\eta = -\int_{d\Omega} \tau \cdot \mathbf{V} dA \tag{5.96}$$

To summarize the work done is given by:

$$\dot{W} = \dot{W}_s + \int_{\partial\Omega} p\,(\mathbf{V} \cdot \mathbf{n}) dA - \int_{\partial\Omega} (\tau \cdot \mathbf{V}) dA \tag{5.97}$$

So the total energy equation becomes:

$$\dot{Q} - \dot{W}_s - \dot{W}_v = \frac{\partial}{\partial t}\left(\int_\Omega \left[\hat{u} + \frac{1}{2}v^2 + gz\right]\rho dV\right) + \int_{\partial\Omega}\left[\hat{u} + \frac{1}{2}v^2 + gz + \frac{p}{\rho}\right]\rho\,(\mathbf{V}\cdot\mathbf{n})\,dA \tag{5.98}$$

In the present case of the Grosch wheel the heat transfer is neglected and there is no shaft work. The current simulation is steady state so the time derivative terms are zero. In the last boundary integral the effect due to gravity is neglected and the internal energy drops out of the equation.

For the work of the viscous stresses there are several cases; When the control surface is a fixed wall where the no-slip condition applies the work done by the viscous stresses is zero. At an inlet or outlet the flow is approximately perpendicular to the inlet or outlet and the viscous work comes only from the normal stresses which are extremely small in this case and will therefore be neglected.

The resulting equation to update the inlet pressure is then given by:

$$\int_{\partial\Omega} p\,(\mathbf{V}\cdot\mathbf{n})\,dA + \int_{\partial\Omega} \frac{1}{2}v^2\rho\,(\mathbf{V}\cdot\mathbf{n})\,dA = 0 \tag{5.99}$$

Applying this to the following control volume:

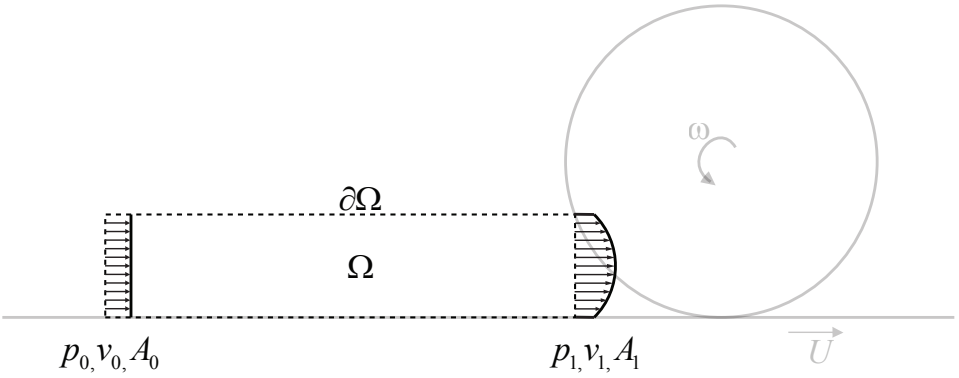

Figure 5.6: Control volume for inlet condition

With the uniform velocity on the inlet of the control volume and the parabolic pressure profile on the outlet, this gives the update:

$$p_1 \int_{A_1} v_1 dA - p_0 v_0 A_0 + \frac{1}{2}\rho \left[\int_{A_1} v_1^3 dA - \int_{A_0} v_0^3 dA \right] = 0 \tag{5.100}$$

Where v_0 is the uniform velocity at the inlet of the control volume, p_0 is the pressure in the far field, equal to zero, v_1 is given by:

$$v_1 = \frac{1}{2\mu}\frac{\partial p}{\partial x}\left(z^2 - hz\right) + \frac{U_1 + U_2}{h} z + U_1 \tag{5.101}$$

The pressure update is then found by:

$$p_1 = \frac{\frac{1}{2}\rho \left[v_0^3 A - \int_{A_1} v_1^3 dA \right]}{\int_{A_1} v_1 dA} \tag{5.102}$$

Which can be evaluated to:

$$
\begin{aligned}
p_1 &= \frac{-3}{140}\begin{pmatrix} 140v_0^3 + C_1^3h^6 - 7C_1^2C_2h^5 + \left(21C_1C_2^2 - 14C_1^2C_3\right)h^4 \\ +70C_1C_2C_3h^3 - 35C_2^2h^3 + \left(70C_1C_3^2 - 140C_2^2C_3\right)h^2 \\ -210C_2C_3^2h - 140C_3^3 \end{pmatrix} \\
C_1 &= \frac{1}{2\mu}\frac{\partial p}{\partial x} \\
C_2 &= \frac{U_2 - U_1}{h} \\
C_3 &= U_1
\end{aligned}
\tag{5.103}
$$

To determine the pressure at the inlet the following iteration scheme is used:

- Assume stagnation at the inlet: $v_1^0 = 0$ (the upper index indicates the iterate)
- Determine initial inlet pressure, $p_1^0 = \frac{1}{2}\rho v^2$
- Solve the pressure profile using Reynolds equation
- Determine the velocity profile
- Determine the new inlet pressure, p_1^1 from 5.103
- Iterate equation 5.103 until $p_1^{i+1} - p_1^i < \epsilon$

Where ϵ indicates the convergence criterion. In applying this scheme divergence sometimes occurs and a scheme using successive under-relaxation is a possible solution.

5.2.3. Inlet condition with momentum correction

To determine the inlet pressure the Bernoulli equation is used with the following assumptions:

- The far field velocity profile is uniform
- The velocity profile in the inlet is according to the Reynolds equation, thus a combination of Poisseuille and Couette flow.

The point of application of the inlet pressure is chosen to be at the point where the water layer first contacts the wheel.

Next, the Bernoulli equation is applied along the streamlines of the flow with an averaging of the velocity profile along the height of the flow in the inlet:

$$
p_0 + \frac{1}{2}\rho v_0^2 = p_1 + \frac{1}{h}\int_0^h \frac{1}{2}\rho v_1^2 dz \tag{5.104}
$$

Where:

- p_0 is the far field pressure
- p_1 is the inlet pressure
- v_0 is the far field uniform velocity
- v_1 is the velocity profile in the inlet, given by the Reynolds equation, i.e.:
  - $$v_1 = \sqrt{u^2 + v^2}$$
  - $$u = \frac{1}{2\eta}\frac{\partial p}{\partial x}\left(z^2 - hz\right) + \frac{U_2 - U_1}{h}z + U_1$$
  - $$v = \frac{1}{2\eta}\frac{\partial p}{\partial y}\left(z^2 - hz\right) + \frac{V_2 - V_1}{h}z + V_1$$

The integration over the height yields the following inlet pressure:

$$p_1 = p_0 + \frac{1}{2}\rho v_0^2 - \frac{1}{2}\rho \begin{pmatrix} \frac{1}{5}\left(C_1^2 + C_4^2\right)h^4 + \\ \frac{1}{2}\left(\left(-C_4 h + C_5\right)C_4 + \left(-C_1 h + C_2\right)C_1\right)h^3 + \\ \frac{1}{3}\left(2C_6 C_4 + \left(-C_4 h + C_5\right)^2 + 2C_3 C_1 + \left(-C_1 h + C_2\right)^2\right)h^2 + \\ \left(C_6\left(-C_4 h + C_5\right) + C_3\left(-C_1 h + C_2\right)\right)h \\ \frac{1}{2}\left(C_3^2 + C_6^2\right) \end{pmatrix} \tag{5.105}$$

Where:

$$\begin{aligned} C_1 &= \tfrac{1}{2\eta}\tfrac{\partial p}{\partial x} \\ C_2 &= \tfrac{U_2 - U_1}{h} \\ C_3 &= U_1 \\ C_4 &= \tfrac{1}{2\eta}\tfrac{\partial p}{\partial y} \\ C_5 &= \tfrac{V_2 - V_1}{h} \\ C_6 &= V_1 \end{aligned} \tag{5.106}$$

To determine the inlet pressure the following iteration scheme is used:

- Assume stagnation at the inlet: $v_1^0 = 0$ (the upper index indicates the iterate)
- Determine initial inlet pressure, $p_1^0 = \frac{1}{2}\rho v^2$
- Determine the pressure and velocity profile at the inlet according to the Reynolds equation, v_1^1
- Determine the new inlet pressure, p_1^1 from 5.105
- Iterate equation 5.105 until $p_1^{i+1} - p_1^i < \epsilon$

Where ϵ indicates the convergence criterion. In applying this scheme divergence sometimes occurs and a scheme using successive under-relaxation is a possible solution.

It is now possible to take the effects at the inlet into account, by a rather crude approximation assuming stagnation of the fluid at the inlet. This can be corrected by iteration of either an energy scheme or a momentum scheme as outlined. With these methods the effect of inertia is most likely overestimated but for a design tool this is deemed appropriate.

The different models have been implemented in Matlab in a finite element model, found in appendix B.

5.3. Fill rate model

Since the previously outlined models assumed fully flooded conditions an extension is needed to deal with starved lubrication where not the entire wheel is flooded with water, as is usually the case of a tire rolling on a wet road. A cavitation model is applied that allows the calculation of the position of the inlet which in essence is a reformation boundary. A reformation boundary is a boundary where the transition from cavitated to full film occurs. See figure:

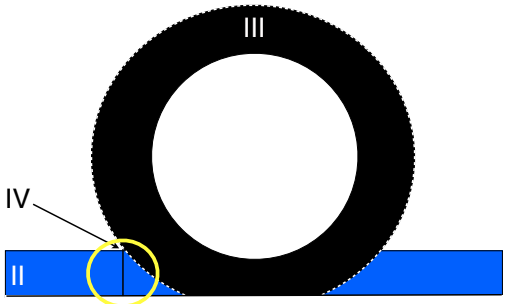

- Section II: Fluid dynamics: Lubrication theory
  - Navier Stokes
  - **Reynolds**
    - Inertia in the fluid film
    - Inertia in the inlet
    - **Fill rate**
- Section III: Solid Mechanics: Tire modelling
  - Linear elastic half space model
  - Hyper elastic finite element model
- Section IV: Fluid Structure Interaction
  - Classical staggering
  - Interface Quasi Newton method
  - Coupling ABAQUS to Matlab

The model adapted here has been developed from a cavitation model [24] and introduces the new variable, the film fraction: f. In the full film area the film fraction is equal to one such that the Reynolds equation as before appears. Assume the Reynolds equation takes the following form:

$$\nabla \cdot \left(\frac{-h^3}{12\mu} f \nabla p + \bar{U} h f \right) = 0 \tag{5.107}$$

Apply a variable transformation, introducing a new variable ξ, where in the full film area:

$$p = \xi \tag{5.108}$$

And in the cavitated area, the film fraction is given by:

$$f = 1 + c_f \xi \tag{5.109}$$

Where c_f is to be determined from continuity on the reformation boundary. Write the expressions using a boolean operator between parentheses:

$$p = (\xi \geq 0)\, \xi \tag{5.110}$$

$$f = 1 + (\xi < 0)\, c_f \xi \tag{5.111}$$

The Reynolds equation becomes:

$$\nabla \cdot \left(\frac{-h^3}{12\mu} (\xi \geq 0) \left(1 + (\xi < 0)\, c_f \xi\right) \nabla \xi + \bar{U} h \left(1 + (\xi < 0)\, c_f \xi\right) \right) = 0 \tag{5.112}$$

Since for the boolean operator one knows that: $(\xi \geq 0)(\xi < 0) = 0$:

$$\nabla \cdot \left(\frac{-h^3}{12\mu} (\xi \geq 0) \nabla \xi + \bar{U} h (1 + (\xi < 0) c_f \xi) \right) = 0 \tag{5.113}$$

Now it is clear that this equation holds for both the full film and cavitated area, assuming that the fluid flow through the cavitated area is equal to $\bar{U}$. To determine c_f apply mass conservation on the reformation boundary:

$$\bar{U} h (1 + c_f \xi) = -\frac{h^3}{12\mu} \frac{\partial \xi}{\partial x} + \bar{U} h \tag{5.114}$$

Discretize this equation using a finite difference, assuming that the reformation boundary is somewhere between point i (cavitated: $\xi_i \leq 0$) and i + 1 (full film: $\xi_{i+1} \geq 0$):

$$\bar{U} h c_f \xi_i = -\frac{h^3}{12\mu} \frac{\xi_{i+1} - \xi_i}{\Delta x} \tag{5.115}$$

Where Δx indicates the mesh size of the discretization. To obtain for c_f:

$$c_f = \frac{h^2}{12\mu\bar{U}} \frac{\left(1 - \frac{\xi_{i+1}}{\xi_i}\right)}{\Delta x} \tag{5.116}$$

Which can be witten as:

$$c_f = \frac{h^2}{12\mu\bar{U}} \frac{1 + \varepsilon}{\Delta x} \tag{5.117}$$

Using $\varepsilon = -\frac{\xi_{i+1}}{\xi_i}$. According to numerical simulations [24] the optimal value for ϵ is 1 such that one obtains:

$$c_f = \frac{h^2}{6\mu\bar{U}\Delta x} \tag{5.118}$$

Knowing c_f the model can be implemented in a finite element code, however also the boundary conditions change as in this case the boundary condition is not given by a pressure but by variable ξ, the boundary condition can be determined from the fill rate:

$$f = \frac{h_0}{h} = 1 + \frac{h^2}{6\mu\bar{U}\Delta x} \xi \tag{5.119}$$

Where h_0 is the fluid film thickness far in front of the wheel, such that the value for ξ on the boundary becomes:

$$\xi = \left(\frac{h_0}{h} - 1 \right) \frac{h^2}{6\mu\Delta x\bar{U}} \tag{5.120}$$

As mentioned the equation can be implemented in a finite element model, however, in the cavitated area one is now confronted with the transport dominated terms. Commonly this results in wiggles in the solution due to the convective terms. These can be stabilized by adding anisotropic artificial diffusion in the direction of the fluid velocity vector $\bar{U}$ is added to the diffusion part of general Reynolds equation:

$$\nabla\left(\frac{-h^3}{12\mu}\left(\left(\xi\geq 0\right)+\alpha_{ad}\alpha_{cf}\left(\xi\leq 0\right)\left[\begin{array}{cc}\frac{U_x}{U} & 0\\ 0 & \frac{U_y}{U}\end{array}\right]\right)\right)\nabla\xi+ \\ Uh\left(1+\left(\xi\leq 0\right)c_f\xi\right)=0 \tag{5.121}$$

This directional anisotropic diffusion is mathematically not correctly implemented. Better would be to start with diffusion in the convection direction, and then rotate it to the global coordinate system. However, this formulation gives more stable numerical results. This equation can be implemented in a finite element model using $\alpha_{ad}=1$ and $\alpha_{c_f}=1$ for linear elements and $\alpha_{ad}=0.5$ for quadratic elements. Alternatively stream upwinding could be used. In order to further improve the solution, in the cavitated areas a small artificial diffusion may be added perpendicular to the flow direction U:

$$\nabla\left(\frac{-h^3}{12\mu}\left(\left(\xi\geq 0\right)+\left(\xi\leq 0\right)\left(D+\alpha_{ad}\alpha_{cf}\left(1-D\right)\right)\left[\begin{array}{cc}\frac{U_x}{U} & 0\\ 0 & \frac{U_y}{U}\end{array}\right]\right)\right)\nabla\xi+ \\ Uh\left(1+\left(\xi\leq 0\right)c_f\xi\right)=0 \tag{5.122}$$

With the fill rate model the Reynolds equation can be solved for non fully flooded conditions.

6. Summary

Section II has shown the application possibilities of the Reynolds equation under the thin film assumption and its limitations, mainly the inertia effects. This inertia effects appears in two different ways, first of all in the fluid film and can be included in an iterative or averaged method. For 2D a novel approach has been introduced combining the average and iterative method. Secondly inertia plays an important role in the inlet and can be taken into account by assuming a velocity profile and calculating the according pressure. A, rather crude, first approximation is done assuming the fluid is stagnating at the inlet. To this approximation two corrections are set-up, one based on energy and one based on momentum. Finally a fill rate model has been introduced that is based on a cavitation algorithm and allows the calculation of the position of the inlet and the according fluid film height.

With the fluid modelling described the next section will dive into the tire modelling.

Section III
Solid mechanics: Tire modelling

In the previous section the fluid modelling has been explained, this section will develop several tire models. To start with an overview of the tire components and construction is given and the most common materials are listed. Then a linear elastic model is explained after which a hyper elastic model is described. Two basic geometries will be used, a simple Grosch wheel which is a small scale solid wheel and a full scale realistic tire model, with three grooves and a cavity.

7. Tire construction

The following description of tire construction is taken from wikipedia [Nov 2009], it gives a good simple overview of how a tire is built up.

The tire is an assembly of numerous components that are built up on a drum and then cured in a press under heat and pressure. Heat facilitates a polymerization reaction that crosslinks rubber monomers to create long elastic molecules. These polymers create the elastic quality that permits the tire to be compressed in the area where the tire contacts the road surface and spring back to its original shape under high-frequency cycles. Typical components used in tire assembly are listed below.

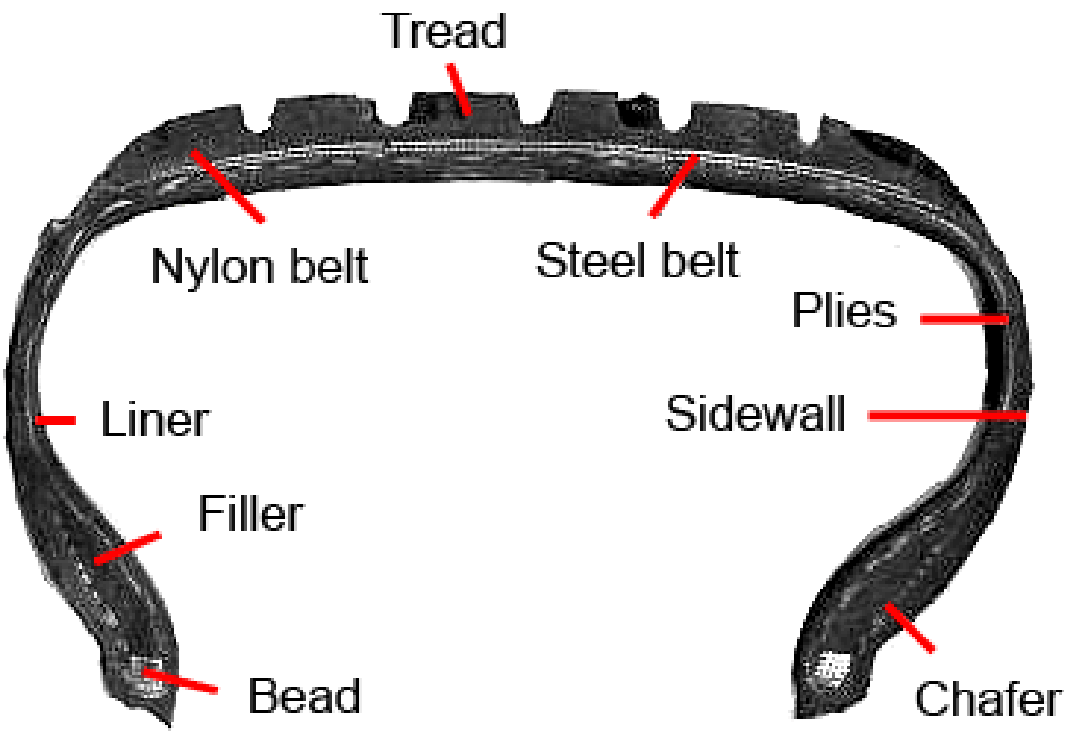

Figure 7.1:

The tire is build up from different functions of which the different sections are:

Inner liner The inner liner is an extruded halobutyl rubber sheet compounded with additives that result in low air permeability. The inner liner assures that the tire will hold

high-pressure air inside, without the air gradually diffusing through the rubber structure.

Body ply The body ply is a calendered sheet consisting of one layer of rubber, one layer of reinforcing fabric, and a second layer of rubber. The earliest textile used was cotton; later materials include rayon, nylon, polyester, and Kevlar. Passenger tires typically have one or two body plies. Body plies give the tire structure strength. Truck tires, off-road tires, and aircraft tires have progressively more plies. The fabric cords are highly flexible but relatively inelastic.

Sidewall Sidewalls are non-reinforced extruded profiles with additives to give the sides of the tire good abrasion resistance and environmental resistance. Additives used in sidewall compounds include antioxidants and antiozonants. Sidewall extrusions are nonsymmetrical and provide a thick rubber area to enable molding of raised letters and sidewall ornamentation.

Beads Beads are bands of high tensile-strength steel wire encased in a rubber compound. Bead wire is coated with special alloys of bronze or brass. Coatings protect the steel from corrosion. Copper in the alloy and sulfur in the rubber cross-link to produce copper sulfide, which improves bonding of the bead to the rubber. Beads are inflexible and inelastic, and provide the mechanical strength to fit the tire to the wheel. Bead rubber includes additives to maximize strength and toughness.

Apex or Filler The apex or filler is a triangular extruded profile that mates against the bead. The apex provides a cushion between the rigid bead and the flexible inner liner and body ply assembly.

Chafer Chafers are strips of protective fabric laid over the outer carcass plies in the bead area of the tire. Their purpose is to protect the carcass plies from damage when mounting or dismounting and to reduce the effects of wear and chafing between the wheel and the tire bead.

Belts Belts are calendered sheets consisting of a layer of rubber, a layer of closely-spaced steel cords, and a second layer of rubber. The steel cords are oriented radially in radial tire construction, and at opposing angles in bias tire construction. Belts give the tire strength and dent resistance while allowing it to remain flexible. Passenger tires are usually made with two or three belts.

Tread The tread is a thick extruded profile that surrounds the tire carcass. Tread compounds include additives to impart wear resistance and traction in addition to environmental resistance. Tread compound development is an exercise in compromise, as hard compounds have long wear characteristics but poor traction whereas soft compounds have good traction but poor wear characteristics.

Breaker The breaker of a Bias tire is rubber-coated layers of cord between the tread and carcass, binding the two together. The breaker prevents cuts in the tread from reaching the carcass and helps absorb shocks.

As seen in the different sections the number of materials used is very large, a short overview:

- Natural rubber, or polyisoprene is the basic elastomer used in tire making
- Styrene-butadiene co-polymer (SBR) is a synthetic rubber which is often substituted in part for natural rubber based on the comparative raw materials cost
- Polybutadiene is used in combination with other rubbers because of its low heat-buildup properties
- Halobutyl rubber is used for the tubeless inner liner compounds, because of its low air permeability. The halogen atoms provide a bond with the carcass compounds which are mainly natural rubber. Bromobutyl is superior to chlorobutyl, but is more expensive
- Carbon Black, forms a high percentage of the rubber compound. This gives reinforcement and abrasion resistance
- Silica, used together with carbon black in high performance tires, as a low heat build up reinforcement
- Sulphur crosslinks the rubber molecules in the vulcanization process
- Vulcanizing Accelerators are complex organic compounds that speed up the vulcanization
- Activators assist the vulcanization. The main one is zinc oxide
- Antioxidants and antiozonants prevent sidewall cracking due to the action of sunlight and ozone
- Textile fabric reinforces the carcass of the tire

To capture the character of a tire in a computationally simple model several models have been made, which will be outlined in the next sections. First a solid tire model is explained, of which the deformation is calculated with an linear elastic half-space model. Then a finite element model of the solid tire model is explained using two different hyper-elastic materials. Then a cavity is added to the model and finally a more realistic finite element model of a tire is explained.

8. Linear elastic solid tire model

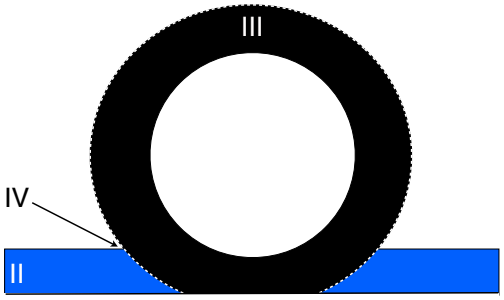

- Section II: Fluid dynamics: Lubrication theory
  - Navier Stokes
  - * Inertia in the fluid film
    * Inertia in the inlet
    * Fill rate
- Section III: Solid Mechanics: Tire modelling
  - **Linear elastic half space model**
  - Hyper elastic finite element model
- Section IV: Fluid Structure Interaction
  - Classical staggering
  - Interface Quasi Newton method
  - Coupling ABAQUS to Matlab

A solid tire model is build by using an analytical expression for the deformation in the contact patch. To determine the deformation in the contact area an elastic half space approximation is done [25] which allows an explicit expression for the influence matrix.

Half-space approximation The half space approximation consists of points on one side of a plane, called the bounding plane. This theory is applicable when the contact area is small compared to the typical dimensions of the elastic body, such that in the majority of the body, outside the contact area, the deformations are small.

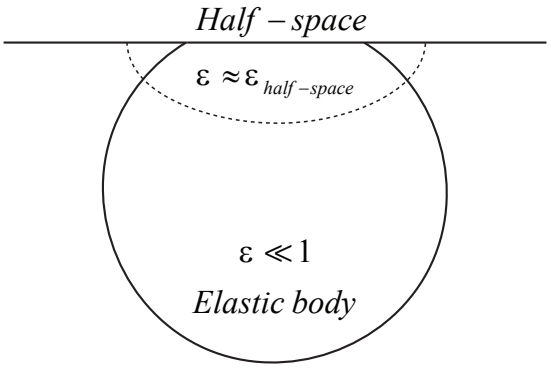

Figure 8.1: Half-space approximation

Influence matrix Exact expression for the influence matrix in the half-space area are determined by Boussinesq [26] and Cerruti. The deformation is then defined by:

$$w\left(x,y\right)=\frac{2}{\pi E'}\int_{-\infty}^{\infty}\int_{-\infty}^{\infty}\frac{p\left(x',y'\right)}{\sqrt{\left(x-x'\right)^{2}+\left(y-y'\right)^{2}}}dx'dy' \tag{8.1}$$

Where E' indicates the resultant modulus of elasticity, which will be defined later, $w(x,y)$ indicates the deformation at point (x,y) and $p(x',y')$ indicates the pressure at

point (x', y'). This influence matrix can also be used to determine the discrete elastic deformation, which is then given by an discrete influence matrix which relates the deformation in one node to the pressure in a different node.

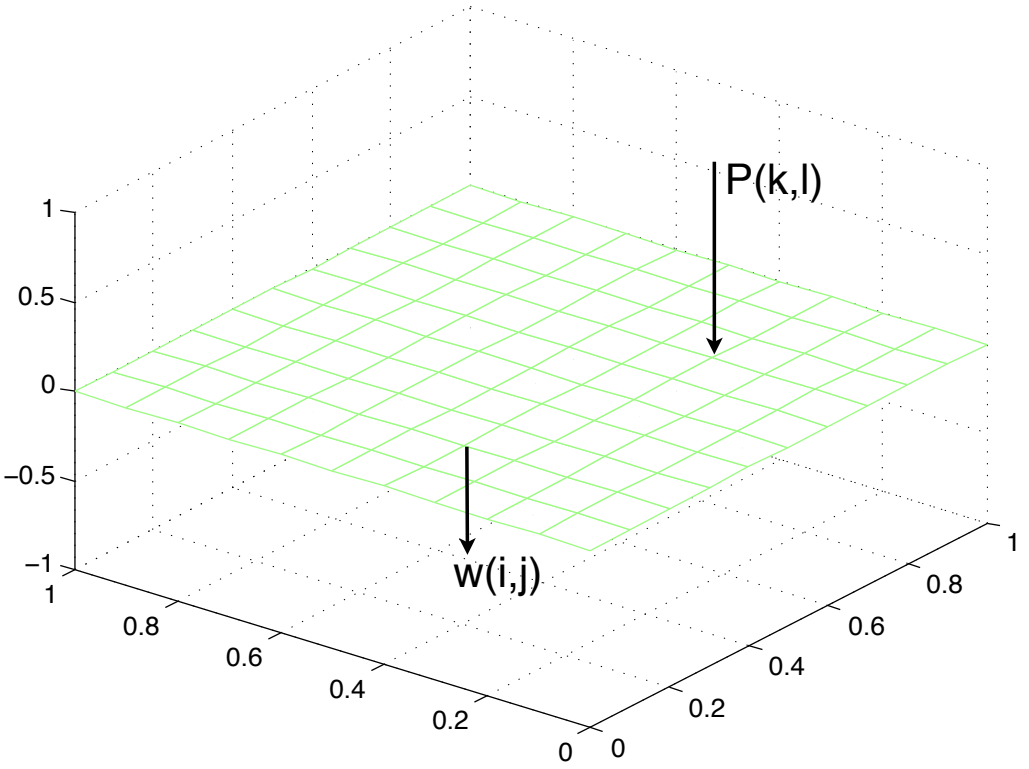

Figure 8.2: Discrete influence matrix

The deformation in node (i, j) as a result of pressure in point (k, l) is given by:

$$w\left(x_i, y_j\right) = w_{i,j} \approx \frac{2}{\pi E'} \sum_{k=1}^{n_x} \sum_{l=1}^{n_y} D_{ijkl} p_{kl} \tag{8.2}$$

Where the influence coefficients are found from:

$$D_{ijkl} = \int \int_{elem} \frac{1}{\sqrt{\left(x_i - x'\right)^2 + \left(y_j - y'\right)^2}} dx' dy' \tag{8.3}$$

An analytical solution for this integral is given by Love [27]:

$$\begin{aligned} D_{ijkl} = & x_p \ln\left(\frac{y_p + \sqrt{x_p^2 + y_p^2}}{y_m + \sqrt{x_p^2 + y_m^2}}\right) + y_m \ln\left(\frac{x_m + \sqrt{x_m^2 + y_m^2}}{x_p + \sqrt{x_p^2 + y_m^2}}\right) \\ & + x_m \ln\left(\frac{y_m + \sqrt{x_m^2 + y_m^2}}{y_p + \sqrt{x_m^2 + y_p^2}}\right) + y_p \ln\left(\frac{x_p + \sqrt{x_p^2 + y_p^2}}{x_m + \sqrt{x_m^2 + y_p^2}}\right) \end{aligned} \tag{8.4}$$

With:

$$\begin{aligned} x_p &= x_i - x_k + \frac{h_x}{2}, x_m = x_i - x_k - \frac{h_x}{2} \\ y_p &= y_j - y_l + \frac{h_y}{2}, y_m = y_j - y_l - \frac{h_y}{2} \end{aligned} \tag{8.5}$$

Where h_x and h_y indicate the mesh size in x and y direction. The resultant modulus (E') for the two materials in contact, assuming the road infinitely stiff, is given by:

$$E' = \frac{2E}{1 - \nu^2} \tag{8.6}$$

With this matrix the deformation can be calculated for a given pressure profile. The E modulus used in this tire model is of natural rubber: 2.05 MPa and a poisson ratio of 0.5. The geometry of a Grosch wheel is used, which will be explained in the next section. The iteration scheme to determine the static footprint is the following:

- Inititalize vertical tire deflection: t_d, 8.3, I

- While ||contact force - external load|| < tolerance

  - Determine penetration of the nodes in contact, $w(i, j)$,8.3, II

  - Determine contact pressure, $p_c(k, l)$, using the inverse of the influence matrix to place the nodes on the road surface, 8.3, III

  - Determine contact force: $F_c = \sum_{i=1}^{n} p_c \cdot dx \cdot dy$, where dx and dy indicate the mesh size in x and y direction, 8.3, IV

  - Determine residual, i.e. the difference between the contact force, F_c and the external load, L_{ex}, 8.3, V

  - Update tire deflection, 8.3, I

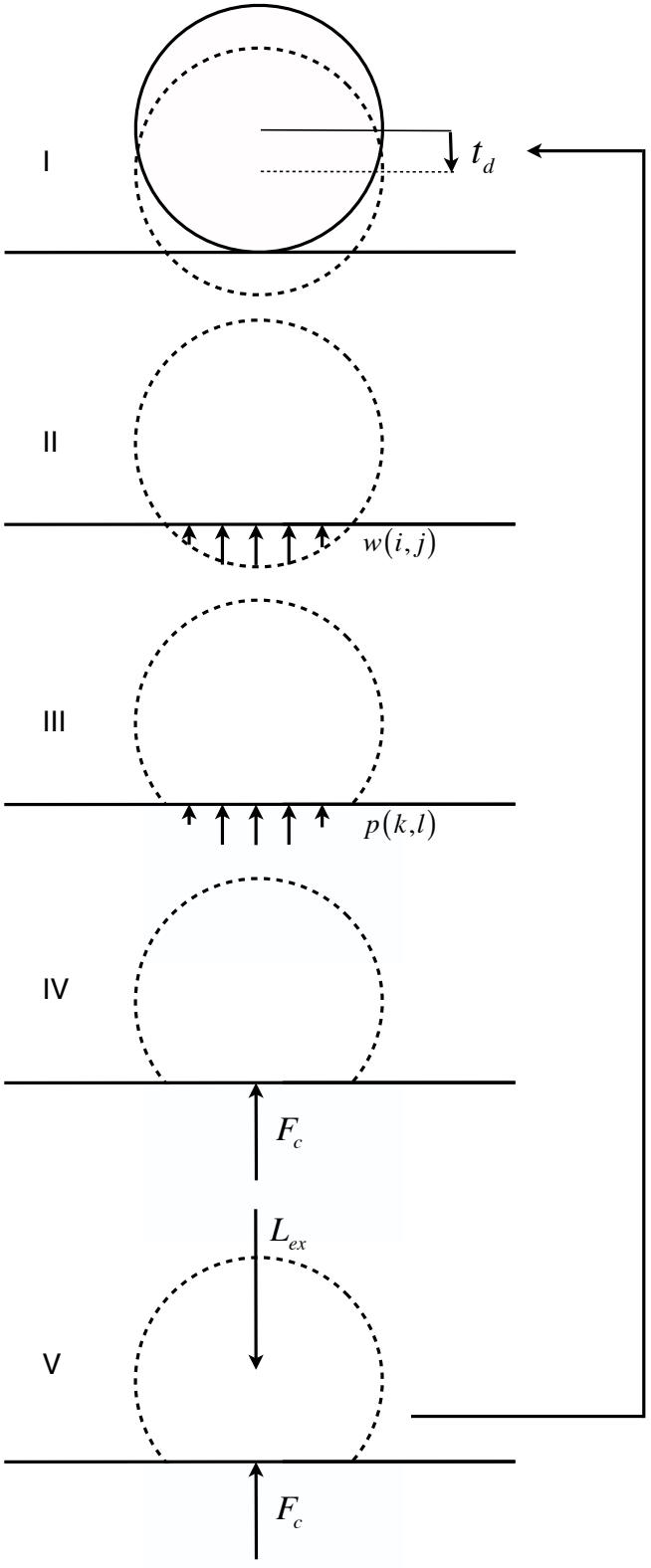

Figure 8.3: Iteration scheme linear elastic half-space

The linear elastic half space model is now ready for the fluid structure interaction, which will be described in section IV. Next the hyper elastic models that are used in

ABAQUS are described.

9. Hyper elastic solid tire model

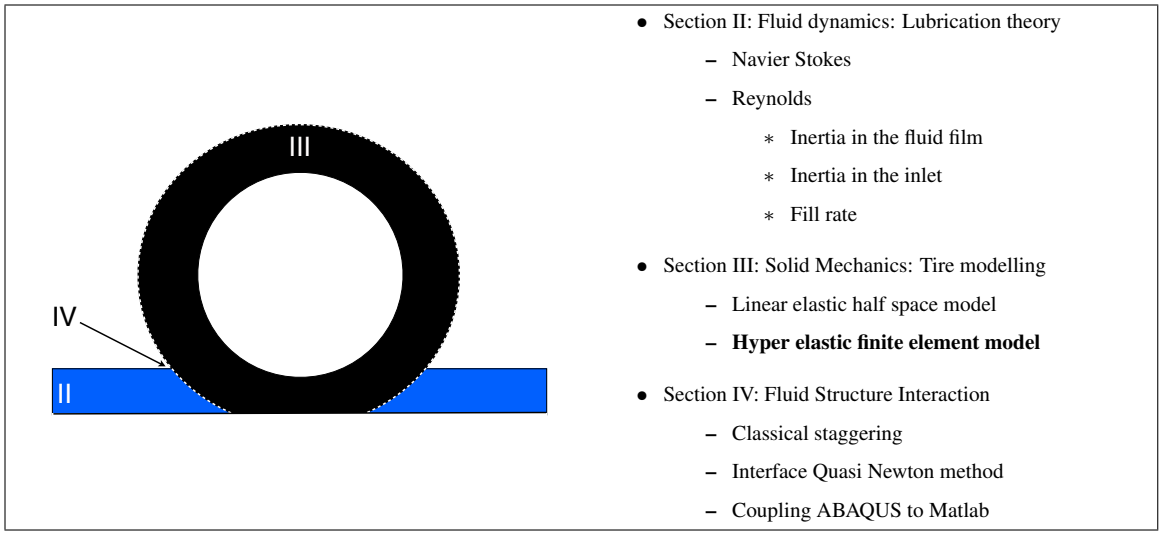

To more realistically represent the behavior of a tire a hyper elastic model is used, with a Grosch wheel, which is a small scale representation of an actual wheel for simulation purposes. The geometry of the wheel is given by the following parameters:

- radius = 40 mm
- width = 20 mm
- groove width = 4 mm
- groove depth = 4 mm

The wheel is modelled with a finite element model in Abaqus Explicit, version 6.8.2 and newer, see figure:

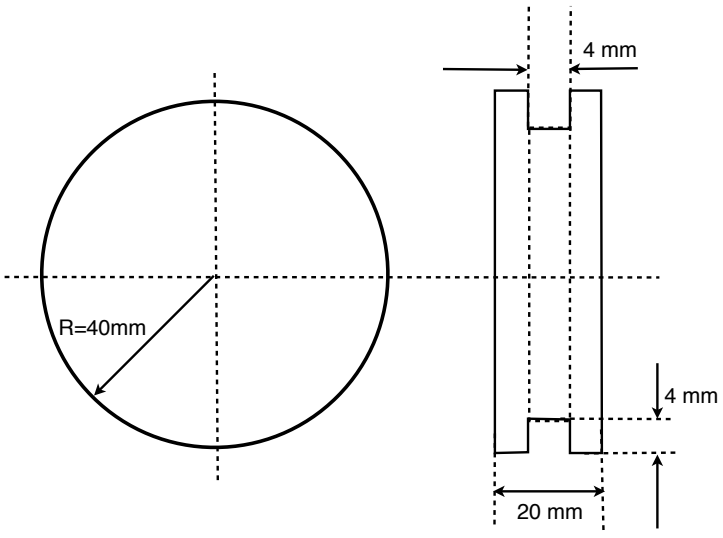

Figure 9.1: Grosch wheel

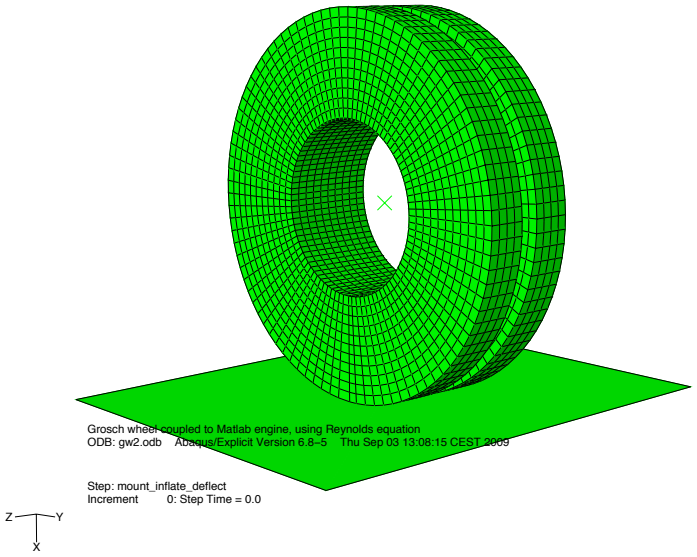

Figure 9.2: Grosch wheel: FEM model

The model is built up using 3D quadrilateral elements, consisting of 8 nodes. Two material models have been used, both neo-Hookean, with the following hyperelastic parameters:

- model 1:
  - Bulk modulus: 200 MPa
  - Shear modulus: 2 MPa
- model 2:
  - Bulk modulus: 200 MPa
  - Shear modulus: 1 MPa

In a linear elastic model this would result in a factor of stiffness difference. A Grosch wheel model with a cavity of 10 mm wide and 10 mm high was also tested as well as a Grosch wheel without a groove. These different models have been tested to compare the problems with the tire model, which will be listed in the next section. No difference appears between the different models and in the final results only the model with a bulk modulus of 200 MPa and a shear modulus of 2 MPa on the Grosch wheel with groove has been used.

9.1. Problems with the tire model

In dry rolling the model remains oscillating, see the movement of the rim node of the wheel:

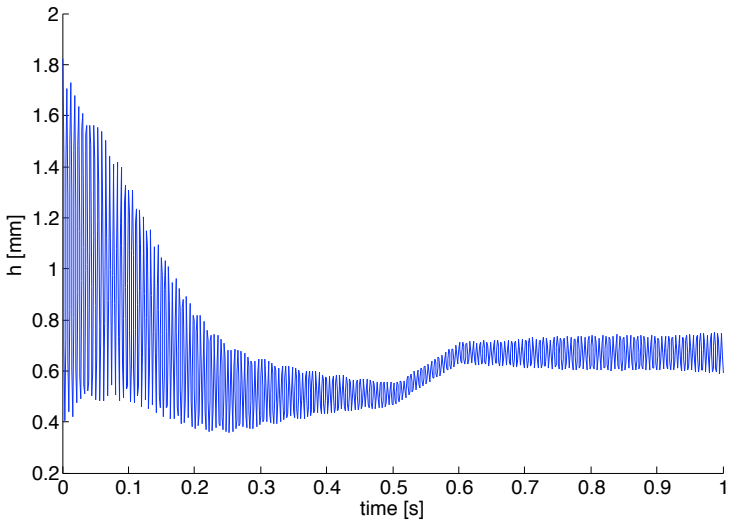

Figure 9.3: Vertical displacement of the wheel

Also the resultant reaction force is oscillating quite a bit:

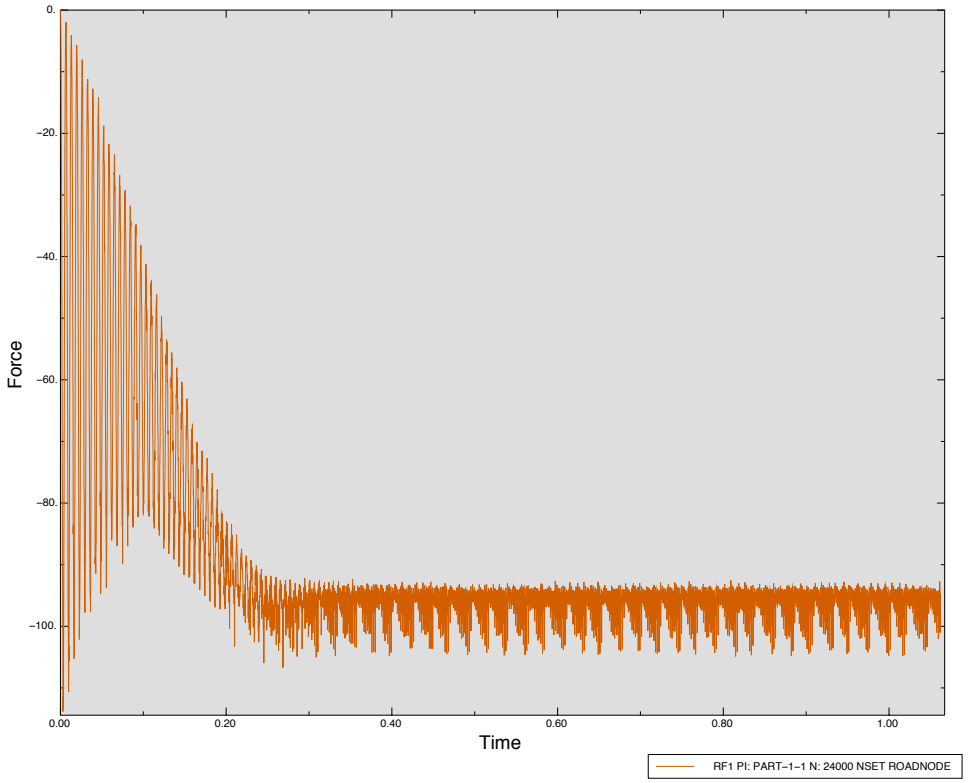

Figure 9.4: Reaction force

Eigen modes The loading conditions of 100 N and 214 N normal load and the rolling speeds of 5, 10, 15, 50, 60 and 70 km/h could be inducing an eigenmode so a modal analysis of the wheel is made. The first few modes are listed:

Table 2: Eigenvalue output

mode no.	frequency (cycles/time)
1	0.0000
2	2.08779E-04
3	361.38
4	361.38
5	367.94
6	367.94
7	375.02
8	448.33
9	448.33
10	448.84
11	563.34
12	586.39
13	586.39
14	656.40
15	656.40
16	750.13
17	750.13
18	754.68
19	824.30
20	824.30

The corresponding eigen shapes are found in the appendix D. The mesh on the Grosch wheel has been made with 90 and with 120 sectors, the "mesh frequency" would then be between 500 and 9300 Hz so there are eigenmodes present in this frequency range are induced by these operating conditions, however more likely is an inaccuracy of the contact penalty method.

Contact Penalty Method Another explanation for the oscillations could be the inaccuracy of contact algorithm. The contact algorithm that ABAQUS uses is the penalty method, in essence it adds an extra spring stiffness and based on the penetration of the contact surface the contact force is updated. The penalty scale factor was changed in 8 different simulations with scale factores: 0.1, 0.5, 1, 2, 10 and the model with and without cavity. The oscillations were unaffected. It seems that the penalty method is the largest cause of the inaccurate contact behavior. Further investigation of how ABAQUS deals with contact is necessary.

Energy level Another problem occurring with the Grosch wheel model as well as with the tire model which will be described in the next section is that the amount of

kinetic energy increases throughout the simulation and becomes more than the total energy.

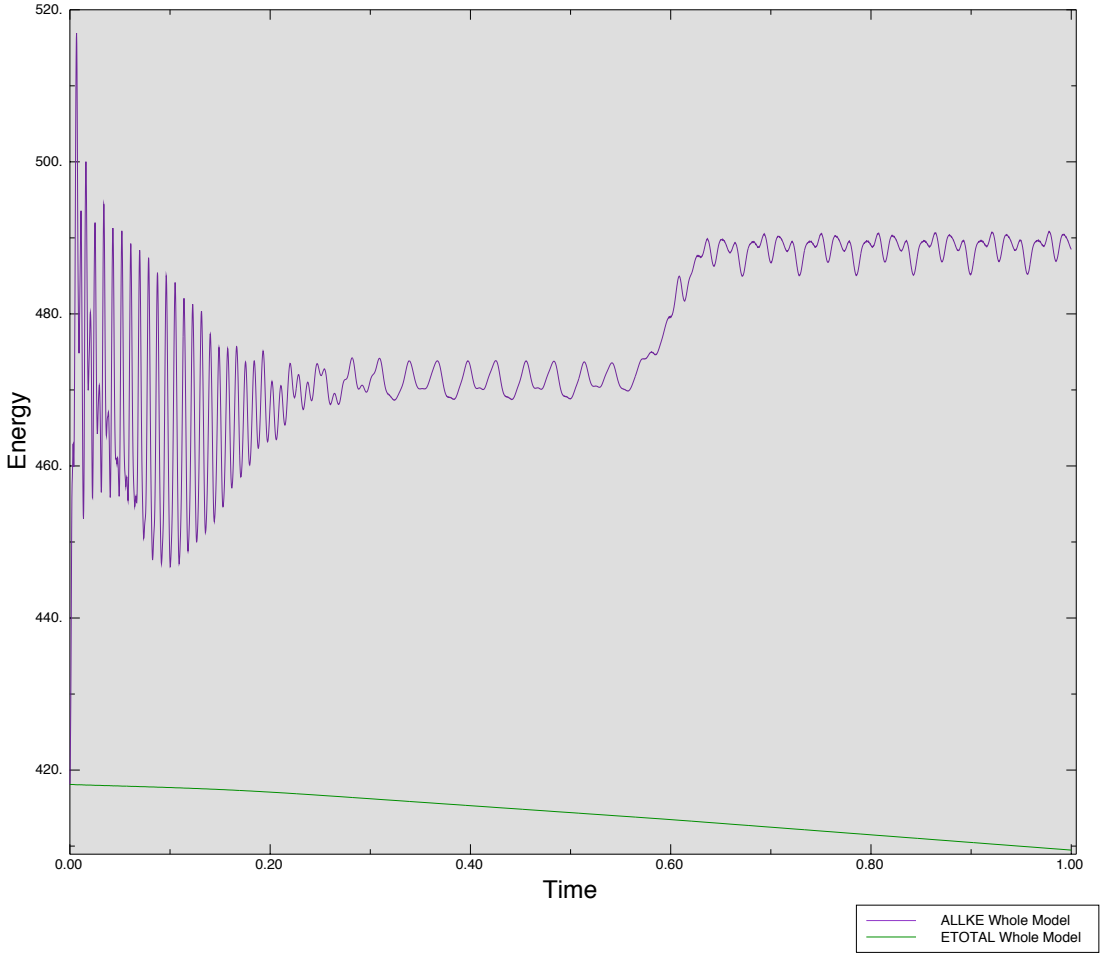

Figure 9.5: Energy level

Upon a restart of the model however the energy level is lower again. This effect is yet unclear and no explanation is found.

10. Real tire model

Finally a tire model, in this thesis also called BMW Coarse model, is made with the following cross section:

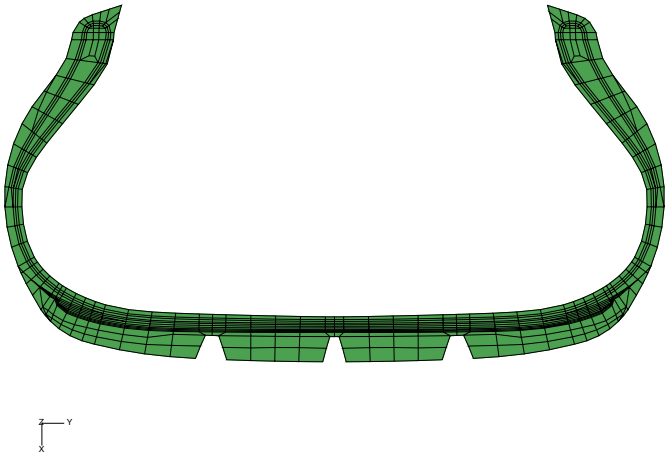

Figure 10.1: BMW Coarse

Which after revolving in 360 sectors looks like:

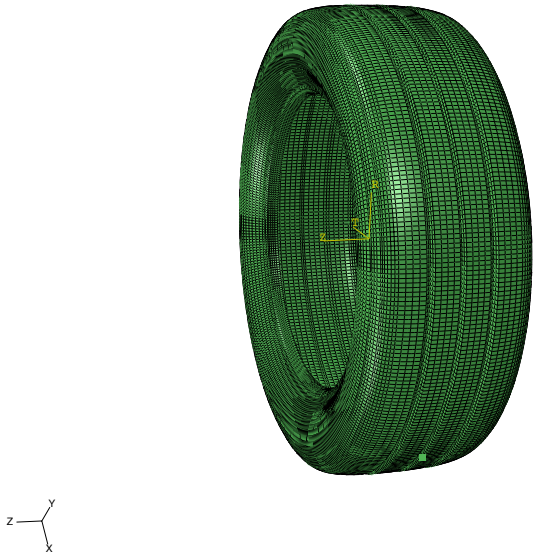

Figure 10.2: BMW Coarse revolved

The tire has a diameter of 315 mm and an inflation pressure of 2.2 bar. The model is build up from 14 different materials:

Compound	Type	E	ν	K	G
Breaker 1& 2	Hyper elastic	-	-	200	8,76
Apex	Hyper elastic	-	-	200	15,6
Ply	Hyper elastic	-	-	200	1,26
Liner	Hyper elastic	-	-	200	0,96
Gstg	Hyper elastic	-	-	200	0,86
Chafer	Hyper elastic	-	-	200	2,76
Sidewall	Hyper elastic	-	-	200	1,10
Miniskirt	Hyper elastic	-	-	200	1,10
Tread	Hyper elastic	-	-	200	2,6
Bead	Elastic	40.000	0,3	-	-
Begs	Hyper elastic	-	-	200	6,08
Overlay	Hyper elastic	-	-	200	5,48
Minibase	Hyper elastic	-	-	200	2,18

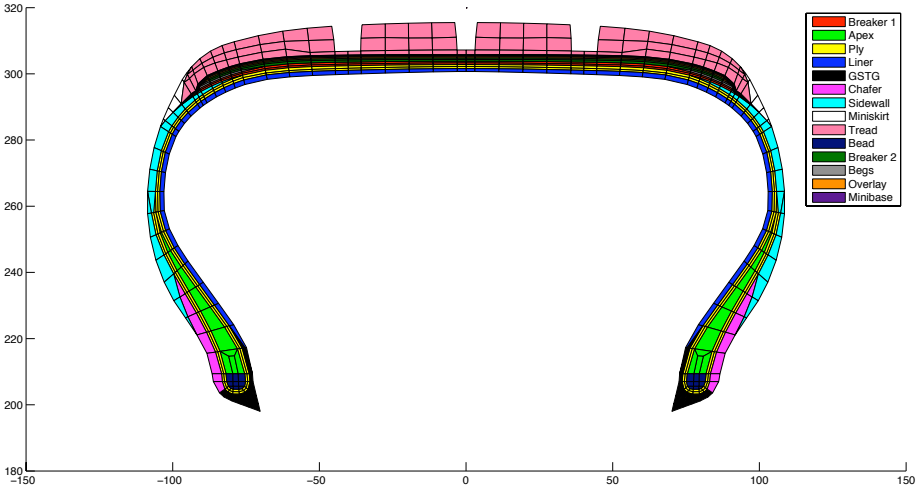

Figure 10.3: BMW Coarse

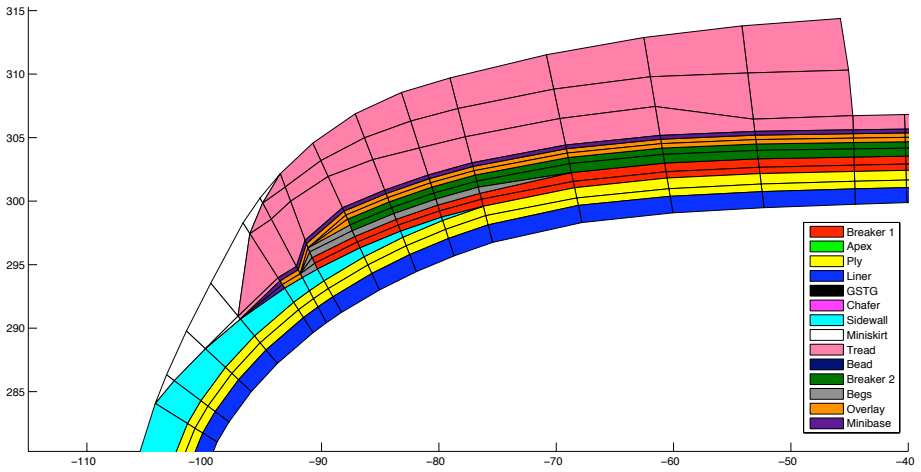

Figure 10.4: BMW Coarse

The tire model contains some additional compounds to what is described before:

Minibase A thin rubber layer between tread and reinforcement package with intermediate stiffness softer than breaker package but stiffer than tread.

Begs The Breaker Ending Gum Strip, sometimes called GumStrip or Breaker Wedge: prevents crack growth in breaker ending region.

Gstg This is usually called ToeGuard

Miniskirt links the tread to the sidewall and is there to prevent the sidewall to enter into contact with the road. It has similar properties than the tread compound, and is not part of the tread only for manufacturing reason.

The 2D cross-section is revolved in Abaqus standard, after which a static footprint is determined, with a normal load of 400 kg. From the undeformed radius and the deflection under static loading the dynamic radius is estimated. With this dynamic radius the initial rotational velocity is predicted and an Abaqus Explicit run is done, having the tire in dry rolling at 90 km/h. Then the model is ready for a restart with a coupling to the fluid code. The problem with the oscillations, as described before, is dealt with by shifting the road in the fluid code. As a result there are more nodes which will be in contact and the contact patch becomes flat instead of with local spikes which will result in pressure spikes in the Reynolds solution. The model can now be implemented in an fluid structure interaction model, which is explained in Section IV.

11. Summary

In this section an overview of the tire construction is given and the most important materials used are listed. Furthermore 2 different tire models have been developed, a linear elastic one and a hyper elastic one. Two basic different geometries have been implemented, a so-called Grosch wheel which is a small scale solid wheel and a more realistic full scale tire model with three grooves and a cavity. There is a problem with the tire model oscillating which has a huge effect for the Reynolds equation, this is solved by shifting the road in the fluid model, i.e. more nodes are assumed to be in contact but this will result in an even contact patch.

With the knowledge of the tire model and the previously developed fluid models a fluid structure coupling can be set up which will be explained in the next section.

Section IV
Fluid Structure Interaction

12. Fluid structure interaction

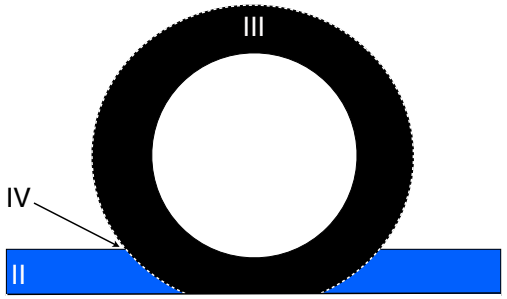

- Section II: Fluid dynamics: Lubrication theory
  - Navier Stokes
  - Reynolds
    - Inertia in the fluid film
    - Inertia in the inlet
    - Fill rate
- Section III: Solid Mechanics: Tire modelling
  - Linear elastic half space model
  - Hyper elastic finite element model
- Section IV: Fluid Structure Interaction
  - **Classical staggering**
  - Interface Quasi Newton method
  - Coupling ABAQUS to Matlab

With the fluid and the structural modelling explained it's time to examine the fluid structure interaction. Fluid Structure interaction is very important in this case due to the strong coupling between the very elastic tire and the incompressible fluid.

Fluid structure interaction can be solved in different ways, monolithic or partitioned. The monolithic approach solves the structural and the fluid equations at once, the partitioned approach uses separate solvers for the fluid and the structure and requires some coupling scheme. Although the monolithic approach could offer more stability it requires extensive coding of the problem whereas the partitioned approach offers the possibility of using existing, well developed and possibly more efficient codes for the fluid and the structure.

For tire modelling a wide variety of finite element models already exist so the partitioned approach is very appealing, if it can be implemented efficiently. In this thesis, to simulate the hydroplaning phenomenon a coupling is made between the (averaged) Reynolds equation and the tire model. It is solved in an iterative manner to determine equilibrium between the fluid pressure and the tire deformation. The output of the model is the percentage of load carried by the tire and the percentage of load carried by the fluid.

In the first section a coupling is made in Matlab between the linear elastic model and the Reynolds equation using classical staggering. However from the iterations it is possible to condense information about the response of the structure and the fluid, this is done in the interface quasi newton method. The second section explains the coupling that was set-up between ABAQUS and Matlab.

12.1. Linear elastic half space model

The iteration scheme, for the linear elastic model is as follows, starting from the dry deformed configuration, see also figure 12.1:

- While the pressure is not converged, i.e $\Delta p <$ tolerance:
- Determine hydrodynamic pressure (p_{hd}) with Reynolds equation, figure 12.1, I
- Determine hydrodynamic lift force: $F_{hd} = \sum_{i=1}^{n} p_{hd} \cdot dx \cdot dy$, where dx and dy indicate the mesh size in x and y direction.
- Determine deformation, w_{hd} due to hydrodynamic pressure p_{hd} using the influence matrix, figure 12.1, II
- While the residual, i.e. the difference between the total lift force, $(F_c + F_{hd})$ and the external load, L_{ex} is larger than the tolerance:
  - Determine penetration of the nodes in contact, w_c, , figure 12.1, III
  - Determine contact pressure: p_c using the inverse of the influence matrix, , figure 12.1, IV
  - Determine contact force: $F_c = \sum_{i=1}^{n} p_c \cdot dx \cdot dy$, figure 12.1, V
  - Determine residual: residual $= L_{ex} - (F_c + F_{hd})$, figure 12.1, V
  - Update tire deflection and re-determine penetration of nodes in contact, figure 12.1, III, until equilibrium is reached
- Update the pressure with the new configuration: p_{hd}, figure 12.1, I
- Determine pressure residual: Δp

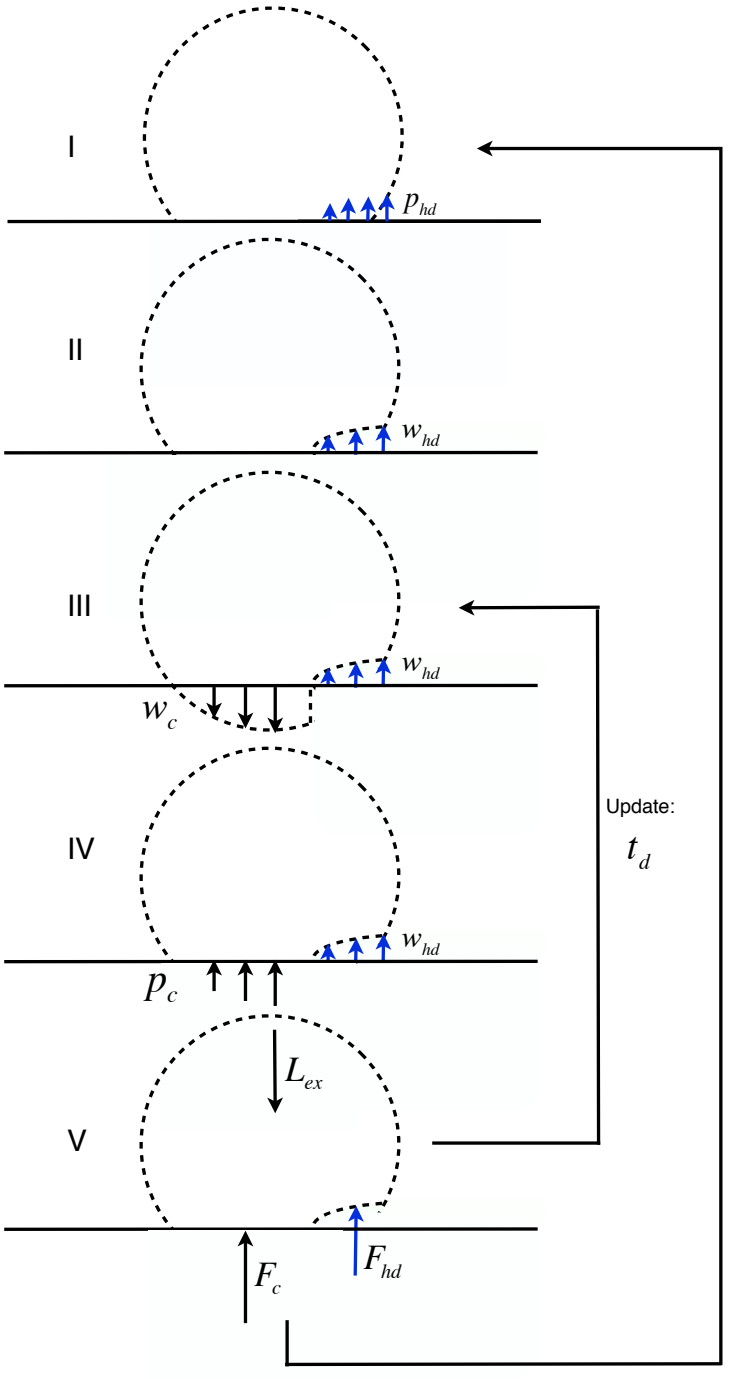

Figure 12.1: Iteration scheme linear elastic half-space

This iteration scheme can be made more efficient by taking into account information of the deformation in previous iterations. This is explained in the next section.

12.1.1. Interface Quasi Newton method

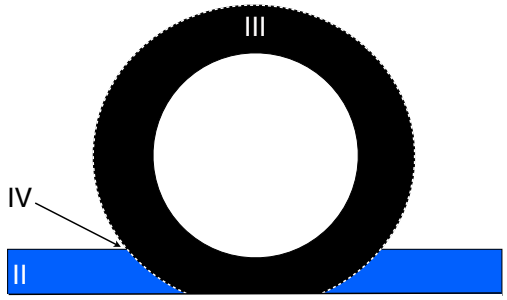

- Section II: Fluid dynamics: Lubrication theory
  - Navier Stokes
  - Reynolds
    - Inertia in the fluid film
    - Inertia in the inlet
    - Fill rate
- Section III: Solid Mechanics: Tire modelling
  - Linear elastic half space model
  - Hyper elastic finite element model
- Section IV: Fluid Structure Interaction
  - Classical staggering
  - **Interface Quasi Newton method**
  - Coupling ABAQUS to Matlab

When using the partitioned approach, in essence the fluid structure interaction problem can be reduced to its boundary, where the position, velocity and acceleration of the boundary is of interest to the fluid and the pressure on the boundary for the structural solver. This, generally non-linear, interface problem can be solved with a Newton-Raphson iteration method, while the structure and the fluid are solved with separate solvers. Some different approaches have been implemented, for example by Gerbeau [28], using an approximation of the Jacobian from a linear, reduced physics model. Another example is van Brummelen [29] who uses a matrix free Krylov solver for the linear system within each Newton-Raphson iteration combined with the approximation of the Jacobian vector product based on a linear combination of the previous residual vectors.

A new scheme, developed by Degroote, Bathe and Vierendeels [30] introduces a new partitioned interface quasi Newton technique. It uses an approximation of the inverse of the Jacobian that appears in the Newton linearization such that no linear system within every Newton-Raphson has to be solved. They named it the IQN-ILS method, the Interface Quasi Newton method with Inverse Jacobian approximation from a Least Squares model.

Governing equations The fluid domain is indicated as: Ω_f and the structural domain as: Ω_s, and the boundaries as: Γ_f and Γ_s. In the next equations the interface is indicated with an underline.

In equilibrium the following conditions should hold:

$$\mathbf{d_s} = \mathbf{d_f} \tag{12.1}$$

and:

$$\mathbf{n_s} \cdot \tau_f = \mathbf{n_s} \cdot \tau_s \tag{12.2}$$

with $\mathbf{d}$ is the displacement, τ the stress and $\mathbf{n}$ the outward normal vector on the boundary of Ω. First reformulate the problem as an equation in the discrete position of the interface:

$$\mathbf{R}\left(\mathbf{d}_s\right) = \mathbf{0} \tag{12.3}$$

Where $\mathbf{R}$ is the residual operator, which is defined for the FSI problem as:

$$\mathbf{R}\left(\mathbf{d}_s\right) = F_s \circ F_f\left(\mathbf{d}_s\right) - \mathbf{d}_s \tag{12.4}$$

Where $\mathbf{d_s}$ is the position of the boundary, $F_f\left(\mathbf{d_s}\right)$ is the result of the fluid code with the boundary as input, in this case the pressure. $F_s \circ F_f\left(\mathbf{d}_s\right)$ is the result of the structural solver with the result of the fluid code as input, so the outcome is the new position of the boundary, and the difference with the previous boundary gives the residual.

This equation is to be solved using a Newton-Raphson iteration:

$$\frac{\partial \mathbf{R}^k}{\partial \mathbf{d}_s}\Delta\mathbf{d}_s^k = -\mathbf{R}^k \tag{12.5}$$

$$\mathbf{d}_s^{k+1} = \mathbf{d}_s^k + \Delta\mathbf{d}_s^k \tag{12.6}$$

The Jacobian matrix has to be known if a direct solver is used or one needs to be able to calculate the product of the Jacobian matrix with a vector if the system is solved iteratively. However this would require knowledge of the Jacobians of the solvers of the fluid and the structural code whereas this is usually not the case in the partitioned method. De Groote et al. developed a method to approximate the inverse of the Jacobian, by a special choice of the inputs and outputs, such that it is not necessary to have the solution of the linear system in every Newton-Raphson iteration.

First the interface position is extrapolated from the previous time steps (where the left superscript indicates the time step), no superscript means the current time step, n+1. Flow and structural equation must be solved to determine an initial residual. To construct an approximate Jacobian two residual vectors are needed, so one iteration with a fixed relaxation factor is used. Attention must be paid to the relaxation factor to avoid divergence.

With at least two residual vectors, difference between the previous values (superscript i) and the last value (superscript k) can be calculated for the residual:

$$\Delta\mathbf{R}^i = \mathbf{R}^i - \mathbf{R}^k \tag{12.7}$$

And for the difference in boundary position:

$$\Delta\tilde{\mathbf{d}}_s^i = \tilde{\mathbf{d}}_s^i - \tilde{\mathbf{d}}_s^k \tag{12.8}$$

with $i = 0, ..., k-1$, these vectors are then stored in a matrix:

$$V^k = \left[\Delta\mathbf{R}^{k-1}...\Delta\mathbf{R}^0\right], \Delta\mathbf{R}^i = \mathbf{R}^i - \mathbf{R}^k \tag{12.9}$$

$$W^k = \left[\Delta\tilde{\mathbf{d}}_s^{k-1}...\Delta\tilde{\mathbf{d}}_s^0\right], \Delta\tilde{\mathbf{d}}_s^i = \tilde{\mathbf{d}}_s^i - \tilde{\mathbf{d}}_s^k \tag{12.10}$$

the number of columns of the matrices is stored in variable q, if this variable would exceed the number of degrees of freedom of the boundary, indicated with p, the number

of columns is limited to p by discarding the rightmost columns. The desired value of $\mathbf{R}$ is the zero vector, and the difference between this and the current value is denoted as:

$$\Delta\mathbf{R} = \mathbf{0} - \mathbf{R}^k \tag{12.11}$$

Approximate this as a linear combination of the known differences, $\Delta\mathbf{R}^i$,

$$\Delta\mathbf{R} \approx \sum_{i=0}^{k-1} \alpha_i^k \Delta\mathbf{R}^i = V^k \alpha^k \tag{12.12}$$

With $q \leq p$ the problem can be solved in the least squares sense, by making a QR decomposition of V^k, which gives an orthogonal matrix Q and an upper triangular matrix R:

$$V^k = Q^k R^k \tag{12.13}$$

Then the coefficient α can simply be determined from the triangular system:

$$R^k \alpha^k = {Q^k}^T \Delta\mathbf{R} \tag{12.14}$$

The $\Delta\tilde{\mathbf{d}}_s$ that corresponds to the $\Delta\mathbf{R}$ is then calculated as a linear combination of the previous $\Delta\tilde{\mathbf{d}}_s^i$:

$$\Delta\tilde{\mathbf{d}}_s \approx \sum_{i=0}^{k-1} \alpha_i^k \Delta\tilde{\mathbf{d}}_s^i = W^k \alpha^k \tag{12.15}$$

Since $\mathbf{R}\left(\mathbf{d}_s\right) = \tilde{\mathbf{d}}_s\left(\mathbf{d}_s\right) - \mathbf{d}_s$ and since α^k is a function of $\Delta\mathbf{R}$ this results in:

$$\mathbf{R}\left(\mathbf{d}_s\right) = \tilde{\mathbf{d}}_s\left(\mathbf{d}_s\right) - \mathbf{d}_s \tag{12.16}$$

Such that the difference in the residual becomes:

$$\Delta\mathbf{R}\left(\mathbf{d}_s\right) = \Delta\tilde{\mathbf{d}}_s\left(\mathbf{d}_s\right) - \Delta\mathbf{d}_s \tag{12.17}$$

Rewrite:

$$\Delta\mathbf{d}_s = \Delta\tilde{\mathbf{d}}_s\left(\mathbf{d}_s\right) - \Delta\mathbf{R}\left(\mathbf{d}_s\right) \tag{12.18}$$

Recall equation 12.15 to obtain:

$$\Delta\mathbf{d}_s = W^k \alpha^k - \Delta\mathbf{R} \tag{12.19}$$

Recall equation 12.11 to write this to:

$$\Delta\mathbf{d}_s = W^k \alpha^k + \mathbf{R}^k \tag{12.20}$$

The inverse of the Jacobian is not determined explicitly but the product of the approximation for the inverse and a vector, recalling equation 12.4:

$$\Delta\mathbf{d}_s = \left(\frac{\partial\hat{\mathbf{R}}^k}{\partial\mathbf{d}_s}\right)^{-1}\left(-\mathbf{R}^k\right) = W^k\alpha^k + \mathbf{R}^k \tag{12.21}$$

So, to summarize, the resulting algorithm starts with an initialization. In this initialization previous iterations are needed, indicated with the left superscript, n, n-1 and n-2.

$$\mathbf{d}_s^0 = \frac{5}{2}\left({}^n\mathbf{d}_s\right) - 2\left({}^{n-1}\mathbf{d}_s\right) + \frac{1}{2}\left({}^{n-2}\mathbf{d}_s\right) \tag{12.22}$$

Then an initial boundary update can be determined by evaluating the result of the fluid code, implement this in the structural code to have the new boundary location $\tilde{\mathbf{d}}_\mathbf{s}^\mathbf{0}$.

$$\tilde{\mathbf{d}}_s^0 = F_s \circ F_f\left(\mathbf{d}_s^0\right) \tag{12.23}$$

Then the initial residual is known $\mathbf{R}^0$:

$$\mathbf{R}^0 = \tilde{\mathbf{d}}_s^0 - \mathbf{d}_s^0 \tag{12.24}$$

The initial update is done $\mathbf{d}_s^1$ using a relaxation factor, ω and the iteration counter (k) is started.

$$\begin{aligned} &\mathbf{d}_s^1 = \mathbf{d}_s^0 + \omega\mathbf{R}^0 \\ &k = 1 \end{aligned} \tag{12.25}$$

Then, while not converged the following is executed, as was described before. Start with calculating the position of the new boundary:

$$\tilde{\mathbf{d}}_s^k = F_s \circ F_f\left(\mathbf{d}_s^k\right) \tag{12.26}$$

Determine the residual

$$\mathbf{R}^k = \tilde{\mathbf{d}}_s^k - \mathbf{d}_s^k \tag{12.27}$$

Construct the matrices, and perform a QR decomposition on V.

$$\begin{aligned} V^k &= \left[\Delta\mathbf{R}^{k-1}...\Delta\mathbf{R}^0\right], \Delta\mathbf{R}^i = \mathbf{R}^i - \mathbf{R}^k \\ W^k &= \left[\Delta\tilde{\mathbf{d}}_s^{k-1}...\Delta\tilde{\mathbf{d}}_s^0\right], \Delta\tilde{\mathbf{d}}_s^i = \tilde{\mathbf{d}}_s^i - \tilde{\mathbf{d}}_s^k \\ V^k &= Q^k R^k \end{aligned} \tag{12.28}$$

Notice that to construct the matrix V the Δ residuals are constructed from the previous residuals, see figure as an example for the first steps:

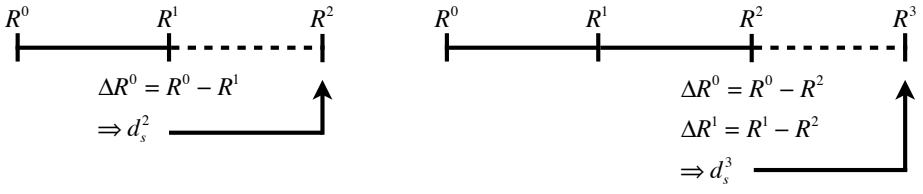

Figure 12.2: Construction of residuals

Determine α using back substitution from:

$$R^k \alpha^k = Q^{k^T} \left(-\mathbf{R^k}\right) \tag{12.29}$$

Determine the prediction of the boundary and update the iteration counter:

$$\begin{aligned} \Delta \mathbf{d}_s &= W^k \alpha^k + \mathbf{R}^k \\ \mathbf{d}_s^{k+1} &= \mathbf{d}_s^k + \Delta \mathbf{d}_s \\ k &= k + 1 \end{aligned} \tag{12.30}$$

The updates boundary is now once more input for the fluid code, from which the result is input for the structural code as in equation 12.26 and the iteration continues. With the interface method it is now possible to take into account the results from previous iterations to speed up convergence.

13. Coupling Abaqus tire model to Reynolds model

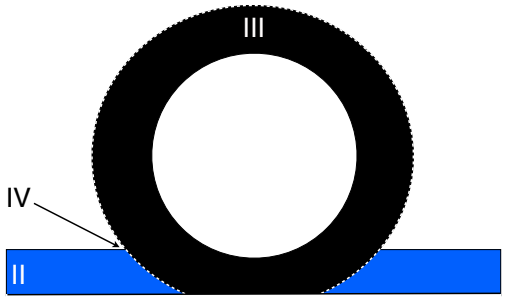

- Section II: Fluid dynamics: Lubrication theory
  - Navier Stokes
  - Reynolds
    - Inertia in the fluid film
    - Inertia in the inlet
    - Fill rate
- Section III: Solid Mechanics: Tire modelling
  - Linear elastic half space model
  - Hyper elastic finite element model
- Section IV: Fluid Structure Interaction
  - Classical staggering
  - Interface Quasi Newton method
  - **Coupling ABAQUS to Matlab**

To couple the Abaqus simulation to the Matlab model there are several options: co-simulation, running the Matlab engine from a user subroutine, programming a user element, and a staggered approach running Abaqus and Matlab sequentially.

Staggered approach The staggered approach was implemented using a file to exchange the information between the programs but this resulted in the wall time of the computation going up with a factor 20 - 30 depending on the model, giving simulation times of over 50 hours for a simple Grosch wheel and therefore the method was deemed inappropriate.

co-simulation Although co-simulation is a very good approach it requires a special contract with Simulia for access to the protocol and the entire model needs to be written in C and is therefore deemed inappropriate for the method development under investigation.

user element Abaqus user elements can be:

- finite elements in the usual sense of representing a geometric part of the model
- feedback links, supplying forces at some points as functions of values of displacement, velocity, etc at other points in the model
- used to solve equations in terms of nonstandard degrees of freedom
- linear or non-linear

The second point seems to be an option to implement the Reynolds equation, however requires significant coding in Fortran, has limitations when dealing with contact and is applied linking predetermined nodes which results in a problem for the current FSI model, as due to the rotating wheel it is not possible to link predetermined nodes.

As a result the chosen approach is running the Matlab engine from the user subroutine, the next sections describe the subroutines and the Matlab engine and its combination.

13.1. Coupling Abaqus to the Matlab engine

This chapter describes the coupling of the Matlab engine to Abaqus via the user subroutines, an overview of the possible user subroutines is found in appendix E

13.2. Abaqus subroutines

Only two subroutines, VDLOAD and VUFIELD, are exemplified here in detail for the specific application to coupling Abaqus/Explicit to Matlab. The VDLOAD subroutine is suited to define a fluid pressure on the surface of a tire, it passes on the following information to the subroutine:

Variable	explanation
nblock	number of points to be processed **NOTE: the number of points processed is determined by Abaqus and is limited to a maximum of 136 at a time**
ndim	number of coordinate directions
stepTime	value of time since step began
totalTime	value of the total time
amplitude	current amplitude value
curCoords	current coordinates for each point **NOTE: this point will be the middle of the surface for which the load is to be specified**
velocity	current velocity
dirCos	current orientation of the face
jltyp	identifier for load type
sname	surface name

The value the subroutine expects to have returned is simply the surface load or body load depending on the specified load, either a DSLOAD or a DLOAD. As mentioned in the table the variable "nblock" is limited to 136, without specifying the node number. To avoid this limitation the user subroutine VUFIELD is used, which passes on the following:

Variable	explanation
nblock	number of points to be processed, user specified **NOTE: in parallel computing on multiple domains the number remains limited to the number of nodes within the domain on one cpu**
nfield	number of field variables to be updated
kfield	field variable number
kstep	current step number
kinc	increment number for step kstep
jnodeuid	user defined node numbers
time	stores current analysis time, time increment, time period of current step and the total analysis time up to this point
coords	current coordinates, the coordinates are this time of the nodes **Although abaqus claims the current coordinates are passed this does not always seem to be the case!**
U, V, A	the displacements, rotations, temperature and pressure and their time derivatives

From user subroutine VUFIELD it is now possible to determine the geometry of the tire, compute the pressure and use VDLOAD to return the pressure to ABAQUS. The variables can be passed on through the different subroutines using a COMMON block in the Fortran code. Next step is to calculate the pressure, this could be done by coding in Fortran, however for method development purposes the ease and flexibility of Matlab is chosen, but this requires a coupling between Matlab and Abaqus, for this purpose the Matlab engine is used which will be explained in the next section. The implemented subroutines have the following flowchart:

User subroutine VUFIELD The user subroutine VUFIELD executes the following scheme:

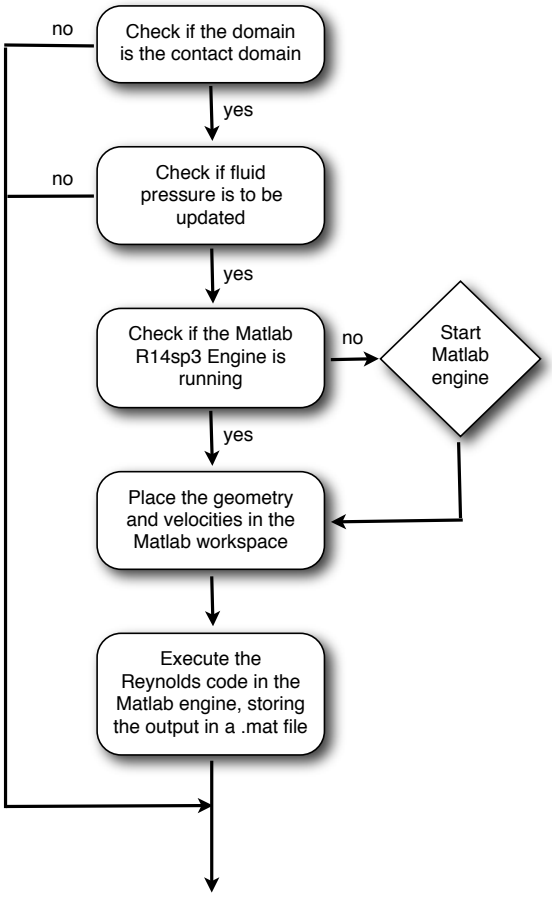

Figure 13.1: VUFIELD subroutine

The built in check if the pressure is to be updated indicates that sub-cycling is used. This is done due to the small time step of ABAQUS Explicit which is based on the eigenfrequency of the smallest element in the structural model and during this time step changes of the structural model are of small influence on the fluid. Furthermore a check routine for the start of the Matlab engine is built in which is a critical step in getting the system running as two subroutines a the same time call the Matlab engine. Finally the pressure output is stored in a .mat file which is clearly very negative for the computational time but currently no solution is found for exchanging information between Matlab engines running on different CPUs.

User subroutine DSLOAD The user subroutine DSLOAD executes the following scheme:

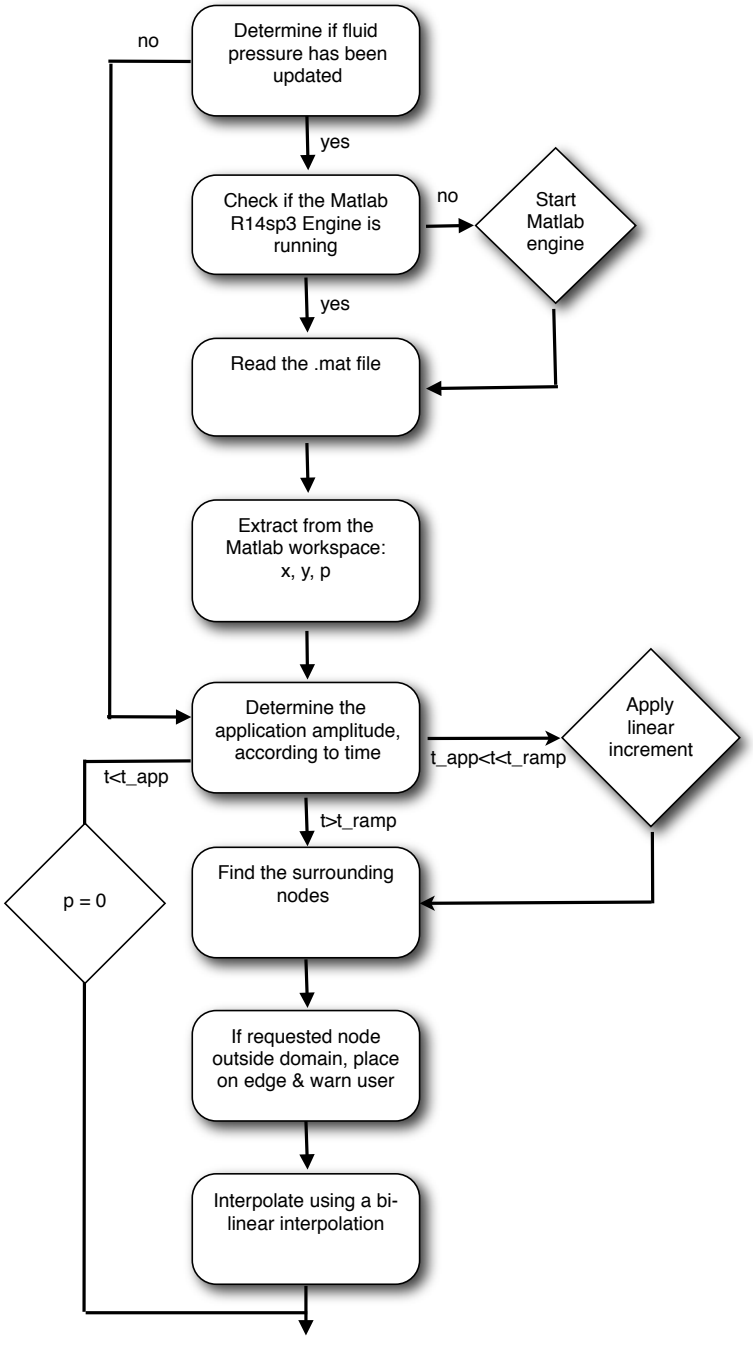

Figure 13.2: DSLOAD subroutine

In this flowchart the x,y and p that are extracted from the Matlab workspace are the coordinates and the pressures at these coordinates.

bi-linear interpolation Since the DSLOAD routine requests the pressure at the middle of the surface element, an interpolation is needed. In this case a bi-linear interpo-

lation is applied. The scheme is used to find the unknown value in point $P(x, y)$ from the data in points $Q_{11} = (x_1, y_1)$, $Q_{12} = (x_1, y_2)$, $Q_{21} = (x_2, y_1)$ and $Q_{22} = (x_2, y_2)$. Intermediate point are $R_1 = (x, y_1)$ and $R_2 = (x, y_2)$. The scheme is as follows, starting in x-direction:

$$\begin{aligned} f(R_1) &\approx \frac{x_2 - x}{x_2 - x_1} f(Q_{11}) + \frac{x - x_1}{x_2 - x_1} f(Q_{21}), R_1 = (x, y_1) \\ f(R_2) &\approx \frac{x_2 - x}{x_2 - x_1} f(Q_{12}) + \frac{x - x_1}{x_2 - x_1} f(Q_{22}), R_1 = (x, y_2) \end{aligned} \tag{13.1}$$

Next, in y-direction:

$$f(P) \approx \frac{y_2 - y}{y_2 - y_1} f(R_1) + \frac{y - y_1}{y_2 - y_1} f(R_2) \tag{13.2}$$

Combine to end up with:

$$\begin{aligned} f(x, y) \approx \frac{f(Q_{11})}{dx \cdot dy} (x_2 - x)(y_2 - y) + \\ \frac{f(Q_{21})}{dx \cdot dy} (x - x_1)(y_2 - y) + \\ \frac{f(Q_{12})}{dx \cdot dy} (x_2 - x)(y - y_1) + \\ \frac{f(Q_{22})}{dx \cdot dy} (x - x_1)(y - y_1) \end{aligned} \tag{13.3}$$

Where dx and dy indicate the mesh size in x and y direction.

linear increment The linear increment on the amplitude of the pressure is applied to avoid the wheel to start bouncing immediately after the pressure is applied. This was also implemented in the benchmark models and adopted here for comparison.

13.2.1. Matlab engine

The MATLAB engine library is a set of routines that allows you to call MATLAB from your own programs, thereby employing MATLAB as a computation engine. MATLAB engine programs are C or Fortran programs that communicate with a separate MATLAB process via pipes, on UNIX, and through a Component Object Model (COM) interface, on Windows. There is a library of functions provided with MATLAB that allows you to start and end the MATLAB process, send data to and from MATLAB, and send commands to be processed in MATLAB [31]. The details on how to get the Matlab engine running are found in appendix F

13.2.2. Matlab engine from Abaqus subroutine

Now that the background of the Matlab engine and the Abaqus subroutine is somewhat clear the next step is to combine both at the same time. Details are found in appendix G. The important part is the compatibility of the compilers which have been used to

compile the programs themselves. Abaqus 6.8 and 6.9 require a a Matlab version compiled with a GCC compiler version 3.3.0 to be compatible, and in fact the following compatible versions of Matlab and Abaqus have been tested:

Compatibility				
Matlab version	Abaqus version			
	6.8-1	6.8-2	6.8-5	6.9-1
R14SP2	ok	ok	ok	ok
R14SP3	ok	ok	ok	ok
2006b	-	-	-	-
2007a	-	-	-	-
2008a	-	-	-	-
2009a	-	-	-	-

13.2.3. Domain decomposition and the Matlab engine

Since the structural calculation in ABAQUS/Explicit is rather computational intensive a domain decomposition is desirable to reduce wall time for the computation. One of the limitations of ABAQUS in the domain decomposition algorithm is that it is not able to decompose a contact domain, if a contact pair is used, which will therefore always be in one domain. Since this contact domain for the wheel is between the road and the outer surface of the tire, this can be used to determine the fluid pressure using the Matlab engine. The only requirement is to have the subroutine determine if the domain for which the calculation is to be done is the domain that includes the contact. From each domain the subroutine will start a separate Matlab engine. This is clarified in the next figure, the ABAQUS model is decomposed on multiple domains, i.e. on multiple CPUs which can communicate with each other. Each domain runs the subroutine VDLOAD to apply the pressure on the wheel, the pressure is extracted from the stored .mat file. Only the contact domain will run the VUFIELD subroutine as this will be the only domain from which it is possible to reconstruct the wheel geometry for the fluid model. This routine stores the pressure profile in a .mat file.

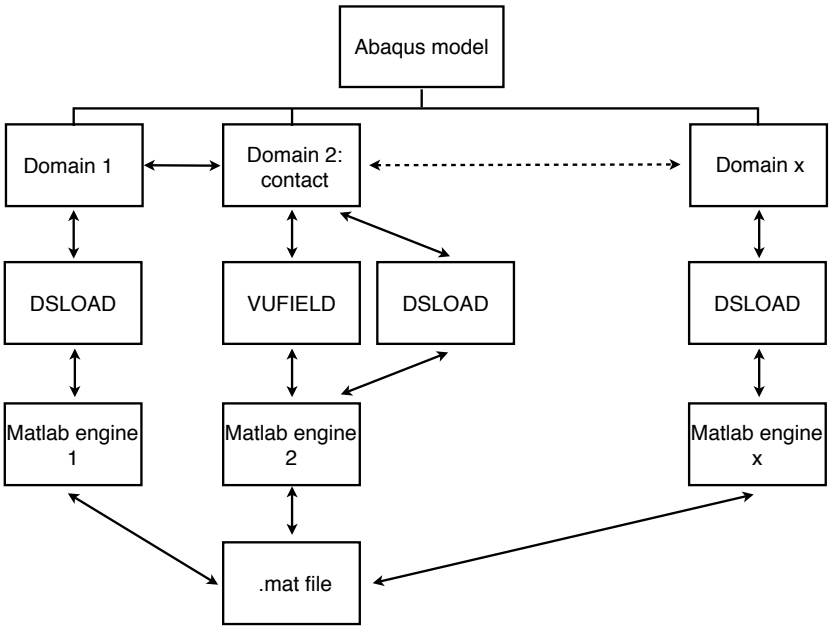

Figure 13.3: Domain decomposition

This way to pass on the information from the domain where the fluid pressure is calculated to the other domains so the VDLOAD routine can apply the surface load is probably the slowest option but the author is up to now unaware how to have multiple matlab engines, running on multiple machine communicating with each other.

Details on how to start the Matlab engine on multiple domains is given in appendix H

13.2.4. Mesh mapping

The ABAQUS tire model is a full 3D model, and therefore a 3D mesh. The Reynolds model is a 2D mesh with only the film height and the velocities of the boundaries as input. It is therefore necessary to map the 3D mesh onto a 2D mesh, which is not a trivial thing to do.

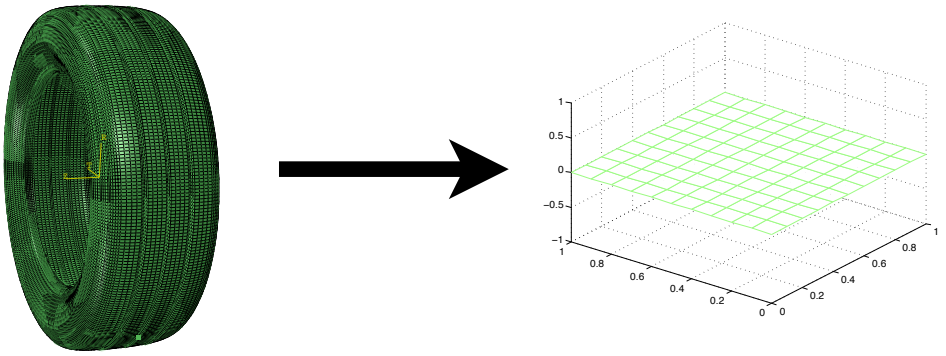

Figure 13.4: Mesh mapping of a 3D mesh onto a 2D mesh

To transfer the mesh from the structure to the fluid several options are possible:

- Direct Delaunay [32] triangulation on the grid points, resulting in a non-equidistant grid
- Using Matlab's griddata [33] algorithm, resulting in an equidistant grid
- Using a smoothing function, such as gridfit [34], to deal with discontinuities

Direct Delaunay triangulation The most simple and straightforward mesh mapping is a direct Delaunay triangulation on the nodes, however this also means that the fluid mesh will be as coarse as the structural mesh which may not be sufficient. Furthermore the nodes must form a convex hull for the algorithm to function adequately. Bad scaling of the nodes, i.e. large variations in length scale over the length and width of the mesh can result in a mesh with nodes hopping. See figure, where the 2D reynolds mesh is plotted with the height at the nodes, resulting in the 3D image:

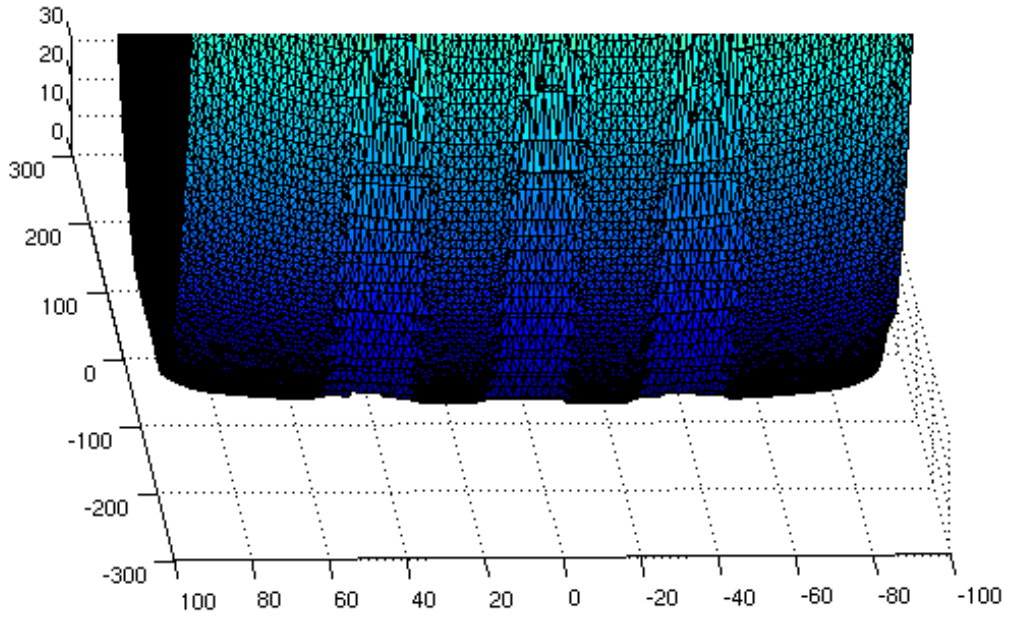

Figure 13.5: Delaunay triangulation failed due to bad scaling, the grooves are not visible

In this figure one cannot see the grooves that are present in the BMW Coarse model 10.2 and the failure of the algorithm is clear. To have the grooves represented two methods are applied, first of all the griddata algorithm and second of all the smooth approximation by the gridfit algorithm, explained in the next sections.

Matlab's Griddata algorithm To deal with the possibility of needing a more refined mesh on the fluid side the griddata algorithm from Matlab is very well suited, the requirement of the convex hull remains but refinement is possible. Next to that the scaling also remains an issue, as griddata uses the Delaunay triangulation first before the refinement is made.

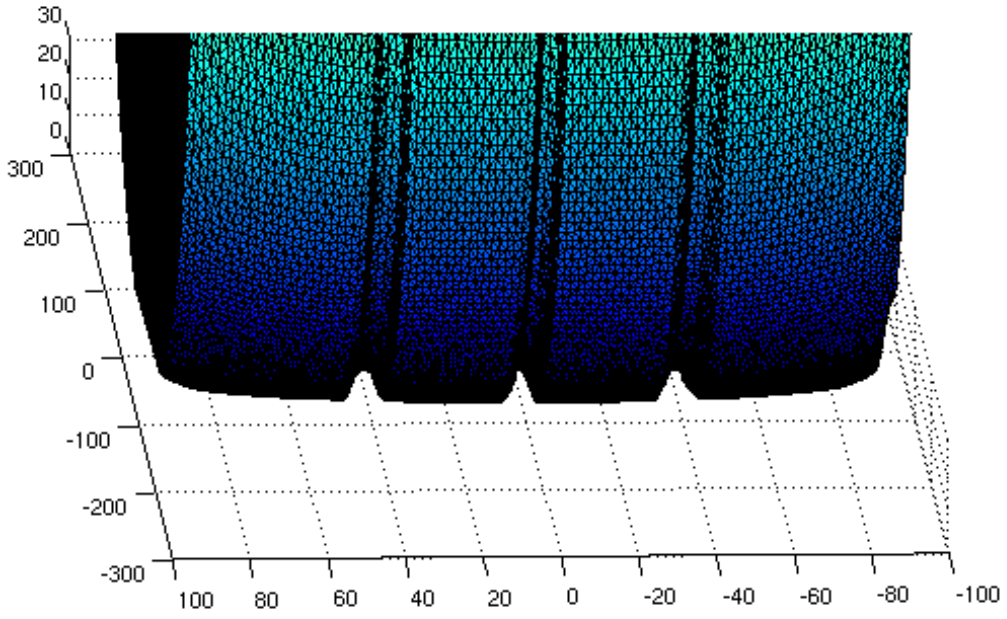

Figure 13.6: Griddata mesh mapping succesfully represents the three grooves and allows mesh refinement on the fluid side

A smooth approximation A solution to deal with the bad scaling is a mesh mapping algorithm where some sort of smoothing is applied. In this work the gridfit function has been used, developed by John D'Errico, available at the Mathworks website [34]. Gridfit solves all of the mentioned problems, although it is not an interpolant. It builds a surface over a complete lattice, extrapolating smoothly into the corners. You have control of the amount of smoothing done, as well as interpolation methods, which solver to use, etc. The algorithm will introduce some extra CPU time in the mesh mapping, depending on the mesh size of course. Furthermore since it is not an interpolant the actual geometry is lost and the approximation might not be sufficiently close to the original geometry.

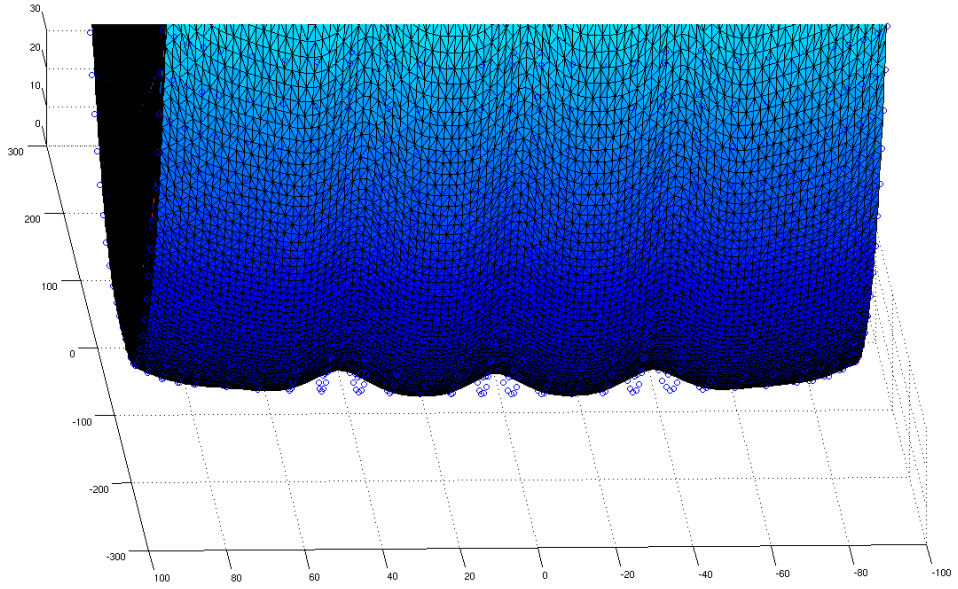

Figure 13.7: Gridfit smooth approximation

To summarize, mesh mapping of a 3D geometry to a 2D mesh is not trivial, either the geometry is represented less accurate, as with the gridfit algorithm, or a refinement on the structural side is necessary which inevitably results in an increase of computational time. For the current simulations the griddata algortihm is chosen as it allows accurate representation of the geometry and the additional computational time is taken for granted for now.

13.3. Summary

Fluid structure interaction is very important in the case of modelling hydroplaning as there is a strong coupling between the incompressible fluid and the highly elastic tire.

Besides classical staggering an interface method has been described that speeds up convergence as it takes into account the behavior of the structre in previous iterations. Next to that a coupling of the Abaqus finite element model to the Reynolds model in Matlab is described, using user subroutines in Fortran. Domain parallelization is possible if the contact is described with the Abaqus contact pair method. However, mesh mapping is an issue and is currently resolved by a structural refinement such that the griddata algorithm can successfully be implemented.

Section V
Results & Recommendations

14. Results

The previous sections have outlined the fluid modelling with different corrections within the fluid film, with different inlet conditions, and a fill rate model. Next to that the structural modelling, i.e. the tire models used, has been outlined for a linear elastic model and several hyper-elastic finite element models. To couple these models a classical staggering has been implemented and an interface model is described to speed up convergence. In this section the results are presented, where the comparison between the different models is made with the lift force. Next to that, for the BMW Coarse tire model a comparison is made of the resulting footprint.

14.1. Grosch wheel, Linear Elastic half space

The deformable Grosch wheel with groove has also been simulated with the ABAQUS CEL method and with an ABAQUS to FlowVision coupling I.1 , results of these simulations have also been incorporated in the comparison as the benchmark. The operating conditions are 214 N normal load, 50, 60 and 70 km/h. The material properties for the tire are: E = 2,05 MPa, ν = 0,5 and for the fluid: $\rho = 1 \cdot 10^3 \frac{kg}{m^3}$ and $\mu = 1 \cdot 10^{-3} Pas$. The water layer thickness is 5 mm.

Table 3: Lift forces in Newton, 50 km/h, 214 N, 5 mm water layer

Model / Boundary condition	Reynolds	Re + Inertia	Fill rate	CEL	FlowVision
$p = 0$	3,14	3,14	3,05	33	16,36
$p = \frac{1}{2}\rho v^2$	25,56	25,56	-	-	-
$p = \frac{1}{2}\rho v^2$ + energy	3,14	3,14	-	-	-
$p = \frac{1}{2}\rho v^2$ + momentum	3,14	3,14	-	-	-

Table 4: Lift forces in Newton, 60 km/h, 214 N, 5 mm water layer

Model / Boundary condition	Reynolds	Re + Inertia	Fill rate	CEL	FlowVision
$p = 0$	3,77	3,77	3,55	48	33,93
$p = \frac{1}{2}\rho v^2$	36,09	36,09	-	-	-
$p = \frac{1}{2}\rho v^2$ + energy	3,77	3,77	-	-	-
$p = \frac{1}{2}\rho v^2$ + momentum	3,77	3,77	-	-	-

One can see that both the energy correction on the inlet pressure and the momentum correction on the inlet pressure convergence to the same value as the Reynolds model without the stagnation pressure at the inlet.

Table 5: Lift forces in Newton, 70 km/h, 214 N, 5 mm water layer

Model / Boundary condition	Reynolds	Re + Inertia	Fill rate	CEL	FlowVision
$p = 0$	4,39	4,39	4,12	64	46,66
$p = \frac{1}{2}\rho v^2$	48,45	48,45	-	-	-
$p = \frac{1}{2}\rho v^2$ + energy	4,39	4,39	-	-	-
$p = \frac{1}{2}\rho v^2$ + momentum	4,39	4,39	-	-	-

The inertia correction has an effect that is smaller than 1% and therefore the thin film assumption, for the Reynolds equation, seems correct.

Also the inlet pressure from the Bernoulli equation seems to be a necessary condition and is therefore implemented in the next models where the Reynolds model is coupled to the ABAQUS model through the user subroutines.

Finally the interface quasi Newton method is compared, this results in the same values but converges faster, it uses half the amount of iterations needed compared to the other staggered scheme.

14.2. Grosch wheel, Hyperelastic, Coupled Matlab with Abaqus

For the Grosch wheel coupled to the Matlab engine only the wheel without the groove gave stable results, the wheel with cavity was only used to test the stability of dry rolling and the wheel with the groove gave unstable results due to the mesh mapping issues. The two different compounds that have been used resulted in no difference for the lift force.

The Grosch wheel without groove, using hyperelastic material with a bulk modulus of 200 MPa and a shear modulus of 2 MPa , solved with ABAQUS and coupled to the Matlab engine gave the following results, using a stagnation pressure at the inlet:

Table 6: Lift forces in Newton, 50 km/h, 214 N, 5 mm water layer

Model / Boundary condition	Reynolds	Re + Inertia	Fill rate	CEL	FlowVision
$p = 0$	-	-	-	-	16,36
$p = \frac{1}{2}\rho v^2$	30,80	-	-	-	-
$p = \frac{1}{2}\rho v^2$ + energy	-	-	-	-	-
$p = \frac{1}{2}\rho v^2$ + momentum	-	-	-	-	-

The results need to be interpreted with care, the lift force has been averaged over a period of rolling of 1 second, in which the lift force is oscillating due to the oscillations of the wheel which were already present in the dry rolling. One observes that for the 50 km/h case the lift force for the hyper elastic model is higher than for the linear elastic

half space, due to the larger deformation a larger full film area is present underneath the wheel.

14.3. Real tire

For the real tire model the following results were obtained, with a normal load of 3924 N (400 kg), rolling at 90 km/h with a water layer of 3 mm.

Table 7: Lift forces in Newton, 90 km/h, 3924 N, 3 mm water layer

Model / Boundary condition	Reynolds	Re + Inertia	Fill rate	CEL	FlowVision
$p = 0$	200	-	-	-	2000
$p = \frac{1}{2}\rho v^2$	2200	-	-	-	-
$p = \frac{1}{2}\rho v^2$ + energy	-	-	-	-	-
$p = \frac{1}{2}\rho v^2$ + momentum	-	-	-	-	-

Next to the lift force also the footprint shape is compared, in this figure the ABAQUS data has been post-processed. The identification block is self explanatory, as well as the parameters block, the conditions block gives the operating conditions and the dimensions/ratio block gives the following factors, which are used to compare different tires:

- ISL: inside shoulder length
- OSL: outside shoulder length
- CL: centerline length
- AFPL: average footprint length
- FSF: footprint shape factor
- CSF: camber sensitivity factor
- CL/SH: centerline length / shoulder length
- N/G: nett area / gross area

The middle left figure indicates the footprint, the middle right gives the contact pressure, the colors match with the pressure sections 1 to 5 as seen in the middle left figure. The bottom figure gives the contact pressure profiles in the sections A to E. Finally the bottom right table gives the weighted average pressure in the different sections of the footprint.

Footprint Contact Pressure Postprocessing - V 571M : ABAQUS
File name : reynolds691
Comment : FSI Footprint @ 90 km/h, Reynolds

IDENTIFICATION		PARAMETERS		
TIRE SIZE :	205/55R16	SURF :	0.5625	mm^2
RIM :	*	RECT :	1.000	
ABAQUS :	6.9.1	PMIN / PMAT :	0.200/0.200	Bar
OPERATOR :	WAPSTRA Henk-Ja	SHOULD. WIDTH :	0.80	
DATE :	OCT 26 2009	C.PRESS LAT/CIRC :	-2.0/-17.9	mm
STEP / INC :	1 /89848	CONTOURING RADIUS:	82.9	mm
		Radius computed by default (APDR: 5.0%)		

CONDITIONS		DIMENSIONS/RATIO					
LOAD :	3923	ISL :	70.50	mm	AFPL :	66.56	mm
INFLATION :	2.20 Bar	OSL :	72.75	mm	FSF :	0.86	
NB OF SECTORS :	360	CL :	61.50	mm	CSF :	1.03	
NB OF NODES :	356400	WIDTH :	168.00	mm	SSI :	-41.62	%
NB OF ELEMENTS :	332640	GROSSAREA:	109.76	cm^2	CL/SH :	0.63	
DEG OF FREEDOM :	2	NETAREA :	78.74	cm^2	N/G :	0.72	

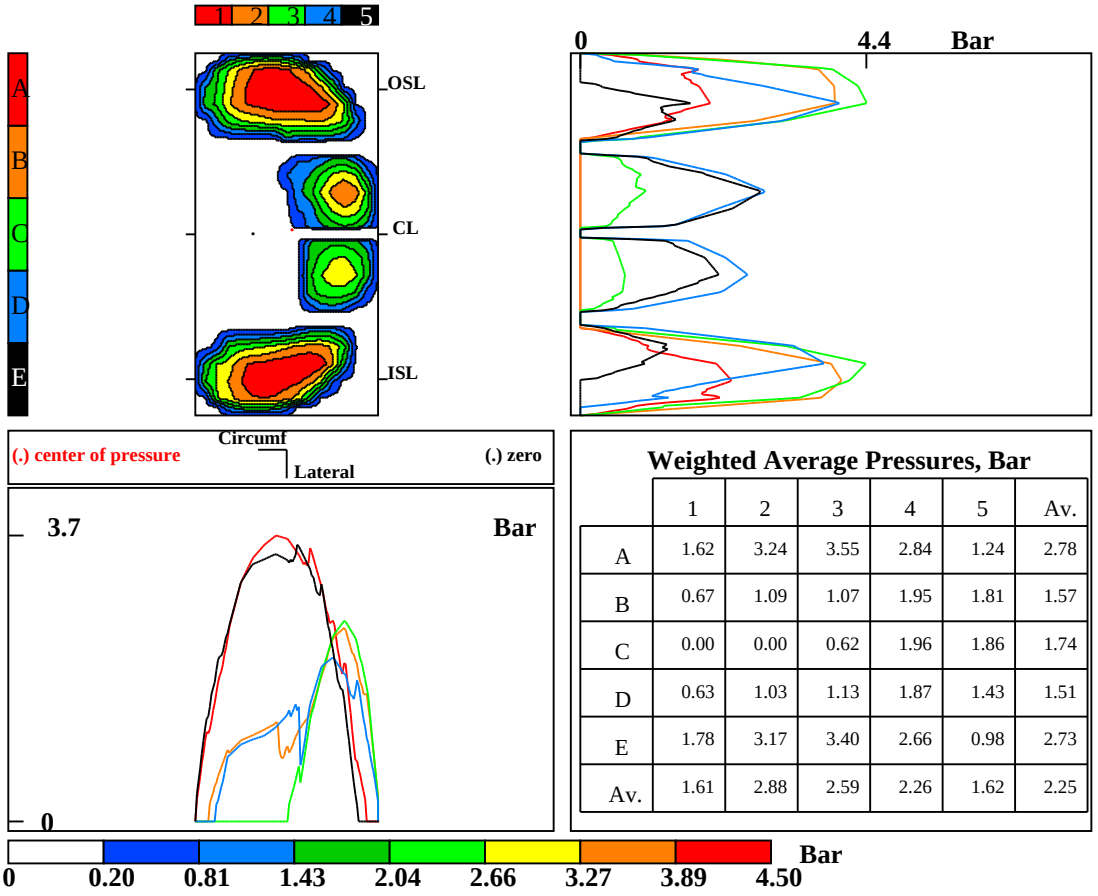

Weighted Average Pressures, Bar

	1	2	3	4	5	Av.
A	1.62	3.24	3.55	2.84	1.24	2.78
B	0.67	1.09	1.07	1.95	1.81	1.57
C	0.00	0.00	0.62	1.96	1.86	1.74
D	0.63	1.03	1.13	1.87	1.43	1.51
E	1.78	3.17	3.40	2.66	0.98	2.73
Av.	1.61	2.88	2.59	2.26	1.62	2.25

Figure 14.1: Reynolds footprint

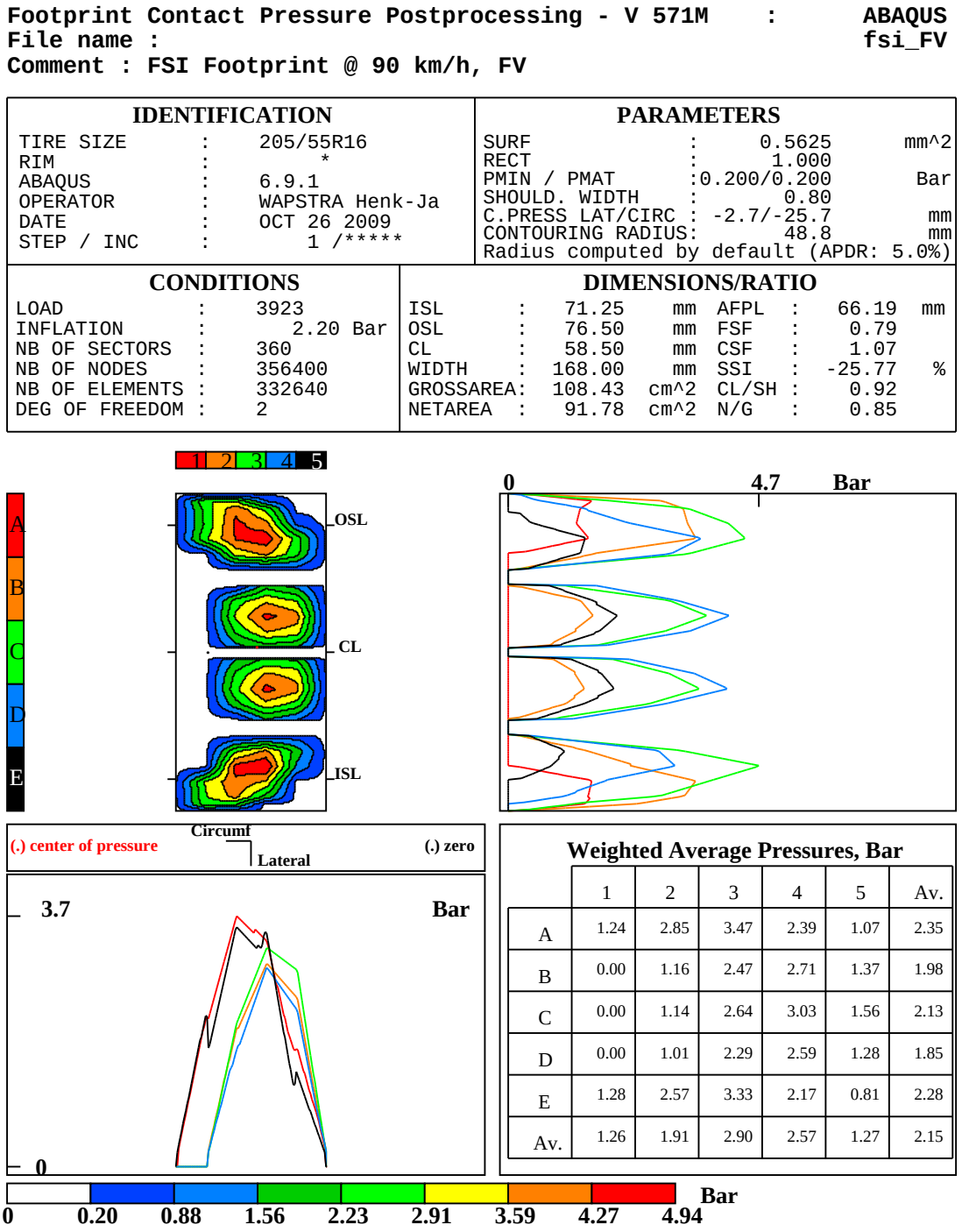

Figure 14.2: FlowVision footprint

These results were obtained after adding to the Matlab code a shift of the road of 1

mm upward to filter the nodes in contact. This was due to the inaccuracy of the contact algorithm resulting in nodes lifted in the footprint and therefore very high pressure peaks within the footprint. One can see that the Reynolds equation with stagnation pressure at the inlet gives an overestimation of the lift force compared to the FlowVision result, which is to be expected as the stagnation over the entire tire width gives an overestimation of the pressure.

Computational time As stated in the introduction the computational time has to be reduced to be able to use the hydroplaning model as a useful tool in tire design. The current models have a CPU time which ranges from 24 to 48 hours on 16 CUPs. The models implemented here are currently just as slow, mainly due to the implementation of the subroutines. A lot of computational time is lost in the file exchange via the .mat file between the Matlab engines. The potential for gain in computational time is clearly present as the fluid modelling is reduces from a 3D model to a 2D model with only one variable, the pressure. The computational time of the fluid code in Matlab is several seconds, the rest of the time is lost in communication with ABAQUS and the file exchange. More efficient ways to implement the Reynolds model need to be investigated.

14.4. Summary

The developed models have been run with different operating conditions, the results show that the assumptions for the Reynolds equation are valid in the footprint region but an inlet condition is needed. The stagnation pressure, $\frac{1}{2}\rho v^2$, gives an over-estimation of the the lift force, the introduced iterative energy and momentum correction converge to zero inlet pressure. The Abaqus tire model gives higher lift forces than the linear elastic model due to the higher deformations in the footprint area.

15. Conclusions & Recommendations

15.1. Fluid modelling

The results obtained are not conclusive but the Reynolds modelling has potential to offer a fast modelling approach for hydroplaning. Since only one variable needs to be solved, the potential for gain in computational time is present. Unfortunately the present analysis has not shown this, due to the slow coupling between Abaqus and Matlab.

The thin film assumption is valid but more work needs to be done on the inlet condition. As can be seen from the results the stagnation pressure results in an overestimation of the pressure profile. A different way to take the inertia effect into account could be the "bulk flow" approximation [35] which is also based on the thin film assumption but includes the inertia terms.

Further improvements that can be made to the fluid model is to include the inlet condition in the fill rate model, as well as taking into account texture effects.

When textures appear in the surfaces fluid flow patterns occur that the Reynolds equation does not accurately describe anymore, mainly due to convective inertia in the textures. One solution would be to solve the full Navier-Stokes equations but this comes with considerable computational cost. To be able to deal with textures in a lubricating film and at the same time take advantage of the computational speed of the Reynolds equation a texture averaged Reynolds equation has been proposed [36]. In this model a distinction is made between the macro and micro level of the fluid flow, at a micro level the fluid flow in the texture is modelled using Navier-Stokes equations. The outcome at micro level are averaged to flow factors which are taken into account on macro level in the Reynolds equation. It is interesting to note that the convective inertia effects can, depending on the scale of the texture, result in either an increase or a reduction of load carrying capacity.

Another option to take textures into account in the Reynolds model would be an Arbitrary Lagrangian Eulerian (ALE) approach which would result in a moving mesh and the patterns can be explicitly defined.

15.2. Structural modelling

The tire model of Abaqus is causing the most problems in the current simulations, the contact algoritm is not accurate enough to have a stable rolling wheel or an accurate footprint for the Reynolds equation. The obtained footprint could be different if an accurate representation of the geometry is passed to the fluid code.

On the other hand the use of the influence matrix can be extended to a more realistic tyre model with a linear elastic model, but also to a hyper-elastic model, by using a linearization around an average indentation, and even to a visco-hyper-elastic model by assuming constant speed and only small deviations of the deformation due to the water layer. This eliminates the need for an Abaqus Matlab coupling and has the most potential for gain in computational time.

15.3. Fluid structure interaction

The coupling scheme could work much faster if the interface quasi Newton method can be implemented in the coupling to the ABAQUS model, but this would require to possibility to interact within a time step. Recommended is to develop an own finite element code to be able to do this. This would also eliminate the necessity to re-mesh every time as the connectivity matrix would be known for the different nodes. If the current coupling is continued then improvements can be made in the mesh mapping algorithm such that the structural model can remain coarser and therefore faster. Other improvements are the elimination of the file exchange to transfer the information along the different Matlab engines.

15.4. Summary

To summarize, the first result are promising for modelling hydroplaning using modified Reynolds equation but more efficient implementation is needed to reduce the current computational times of up to 48 hours on 16 CPUs. The potential is clear as the fluid modelling is reduced from a 3D model to a 2D model with only one variable, the pressure. The structural modelling needs to be more accurate in the footprint. The fluid structure interaction model can converge faster if the interface quasi Newton method is implemented further.

References

[1] E. N. Harrin, “Low tire friction and cornering forces on a wet surface,” Tech. Rep. TN 4406, NACA, 1958.

[2] W. B. Horne and R. C. Dreher, “Phenomena of pneumatic tire hydroplaning,” Tech. Rep. TN D-2056, NASA, 1962.

[3] FAA and NASA, “Joint technical conference on slush drag and braking problems.,” 1961.

[4] E. P. K. Daniel E. Sommers, John F. Marcy and D. W. Conley, “Runway slush effects on the takeoff of a jet transport,” Tech. Rep. 308-3X, FAA, 1962.

[5] D. Moore in *18th Leeds Lyon Conference*.

[6] D. Moore, “A theory of viscous hydroplaning,” *International Journal of Mechanical Sciences*, 1967.

[7] T. K. Y. Nakijima, E. Seta and H. Ogawa, “Hydroplaning analysis by fem and fvm: Effect of tire rolling and tire pattern on hydroplaning,” *International Journal of automotive technology, 1(1):26Ð34*, 2000.

[8] J. S. G. K. J.R. Cho, H.W. Lee and J. Woo, “Numerical investigation of hydroplaning characteristics of three-dimensional patterned tire,” *European Journal of Mechanics A/Solids, 25:914Ð926*, 2006.

[9] M. Zmindak and I. Grajciar, “Simulation of the aquaplane problem,” *Computers Strucrures Vol. 64, No. 5/6, pp. I lSS11*, 1997.

[10] F. Ong, “Modeling of the hydroplaning phenomenon,” tech. rep., Department of Civil Engineering National University of Singapore.

[11] H. C. A. BROWNE and A. KISTLER, “Dynamic hydroplaning of pneumatic tires,” *Wear*, 1971.

[12] P. M. Minh-Tan Do and A. Mosset, “Tribology approach to predict the variation , of tire/wet road friction with slip speed,”

[13] A. J. Peter Andren, “Elastohydrodynamic aspects on the tire-pavement contact at aquaplaning,” Tech. Rep. 438A, Swedish National Road and Transport Research Institute, 2003.

[14] L. B. Robert D. Ervin, “Hydroplaning with lightly-loaded truck tires,” tech. rep., The University of Michigan Transportation Research Institute, 1990.

[15] J. Padovan, “Advanced tire modeling,” *Tire Mechanics Short Course*, 2007.

[16] D. Hays and A. Browne, “Physics of tire traction: Theory and experiment,” 1973.

[17] J. Meyer, W.E. Walter, “Frictional interaction of tire and pavement,” 1981.

[18] A. H. d. W. Claeys, Yi and Richard., "Tire frictional modeling under wet road conditions," 2001.

[19] O. Reynolds, "On the theory of lubrication and its application to mr. b. towers experiments, including an experimental determination of the viscosity of olive oil," *Philosophical transactions of the Royal Society*, vol. 177, pp. 157–234, 1886.

[20] B. Towers, "First report on friction experiments," *Proceedings of the Institution of Mechanical Engineers*, pp. 29 – 35, 632–59, 1884.

[21] Stokes, "On the theories of internal friction of fluids in motion, and of the equilibrium and motion of elastic solids," *Transaction of the Cambridge Philosophical Society*, vol. 8, p. 287.

[22] A. van Beek, *Machine lifetime performance and reliability*. 2004.

[23] B. S. O. Pinkus, *Theory of hydrodynamic lubrication*. McGraw-Hill, 1961.

[24] t. . p. R.A.J. van Ostayen

[25] J. J. Kalker, *Three dimensional elastic bodies in rolling contact*, vol. 2. Kluwer Academic Publishers, 1990.

[26] J. Boussinesq, *APPLICATION DES POTENTIELS À L'ÉTUDE DE L'ÉQUILIBRE ET DU MOUVEMENT DES SOLIDES ÉLASTIQUES*. 1885.

[27] A. Love, *A treatise on the mathematical theory of elasticity*. Dover publications, 1944.

[28] V. M. Gerbeau JF, "A quasi-newton algorithm based on a reduced model for ßuidÐstructure interaction problems in blood ßows," *ESAIM: Math Model Numer Anal*, 2003.

[29] d. B. R. Michler C, van Brummelen E, "An interface newtonÐkrylov solver for ßuidÐstructure interaction," *Int J Numer Methods Fluids*, vol. 47(10Ð11), p. 1189Ð95, 2005.

[30] J. V. Joris Degroote, Klaus-Jrgen Bathe, "Performance of a new partitioned procedure versus a monolithic procedure in ßuidÐstructure interaction," *Computers and Structures*, vol. 87, pp. 793 – 801, 2009.

[31] `http://www.mathworks.com/access/helpdesk/help/techdoc/matlab_external/f29148.html`.

[32] `http://www.mathworks.com/access/helpdesk/help/techdoc/ref/delaunay.html`.

[33] `http://www.mathworks.com/access/helpdesk/help/techdoc/ref/griddata.html`.

[34] http://www.mathworks.com/matlabcentral/fileexchange/8998.

[35] M. A. JEROME GEHANNIN and O. BONNEAU, “private communication,”

[36] D. R. A. de Kraker, R.A.J. van Ostayen, “Development of a texture averaged reynolds equation,” 2008.

[37] G. Batchelor, *An introduction to fluid dynamics*. Cambridge University Press, 1967.

A. Navier Stokes Equations

Derivation of the Navier-Stokes equations, a special case of the continuity equation, beginning with:

Assumption 8. ***Continuum****, The fluid is a continuous substance*

And:

Assumption 9. ***Differentiable****, The fluid parameters are, at least weakly, differentiable*

Next apply the Reynolds transport theorem which states that the changes of a certain property L defined over a control volume Ω must be equal to what is transported through the boundaries plus what is created or lost by a source or sink within the control volume.

$$\frac{d}{dt}\int_{\Omega} L dV = -\int_{\partial\Omega} L\mathbf{v}\cdot\mathbf{n}dA - \int_{\Omega} Q dV \tag{A.1}$$

Where Ω represents the control volume, $\partial\Omega$ the boundary of the control volume, $\mathbf{v}$ the velocity and Q represents the source or sink.

Apply the divergence theorem to the surface integral to change it into a volume integral:

$$\frac{d}{dt}\int_{\Omega} L dV = -\int_{\Omega} \nabla\cdot(L\mathbf{v})\, dV - \int_{\Omega} Q dV \tag{A.2}$$

Apply Leibniz's rule to the first term:

$$\int_{\Omega} \frac{d}{dt} L dV = -\int_{\Omega} \nabla\cdot(L\mathbf{v})\, dV - \int_{\Omega} Q dV \tag{A.3}$$

Combine all terms in one integral:

$$\int_{\Omega} \left(\frac{d}{dt}L + \nabla\cdot(L\mathbf{v}) + Q\right) dV = 0 \tag{A.4}$$

Since this equation must apply to any arbitrary control volume, the integrand must be zero:

$$\frac{d}{dt}L + \nabla\cdot(L\mathbf{v}) + Q = 0 \tag{A.5}$$

First apply this theorem to the conservation of mass, where the property is density, ρ, and there are no sources or sinks:

$$\frac{\partial\rho}{\partial t} + \nabla\cdot(\rho\mathbf{v}) = 0 \tag{A.6}$$

Now, apply this continuity relation to the conservation of momentum, the most general form of the Navier-Stokes equations, where $\rho\mathbf{v}$ is momentum:

$$\frac{d}{dt}\rho\mathbf{v} + \nabla \cdot (\rho\mathbf{v}\mathbf{v}) + Q = 0 \tag{A.7}$$

$\mathbf{v}\mathbf{v}$ is a dyad, a tensor product resulting in a tensor of which the divergence is again a vector. The sink / source term is in this case represented by $\mathbf{b}$ acting on the fluid element. Expand the derivatives:

$$\begin{aligned}
&\frac{\partial\rho}{\partial t}\mathbf{v} + \rho\frac{\partial\mathbf{v}}{\partial\mathbf{t}} + \nabla(\rho\mathbf{v}) \cdot \mathbf{v} + \rho\mathbf{v}\nabla \cdot \mathbf{v} = \mathbf{b} \\
&\frac{\partial\rho}{\partial t}\mathbf{v} + \rho\frac{\partial\mathbf{v}}{\partial\mathbf{t}} + \nabla(\rho)\,\mathbf{v} \cdot \mathbf{v} + \rho\nabla(\mathbf{v}) \cdot \mathbf{v} + \mathbf{v}\rho\nabla \cdot \mathbf{v} = \mathbf{b} \\
&\mathbf{v}\frac{\partial\rho}{\partial t} + \rho\frac{\partial\mathbf{v}}{\partial\mathbf{t}} + \mathbf{v}\mathbf{v} \cdot \nabla\rho + \rho\mathbf{v} \cdot \nabla\mathbf{v} + \rho\mathbf{v}\nabla\mathbf{v} = \mathbf{b}
\end{aligned} \tag{A.8}$$

The derivative of a vector results in a tensor, the covariant derivative. Rearrange:

$$\mathbf{v}\left(\frac{\partial\rho}{\partial t} + \mathbf{v} \cdot \nabla\rho + \rho\nabla \cdot \mathbf{v}\right) + \rho\left(\frac{\partial\mathbf{v}}{\partial t} + \mathbf{v} \cdot \nabla\mathbf{v}\right) = \mathbf{b} \tag{A.9}$$

Observe that:

$$\mathbf{v} \cdot \nabla\rho + \rho\nabla \cdot \mathbf{v} = \nabla \cdot (\rho\mathbf{v}) \tag{A.10}$$

To end up with:

$$\mathbf{v}\left(\frac{\partial\rho}{\partial t} + \nabla \cdot (\rho\mathbf{v})\right) + \rho\left(\frac{\partial\mathbf{v}}{\partial t} + \mathbf{v} \cdot \nabla\mathbf{v}\right) = \mathbf{b} \tag{A.11}$$

Here, one should recognize A.6 so the equation can be simplified to:

$$\rho\left(\frac{\partial\mathbf{v}}{\partial t} + \mathbf{v} \cdot \nabla\mathbf{v}\right) = \mathbf{b} \tag{A.12}$$

Next step is to define the sources/sinks of momentum. In general the distinction is made between body forces and surface forces, where body forces are due to external fields such as gravity, magnetism, electric potential, which act on the entire mass within the element. The surface forces are due to the stresses on the sides of the control surface, observe the following element volume:

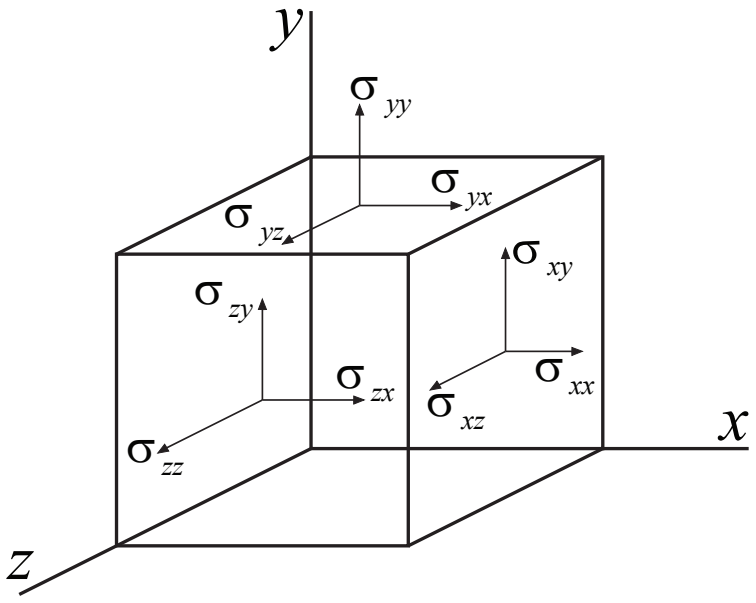

Figure A.1: Control volume with surface forces

The net force on the control volume is due to the gradient of these stresses, see figure where this has been demonstrated for forces in the x-direction:

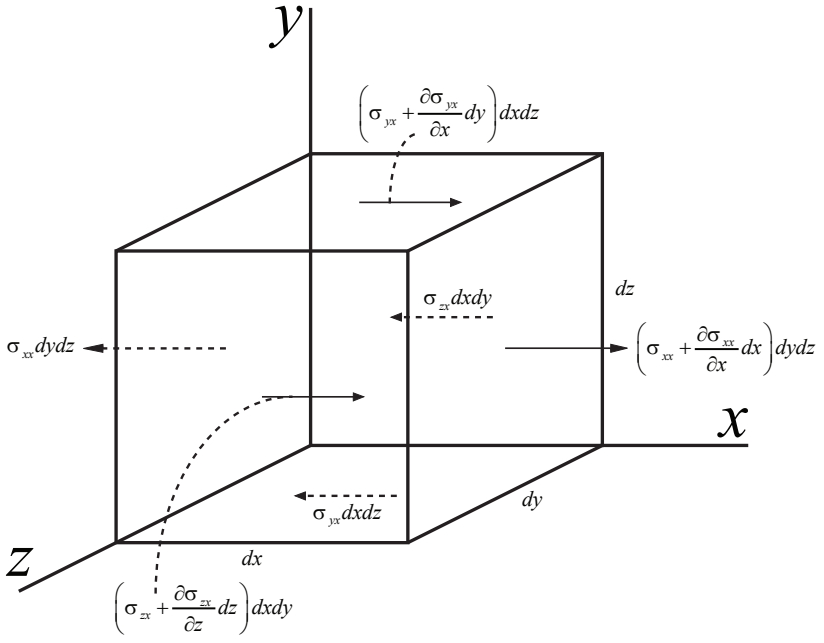

Figure A.2: Control volume with net forces

To end up with the Cauchy momentum equation:

$$\rho\frac{D\mathbf{v}}{Dt} = \nabla\cdot\sigma_{ij} + \mathbf{f} \tag{A.13}$$

Where the stress tensor is defined as:

$$\sigma_{ij} = \begin{pmatrix} \sigma_{xx} & \tau_{xy} & \tau_{xz} \\ \tau_{yx} & \sigma_{yy} & \tau_{yz} \\ \tau_{zx} & \tau_{zy} & \sigma_{zz} \end{pmatrix} \tag{A.14}$$

The stresses are generally written as the sum of the hydrostatic pressure plus the viscous stresses:

$$\sigma_{ij} = -\begin{pmatrix} p & 0 & 0 \\ 0 & p & 0 \\ 0 & 0 & p \end{pmatrix} + \begin{pmatrix} \sigma_{xx} + p & \tau_{xy} & \tau_{xz} \\ \tau_{yx} & \sigma_{yy} + p & \tau_{yz} \\ \tau_{zx} & \tau_{zy} & \sigma_{zz} + p \end{pmatrix} \tag{A.15}$$

Also described as:

$$\rho \frac{D\mathbf{v}}{Dt} = -\nabla p + \nabla \cdot \mathbf{T} + \mathbf{f} \tag{A.16}$$

Where p is the hydrostatic pressure and $\mathbf{T}$ as the deviatoric stress. Now, the following assumptions are made:

Assumption 10. ***Newtonian fluid***

- *The stress tensor is a linear function of the strain rates.*
- *The fluid is isotropic.*
- *For a fluid at rest,* $\nabla \cdot \mathbf{T}$ *must be zero (so that hydrostatic pressure results)*

The stress tensor being a linear function of the velocity gradients is expressed using a fourth order tensor coefficient [37]:

$$T_{ij} = A_{ijkl} \frac{\partial u_k}{\partial x_l} \tag{A.17}$$

This coefficient depends on the state of the fluid and is necessarily symmetrical in indices i and j, now write the velocity gradient as the sum of its symmetrical part (the rate of strain tensor, e_{kl}) and its anti-symmetrical part (the vorticity, ω):

$$\frac{\partial u_k}{\partial x_l} = e_{kl} - \frac{1}{2}\varepsilon_{klm}\omega_m \tag{A.18}$$

Where ε_{klm} indicates the permutation tensor. Now, with the assumption that the fluid is isotropic, the tensor A is an isotropic tensor, having a form where all directional dependence is absent. The basic isotropic tensor is the Kronecker delta tensor and all even order tensors that are isotropic can be written as the sum of products of delta tensors:

$$A_{ijkl} = \mu\delta_{ik}\delta_{jl} + \mu'\delta_{il}\delta_{jk} + \mu''\delta_{ij}\delta_{kl} \tag{A.19}$$

Where μ, μ' and μ'' are scalars. Since A_{ijkl} is symmetrical in i and j:

$$\mu' = \mu'' \tag{A.20}$$

As a result of this the tensor is also symmetric in k and l and therefore the term containing ω drops out:

$$T_{ij} = 2\mu e_{ij} + \mu''\Delta\delta_{ij} \tag{A.21}$$

Where Δ is the rates of expansion $e_{kk} = \nabla \cdot \mathbf{v}$. Since we have also assumed that T_{ij} gives zero contribution to the mean normal stress:

$$T_{ij} = (2\mu + 3\mu'')\,\Delta = 0 \tag{A.22}$$

For all values of Δ, resulting in:

$$(2\mu + 3\mu'') = 0 \tag{A.23}$$

Choosing μ as the only independent variable the deviatoric stress tensor becomes:

$$\mathbf{T}_{ij} = \mu\left(\frac{\partial u_i}{\partial x_j} + \frac{\partial u_j}{\partial x_i}\right) + \delta_{ij}\lambda\nabla\cdot\mathbf{v} \tag{A.24}$$

Where μ is the first viscosity, or simply viscosity, of the fluid and is the second viscosity, related to the bulk viscosity and becomes zero for an incompressible flow.
$2\left(\frac{\partial u_i}{\partial x_j} + \frac{\partial u_j}{\partial x_i}\right)$
Which results in the following form of the Navier Stokes equations for a Newtonian fluid:

$$\rho\frac{Du_i}{Dt} = \rho f_i - \frac{\partial p}{\partial x_i} + \frac{\partial}{\partial x_i}\left\{2\mu\left(e_{ij} - \frac{1}{3}\Delta\delta_{ij}\right)\right\} \tag{A.25}$$

Expanding to obtain:

$$\begin{aligned}
\rho\frac{Du}{Dt} &= -\frac{\partial p}{\partial x} + \frac{\partial}{\partial x}\left(2\mu\frac{\partial u}{\partial x} + \lambda\nabla\cdot\mathbf{v}\right) + \frac{\partial}{\partial y}\left(\mu\left(\frac{\partial u}{\partial y} + \frac{\partial v}{\partial x}\right)\right) + \frac{\partial}{\partial z}\left(\mu\left(\frac{\partial u}{\partial z} + \frac{\partial w}{\partial x}\right)\right) + \rho g_x \\
\rho\frac{Dv}{Dt} &= -\frac{\partial p}{\partial y} + \frac{\partial}{\partial x}\left(\mu\left(\frac{\partial v}{\partial x} + \frac{\partial u}{\partial y}\right)\right) + \frac{\partial}{\partial y}\left(2\mu\frac{\partial v}{\partial y} + \lambda\nabla\cdot\mathbf{v}\right) + \frac{\partial}{\partial z}\left(\mu\left(\frac{\partial v}{\partial z} + \frac{\partial w}{\partial y}\right)\right) + \rho g_y \\
\rho\frac{Dw}{Dt} &= -\frac{\partial p}{\partial z} + \frac{\partial}{\partial x}\left(\mu\left(\frac{\partial w}{\partial x} + \frac{\partial u}{\partial z}\right)\right) + \frac{\partial}{\partial y}\left(\mu\left(\frac{\partial w}{\partial y} + \frac{\partial v}{\partial z}\right)\right) + \frac{\partial}{\partial z}\left(2\mu\frac{\partial w}{\partial z} + \lambda\nabla\cdot\mathbf{v}\right) + \rho g_z
\end{aligned} \tag{A.26}$$

Now, assume:

Assumption 11. ***Incompressibility***

$$\frac{D\rho}{Dt} = 0 \tag{A.27}$$

Combine with the continuity equation A.6, which results in:

$$\rho\left(\nabla\cdot\mathbf{v}\right)=0 \tag{A.28}$$

Now, examine the terms associated with the viscosity in x direction in A.26:

$$\begin{aligned}\frac{\partial}{\partial x}\left(2\mu\frac{\partial u}{\partial x}+\lambda\nabla\cdot\mathbf{v}\right)+\frac{\partial}{\partial y}\left(\mu\left(\frac{\partial u}{\partial y}+\frac{\partial v}{\partial x}\right)\right)+\frac{\partial}{\partial z}\left(\mu\left(\frac{\partial u}{\partial z}+\frac{\partial w}{\partial x}\right)\right)\\ =2\mu\frac{\partial^2 u}{\partial x^2}+\mu\frac{\partial^2 u}{\partial y^2}+\mu\frac{\partial^2 v}{\partial y\,\partial x}+\mu\frac{\partial^2 u}{\partial z^2}+\mu\frac{\partial^2 w}{\partial z\,\partial x}\\ =\mu\frac{\partial^2 u}{\partial x^2}+\mu\frac{\partial^2 u}{\partial y^2}+\mu\frac{\partial^2 u}{\partial z^2}+\mu\frac{\partial^2 u}{\partial x^2}+\mu\frac{\partial^2 v}{\partial y\,\partial x}+\mu\frac{\partial^2 w}{\partial z\,\partial x}\\ =\mu\nabla^2 u+\mu\frac{\partial}{\partial x}\left(\frac{\partial u}{\partial x}+\frac{\partial v}{\partial y}+\frac{\partial w}{\partial z}\right)\end{aligned} \tag{A.29}$$

One clearly observes the last term between brackets as equal to zero due to the incompressibility condition applied to the mass conservation expression. The term associated with viscosity in x-direction therefore reduces to:

$$\mu\nabla^2 u \tag{A.30}$$

Such that the conservation of momentum becomes:

$$\rho\left(\frac{\partial\mathbf{v}}{\partial t}+\mathbf{v}\cdot\nabla\mathbf{v}\right)=-\nabla p+\mu\nabla^2\mathbf{v}+\mathbf{f} \tag{A.31}$$

B. Numerical models to solve the Reynolds equation

B.1. Finite difference model

To solve the Reynolds equation a numerical approach is used, first of all a grid is created, with mesh size dx and dy in respectively x and y direction. A vertical node numbering is used on the nodes, see figure:

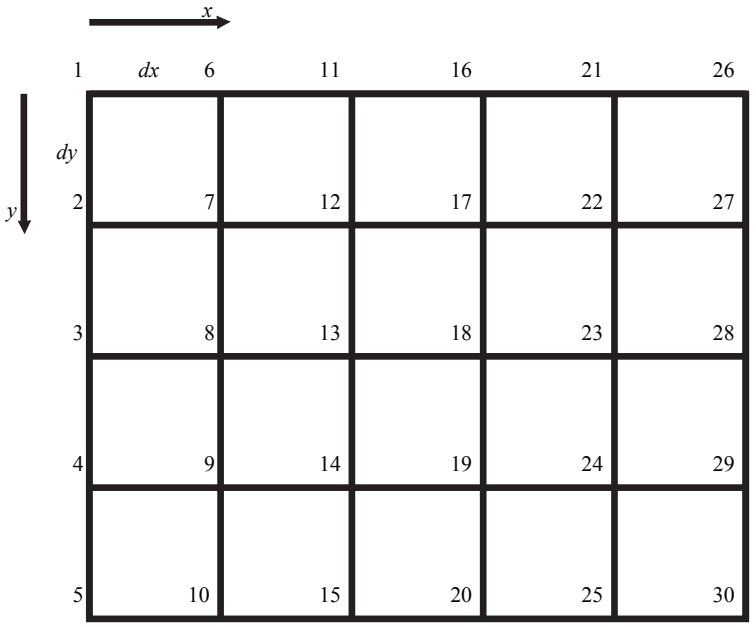

Figure B.1: Mesh with vertical node numbering

Such that the conversion formula for the double index to the single index for the node numbers simply is:

$$\alpha = (i-1)(n_y - 2) + j \tag{B.1}$$

Where n_y is the number of nodes in y-direction.

The governing equations are discretized according to a central difference scheme. The central difference scheme is derived as follows. Assume f a function which satisfies $f \in C^3[a,b]$ and $x-h, x, x+h \in [a,b]$ Then write the second degree Taylor polynomial:

$$f(x+h) = f(x) + f'(x)h + \frac{f^{(2)}(x)h^2}{2!} + \frac{f^{(3)}(c_1)h^3}{3!} \tag{B.2}$$

And:

$$f(x-h) = f(x) - f'(x)h + \frac{f^{(2)}(x)h^2}{2!} - \frac{f^{(3)}(c_2)h^3}{3!} \tag{B.3}$$

Subtract these equations to obtain:

$$f(x+h) - f(x-h) = 2f'(x)h + \frac{f^{(3)}(c_1)h^3 + f^{(3)}(c_2)h^3}{3!} \tag{B.4}$$

Since $f^{(3)}(x)$ is continuous the intermediate value theorem can be used to find a value c such that:

$$\frac{f^{(3)}(c_1) + f^{(3)}(c_2)}{2} = f^{(3)}(c) \tag{B.5}$$

Substitute and rearrange to obtain:

$$f'(x) = \frac{f(x+h) - f(x-h)}{2h} - \frac{f^{(3)}(c)\,h^2}{3!} \tag{B.6}$$

So the truncation error is of order h^2. Apply this to the left hand side of equation 5.15 to obtain:

$$\begin{aligned}
&\frac{\partial}{\partial x}\left(h^3\frac{\partial p}{\partial x}\right) = \frac{h^3_{j,i+\frac{1}{2}}\frac{\partial p_{j,i+\frac{1}{2}}}{\partial x} - h^3_{j,i-\frac{1}{2}}\frac{\partial p_{j,i-\frac{1}{2}}}{\partial x}}{dx} + O\left(h^2\right) \\
&= \frac{h^3_{j,i+\frac{1}{2}}\left(\frac{p_{j,i+1}-p_{j,i}}{dx}\right) - h^3_{j,i-\frac{1}{2}}\left(\frac{p_{j,i}-p_{j,i-1}}{dx}\right)}{dx} + O\left(h^2\right) \\
&= \frac{\left(\frac{h^3_{j,i}+h^3_{j,i+1}}{2}\right)\left(\frac{p_{j,i+1}-p_{j,i}}{dx}\right) - \left(\frac{h^3_{j,i}+h^3_{j,i-1}}{2}\right)\left(\frac{p_{j,i}-p_{j,i-1}}{dx}\right)}{dx} + O\left(h^2\right) \\
&= \frac{\left(h^3_{j,i}+h^3_{j,i+1}\right)\left(p_{j,i+1}-p_{j,i}\right) - \left(h^3_{j,i}+h^3_{j,i-1}\right)\left(p_{j,i}-p_{j,i-1}\right)}{2dx^2} + O\left(h^2\right)
\end{aligned} \tag{B.7}$$

Next apple the central difference to the wedge term:

$$6\eta\left(U_1+U_2\right)\frac{\partial h}{\partial x} = 6\eta\left(U^1_{j,i}+U^2_{j,i}\right)\frac{h_{j,i+1}-h_{j,i-1}}{dx} \tag{B.8}$$

The stretch term:

$$6\eta h\frac{\partial\left(U_1+U_2\right)}{\partial x} = 6\eta h_{j,i}\frac{\left(U^1_{j,i+1}+U^2_{j,i-1}\right)-\left(U^1_{j,i+1}+U^2_{j,i-1}\right)}{2dx} \tag{B.9}$$

The squeeze term is simply:

$$12\eta\frac{\partial h}{\partial t} = 12\eta w_{j,i} \tag{B.10}$$

In Matlab this is implemented and for a vertically numbered grid as shown in figure B.1 one ends up with a matrix of the following shape for the internal elements:

$$
\begin{aligned}
M &= \begin{bmatrix}
A & B & 0 & 0 & D & 0 & 0 & 0 & 0 & 0 \\
C & A & B & 0 & 0 & D & 0 & 0 & 0 & 0 \\
0 & C & A & B & 0 & 0 & D & 0 & 0 & 0 \\
0 & 0 & C & A & B & 0 & 0 & D & 0 & 0 \\
E & 0 & 0 & C & A & B & 0 & 0 & D & 0 \\
0 & E & 0 & 0 & C & A & B & 0 & 0 & D \\
0 & 0 & E & 0 & 0 & C & A & B & 0 & 0 \\
0 & 0 & 0 & E & 0 & 0 & C & A & B & 0 \\
0 & 0 & 0 & 0 & E & 0 & 0 & C & A & B \\
0 & 0 & 0 & 0 & 0 & E & 0 & 0 & C & A
\end{bmatrix} \\
A &= -\frac{h_{j,i-1}^3 + 2h_{j,i}^3 + h_{j,i+1}^3}{2dx^2} - \frac{h_{j-1,i}^3 + 2h_{j,i}^3 + h_{j+1,i}^3}{2dy^2} \\
B &= \frac{h_{j,i}^3 + h_{j+1,i}^3}{2dy^2} \\
C &= \frac{h_{j,i}^3 + h_{j-1,i}^3}{2dy^2} \\
D &= \frac{h_{j,i}^3 + h_{j,i+1}^3}{2dx^2} \\
E &= \frac{h_{j,i}^3 + h_{j,i-1}^3}{2dx^2}
\end{aligned}
\tag{B.11}
$$

Which is a matrix that can be neatly stored using the sparse command. In addition one has to take into account the boundary conditions so matrix M has to be adapted by removing the elements referring to the boundary elements and placing them on the right hand side of the equation. The right hand side is simply built up from the wedge, stretch and squeeze terms.

B.2. Finite Element model

Next to finite difference a finite element model is built, this is more versatile and is the first step towards the fill rate model which is to be implemented later. Start with the Reynolds equation, multiply with a test function and integrate over the domain:

Start with Reynolds:

$$\frac{\partial}{\partial x}\left(\frac{h^3}{12\mu}\frac{\partial p}{\partial x}\right)+\frac{\partial}{\partial y}\left(\frac{h^3}{12\mu}\frac{\partial p}{\partial y}\right)=\frac{U_1+U_2}{2}\frac{\partial h}{\partial x}+\frac{V_1+V_2}{2}\frac{\partial h}{\partial y}+\frac{h}{2}\frac{\partial\left(U_1+U_2\right)}{\partial x}+\frac{h}{2}\frac{\partial\left(V_1+V_2\right)}{\partial y}+\frac{\partial h}{\partial t} \tag{B.12}$$

Or:

$$\nabla\cdot\left(\frac{h^3}{12}\nabla p\right)=\nabla\left(h\bar{U}\right)+\frac{\partial h}{\partial t} \tag{B.13}$$

Multiply with test function, η, and integrate over the domain:

$$\int_\Omega \nabla\cdot\left(\frac{h^3}{12}\nabla p\right)\eta d\Omega=\int_\Omega\left[\nabla\left(h\bar{U}\right)+\frac{\partial h}{\partial t}\right]\eta d\Omega \tag{B.14}$$

Integration by parts:

$$-\int_\Omega \frac{h^3}{12}\nabla p\cdot\nabla\eta d\Omega+\int_\Omega\nabla\cdot\left(\frac{h^3}{12}\eta\nabla p\right)=-\int_\Omega\left(h\bar{U}\right)\nabla\eta d\Omega+\int_\Omega\nabla\cdot\left(h\bar{U}\eta\right)d\Omega+\int_\Omega\frac{\partial h}{\partial t}\eta d\Omega \tag{B.15}$$

Apply divergence theorem to the integral:

$$-\int_\Omega \frac{h^3}{12}\nabla p\cdot\nabla\eta d\Omega+\int_{\partial\Omega}\left(\frac{h^3}{12}\eta\nabla p\right)\cdot\mathbf{n}\partial\Omega=-\int_\Omega\left(h\bar{U}\right)\nabla\eta d\Omega+\int_{\partial\Omega}\left(h\bar{U}\eta\right)\cdot\mathbf{n}d\Omega+\int_\Omega\frac{\partial h}{\partial t}\eta d\Omega \tag{B.16}$$

With the natural boundary condition the boundary integral vanishes. Now apply Galerkin's method, approximating the solution with a finite linear combination of basis functions:

$$p^n\left(\mathbf{x}\right)=\sum_{j=1}^{N}a_j\varphi_j\left(\mathbf{x}\right) \tag{B.17}$$

Since the test function is in the same space as p it is natural to demand that the test function is a linear combination of N basis functions:

$$\eta=\sum_{j=1}^{N}b_i\varphi_i\left(\mathbf{x}\right) \tag{B.18}$$

Also the driving terms are expressed in their nodal values:

$$\begin{aligned} \bar{U}(\mathbf{x}) &= \sum_{j=1}^{N} u_j \varphi_j \\ \tfrac{\partial h}{\partial t}(\mathbf{x}) &= \sum_{j=1}^{N} \tfrac{\partial h}{\partial t}_j \varphi_j \end{aligned} \tag{B.19}$$

to end up with N linear equations:

$$\sum_{j=1}^{N} -a_j \int_{\Omega} \frac{h^3}{12\mu} \nabla\varphi_j \cdot \nabla\varphi_i d\Omega = \int_{\Omega} f\varphi_j d\Omega \tag{B.20}$$

The element matrix and the element vector then become.

$$K_e = -\int_{\Omega} \frac{h^3}{12\mu} \left(\frac{\partial\varphi_i}{\partial x}\frac{\partial\varphi_j}{dx} + \frac{\partial\varphi_i}{\partial y}\frac{\partial\varphi_j}{dy} \right) d\Omega \tag{B.21}$$

$$\begin{aligned} K_{U_x} &= \int_{\Omega} h\tfrac{\partial\varphi_i}{\partial x}\varphi_j d\Omega \\ K_{U_x} &= \int_{\Omega} h\tfrac{\partial\varphi_i}{\partial y}\varphi_j d\Omega \\ K_{\frac{\partial h}{\partial t}} &= \int_{\Omega} \varphi_i\varphi_j d\Omega \\ F &= [K_{U_x}]\bar{U}_x + [K_{U_x}]\bar{U}_x + \left[K_{\frac{\partial h}{\partial t}}\right]\frac{\partial h}{\partial t} \end{aligned} \tag{B.22}$$

Next step is to define the shape functions for the elements. The chosen elements are the simplest for a 2D model, the linear triangle. The element look like:

For the linear triangular element the shape functions are:

$$\begin{aligned} \varphi_1 &= a_0^1 + a_1^1 x^1 + a_2^1 y^1 \\ \varphi_2 &= a_0^2 + a_1^2 x^2 + a_2^2 y^2 \end{aligned} \tag{B.23}$$

The area of the element is defined as:

$$\Delta = (x_2 - x_1)(y_3 - y_2) - (y_2 - y_1)(x_3 - x_2) \tag{B.24}$$

And the coefficients can then be defined as:

$$\begin{aligned} a_1^i &= \tfrac{1}{\Delta}\begin{bmatrix} y_2 - y_3 \\ y_3 - y_1 \\ y_1 - y_2 \end{bmatrix} \\ a_2^i &= \tfrac{1}{\Delta}\begin{bmatrix} x_3 - x_2 \\ x_1 - x_3 \\ x_2 - x_1 \end{bmatrix} \end{aligned} \tag{B.25}$$

The element matrix and vector can be determined by using the Newton-Cotes integration rule:

$$K_p^e(k,l) = a\frac{|\Delta|}{72\mu}\left(h^3(\mathbf{x_1}) + h^3(\mathbf{x}_2) + h^3(\mathbf{x}_3)\right)\left(a_1^k a_1^l + a_2^k a_2^l\right) \tag{B.26}$$

$$K_{U_x}^e(k,l) = -\frac{|\Delta|}{6}h(\mathbf{x}_l)\, a_1^k \tag{B.27}$$

$$K_{U_x}^{e}(k,l) = -\frac{|\Delta|}{6} h(\mathbf{x}_l)\, a_2^k \tag{B.28}$$

For the element generation the Delaunay algorithm is used in Matlab, this uses the Qhull algorithm to return a set of triangles such that no data points are inside the circle that circumscribes the triangle.

C. Benchmark problems Reynolds

C.1. Numerical Model Validation

To determine the correct implementation several analytical solutions of the Reynolds equations are compared to the numerical results. The following analytical solutions are tested for the wedge terms in he Reynolds equation: converging wedge, Rayleigh step bearing, Rayleigh step with zero film thickness and a tapered land pad. The squeeze terms are validated using a band on flat and a solution from a full 3D code.

C.1.1. Analytical solutions, purely driven by wedge terms

Converging wedge The converging wedge is defined by the following geometry, with the bottom surface moving horizontally with velocity U so fluid at the botom is moved with velocity U and the fluid velocity at the top of the wedge is zero.

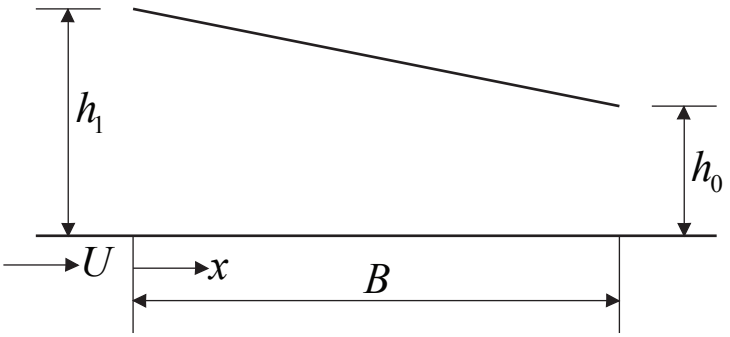

Figure C.1: Converging wedge

Let us define the Couette film thickness h_c which is the film thickness at the point where the pressure gradient is zero and the pressure reaches its maximum. At this point there is a pure Couette flow with a film thickness h_c, the flow is then given by:

$$q_c = \frac{1}{2} U h_c \tag{C.1}$$

Use equation 5.15 and take only terms in x-direction, drop the stretch and squeeze effect to obtain:

$$\frac{dp}{dx} = 6\eta U \frac{h - h_c}{h^3} \tag{C.2}$$

Integrate to obtain:

$$p\left(x\right) = 6\eta U \int \frac{h - h_c}{h^3} dx + C_2 \tag{C.3}$$

The boundary conditions to solve this problem are:

$$\begin{aligned} p\left(x=0\right)&=0\\ p\left(x=B\right)&=0 \end{aligned} \tag{C.4}$$

Substitute:

$$\begin{aligned} 0&=6\eta U\int_0^B \frac{h-h_c}{h^3}dx\\ h_c&=\frac{\int_0^B \frac{1}{h^2}dx}{\int_0^B \frac{1}{h^3}dx} \end{aligned} \tag{C.5}$$

With the given height profile:

$$h\left(x\right)=h_1-\frac{h_1-h_0}{B}x \tag{C.6}$$

Evaluate to obtain:

$$\frac{h_c}{h_0}=\frac{2n}{n-1}, n=\frac{h_1}{h_0} \tag{C.7}$$

Substitute and evaluate:

$$p\left(x\right)=6\eta U\int_0^x \frac{h-h_c}{h^3}dx \tag{C.8}$$

$$p\left(\bar{x}\right)=\frac{\eta UB}{h_0^2}\cdot\frac{6\left(n-1\right)\left(1-\bar{x}\right)\bar{x}}{\left(n+1\right)\left(n-\bar{x}n+\bar{x}\right)^2}, \bar{x}=\frac{x}{B} \tag{C.9}$$

The output of the numerical model compared to the analytical solution, for the numerical model the following parameters are used:

- $B=50mm$
- $L=1m$
- $h_0=1mm$
- $h_1=2mm$
- $\eta == 1\cdot 10^{-3}$
- $U=1$

Since the analytical solution is 1D, a plate is simulated with a length of 1m, to mimic the infinite length, and the pressure profiles are compared in the middle of the plate. is:

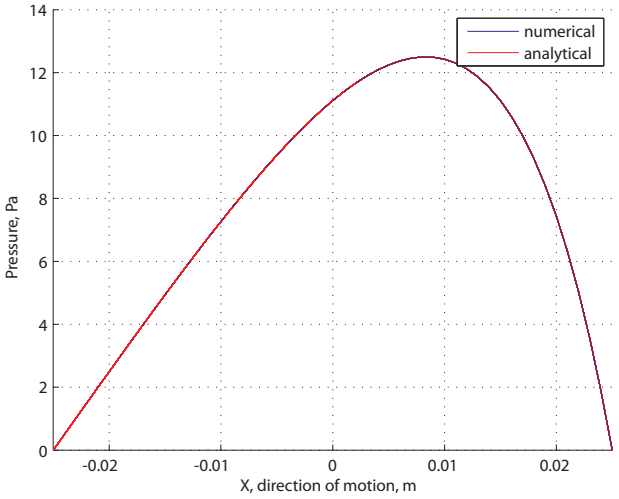

Figure C.2: Converging wedge

Showing very good accordance of the model with the analytical solution.

Tapered land pad Next test problem is a tapered land pad, with the following geometry:

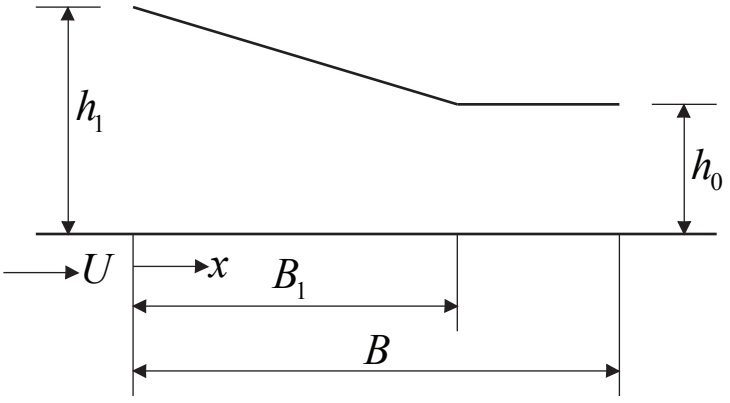

Figure C.3: Tapered land pad

Calculating the pressure distribution of the tapered land pad is similar to that of the wedge, where the difference if a boundary condition $p\,(x = B_1) = p_1$ and a linear pressure drop from p_1 to the end of the land pad where $p\,(x = B) = 0$. Equating the flow in both sections gives:

$$\frac{-h^3}{12\eta}\frac{dp}{dx} + \frac{Uh}{2} = \frac{-h_0^3}{12\eta}\frac{-p_1}{B - B_1} + \frac{Uh_0}{2} \tag{C.10}$$

Rearrange:

$$\frac{dp}{dx} = \left(\frac{h_0}{h}\right)^3 \frac{p_1}{B_1 - B} + 6\eta U \frac{h - h_0}{h^3} \tag{C.11}$$

Integrate:

$$p\left(x\right) = \int_0^x \left(\frac{h_0}{h}\right)^3 \frac{p_1}{B_1 - B} + 6\eta U \frac{h - h_0}{h^3} dx \tag{C.12}$$

$h\left(x\right)$ as shown in figure C.3 and the definition for p_1 the equation can be rewritten to:

$$p_1 = \int_0^{B_1} \left(\frac{h_0}{h}\right)^3 \frac{p_1}{B_1 - B} + 6\eta U \frac{h - h_0}{h^3} dx \tag{C.13}$$

Which gives:

$$p_1 = \frac{6\eta U B}{h_0^3} \frac{\bar{B}\left(\bar{B} - 1\right)\left(n - 1\right)}{-2n^2 + 2n^2\bar{B} - n\bar{B} - \bar{B}}, \bar{B} = \frac{B_1}{B}, n = \frac{h_1}{h_0} \tag{C.14}$$

Substitute to obtain the resulting pressure profile. The comparison of the analytical solution with the numerical model is, with the following parameters:

- $B = 50m$
- $L = 1000m$
- $h_0 = 1m$
- $h_1 = 2m$
- $\eta == 1 \cdot 10^{-6}$
- $U = 1000$

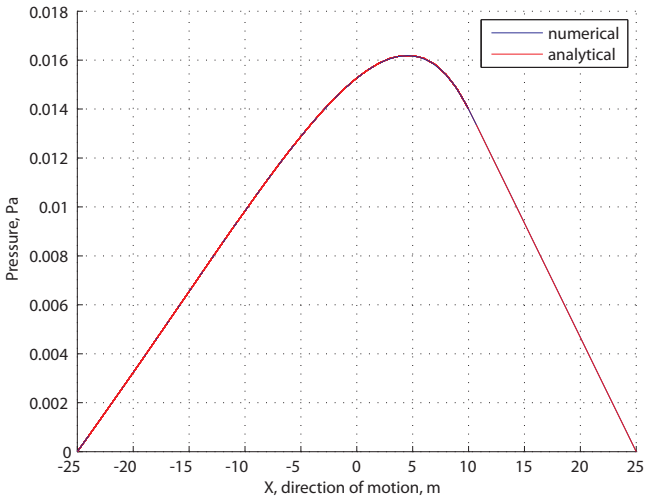

Figure C.4: Tapered land pad

Again, good accordance with the numerical model and the analytical solution.

Rayleigh step bearing The next test problem is a Rayleigh step bearing which is given by:

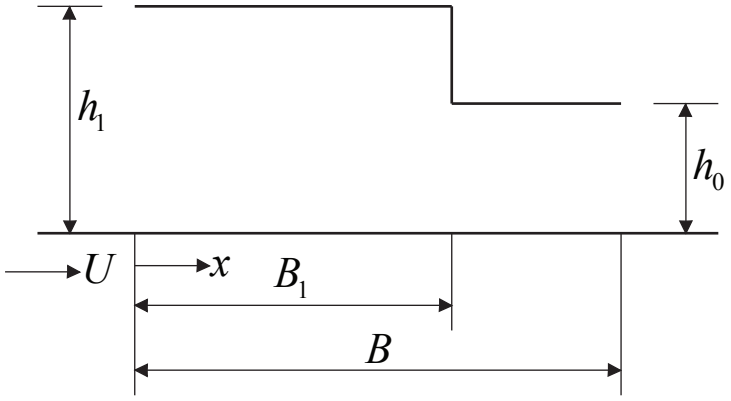

Figure C.5: Rayleigh step

For the parallel sections the pressure distribution is given by:

$$p\left(x\right) = 6\eta U \frac{h - h_c}{h^3} x + C_2 \tag{C.15}$$

Showing a linear relation between pressure and distance, for the step bearing a linear increase is expected to B_1 and a linear decrease from B_1 to B, the maximum pressure is then found by equating the flow on both sides:

$$\frac{-h_1^3}{12\eta}\frac{p_{\max}}{B_1} + \frac{Uh_1}{2} = \frac{-h_0^3}{12\eta}\frac{p_{\max}}{B - B_1} + \frac{Uh_0}{2} \tag{C.16}$$

Giving for the maximum pressure:

$$p_{\max} = \frac{\eta U B}{h_0^2}\frac{6\bar{B}\left(\bar{B}-1\right)(n-1)}{-n^3 + n^3\bar{B} - \bar{B}}, \bar{B} = \frac{B_1}{B}, n = \frac{h_1}{h_0} \tag{C.17}$$

And the entire pressure profile is determined. The numerical model uses the following parameters:

- $B = 50m$
- $L = 1000m$
- $h_0 = 1m$
- $h_1 = 2m$
- $\eta = 1 \cdot 10^{-6}$
- $U = 1000$

The results are:

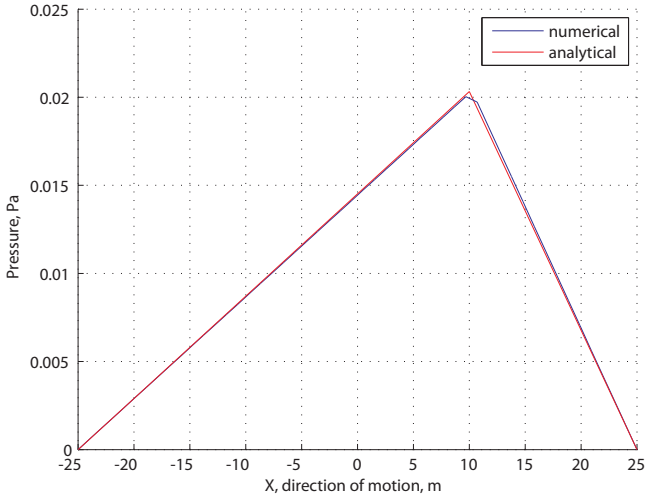

Figure C.6: Rayleigh step

Again, good accordance between the solutions, the only difference is around the pressure peak as the analytical model makes a direct step from h_1 to h_0 whereas the numerical model needs on step of distance dx to change the height from h_1 to h_0.

C.1.2. Analytical solutions, purely driven by squeeze terms

The squeeze terms are validated using a band on flat and a circular disc on flat.

Band on flat A band on flat describes a band being squeezed towards a surface, as shown in figure C.7.

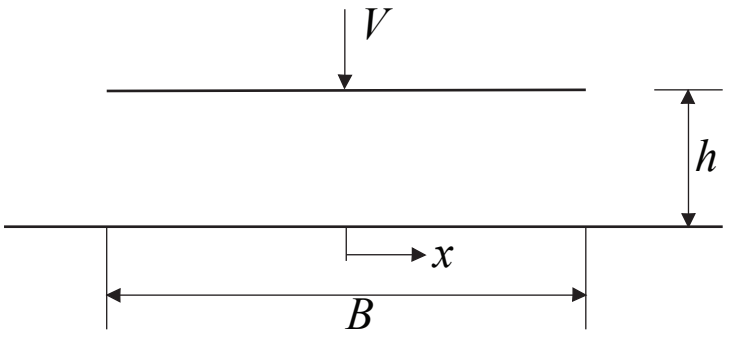

Figure C.7: Band on flat

Using the Reynolds equation with only the squeeze terms:

$$\frac{\partial}{\partial x}\left(\frac{h^3}{12\eta}\frac{\partial p}{\partial x}\right) = \frac{dh}{dt} \tag{C.18}$$

Integrate:

$$\frac{h^3}{12\eta}\frac{\partial p}{\partial x} = \frac{dh}{dt}x + C_1 \tag{C.19}$$

With boundary condition $\frac{\partial p}{\partial x}(x = 0) = 0$, C_1 becomes zero. Apply a second integration:

$$p(x) = \frac{12\eta\frac{dh}{dt}}{h^3}\frac{1}{2}x^2 + C_2 \tag{C.20}$$

With boundary condition $p\left(x = -\frac{B}{2}\right) = 0$ the resulting pressure profile is:

$$p(x) = -\frac{6\eta\frac{dh}{dt}}{h^3}\left(x^2 - \left(\frac{B}{2}\right)^2\right) \tag{C.21}$$

The numerical model uses the following parameters:

- $B = 50mm$
- $L = 1m$
- $h_0 = 5.1mm$
- $\eta == 1 \cdot 10^{-3}$

- $\frac{dh}{dt} = -1 \frac{mm}{s}$

The results are:

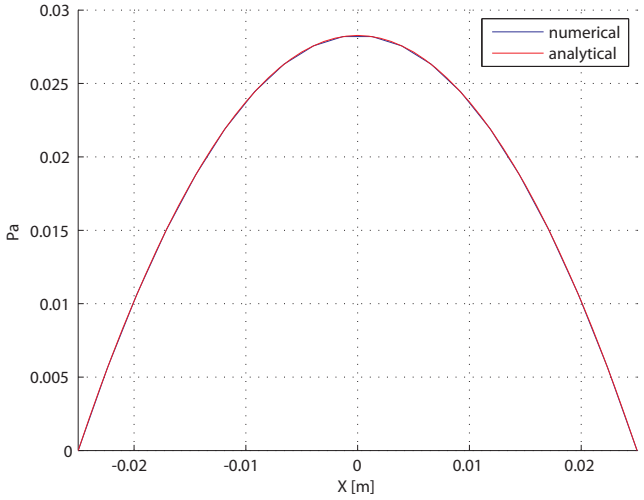

Figure C.8: Band on flat, numerical versus analytical

The results match quite well, again a L of $1m$ has been chosen to apply a 2D model and compare the pressure in the middle with the analytical solution.

Circular disc The circular disc on flat has the following geometry:

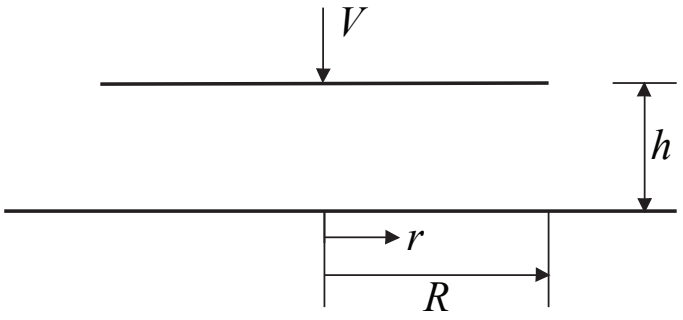

Figure C.9: Circular disc on flat

Apply the Navier-Stokes equations for an incompressible Newtonian fluid in cylindrical coordinates:

$$\begin{aligned}
&\rho\left(\frac{\partial u_r}{\partial t}+u_r\frac{\partial u_r}{\partial r}+\frac{u_\theta}{r}\frac{\partial u_r}{\partial \theta}+u_z\frac{\partial u_r}{\partial z}-\frac{u_\theta^2}{r}\right)=-\frac{\partial p}{\partial r}+\\
&\mu\left[\frac{1}{r}\frac{\partial}{\partial r}\left(\frac{1}{r}\frac{\partial u_r}{\partial r}\right)+\frac{1}{r^2}\frac{\partial^2 u_r}{\partial \theta^2}+\frac{\partial^2 u_r}{\partial z^2}-\frac{u_r}{r^2}-\frac{2}{r^2}\frac{\partial u_\theta}{\partial \theta}\right]+\rho g_r\\
&\rho\left(\frac{\partial u_\theta}{\partial t}+u_r\frac{\partial u_\theta}{\partial r}+\frac{u_\theta}{r}\frac{\partial u_\theta}{\partial \theta}+u_z\frac{\partial u_\theta}{\partial z}-\frac{u_r u_\theta}{r}\right)=-\frac{1}{r}\frac{\partial p}{\partial \theta}+\\
&\mu\left[\frac{1}{r}\frac{\partial}{\partial r}\left(\frac{1}{r}\frac{\partial u_\theta}{\partial r}\right)+\frac{1}{r^2}\frac{\partial^2 u_\theta}{\partial \theta^2}+\frac{\partial^2 u_\theta}{\partial z^2}+\frac{2}{r^2}\frac{\partial u_r}{\partial \theta}-\frac{u_\theta}{r^2}\right]+\rho g_\theta\\
&\rho\left(\frac{\partial u_z}{\partial t}+u_r\frac{\partial u_z}{\partial r}+\frac{u_\theta}{r}\frac{\partial u_z}{\partial \theta}+u_z\frac{\partial u_z}{\partial z}\right)=-\frac{\partial p}{\partial z}+\\
&\mu\left[\frac{1}{r}\frac{\partial}{\partial r}\left(\frac{1}{r}\frac{\partial u_z}{\partial r}\right)+\frac{1}{r^2}\frac{\partial^2 u_z}{\partial \theta^2}+\frac{\partial^2 u_z}{\partial z^2}\right]+\rho g_z
\end{aligned} \tag{C.22}$$

With the continuity equation:

$$\frac{1}{r}\frac{\partial}{\partial r}\left(r u_r\right)+\frac{1}{r}\frac{\partial u_\theta}{\partial \theta}+\frac{\partial u_z}{\partial z}=0 \tag{C.23}$$

In case of axi-symmetric flow this can be reduced to:

$$\begin{aligned}
&\rho\left(\frac{\partial u_r}{\partial t}+u_r\frac{\partial u_r}{\partial r}+u_z\frac{\partial u_r}{\partial z}\right)=-\frac{\partial p}{\partial r}+\\
&\mu\left[\frac{1}{r}\frac{\partial}{\partial r}\left(\frac{1}{r}\frac{\partial u_r}{\partial r}\right)+\frac{\partial^2 u_r}{\partial z^2}-\frac{u_r}{r^2}\right]+\rho g_r\\
&\rho\left(\frac{\partial u_z}{\partial t}+u_r\frac{\partial u_z}{\partial r}+u_z\frac{\partial u_z}{\partial z}\right)=-\frac{\partial p}{\partial z}+\\
&\mu\left[\frac{1}{r}\frac{\partial}{\partial r}\left(\frac{1}{r}\frac{\partial u_z}{\partial r}\right)+\frac{\partial^2 u_z}{\partial z^2}\right]+\rho g_z
\end{aligned} \tag{C.24}$$

With the continuity equation:

$$\frac{1}{r}\frac{\partial}{\partial r}\left(r u_r\right)+\frac{\partial u_z}{\partial z}=0 \tag{C.25}$$

Again, with assumption 5 the squeeze film thickness is much smaller than the radius of the squeeze surface thus:

$$\begin{aligned}
&h \ll r\\
&\frac{\partial p}{\partial z} \ll \frac{\partial p}{\partial r}
\end{aligned} \tag{C.26}$$

Then, the Navier-Stokes equations can be reduced to:

$$\rho\left(\frac{\partial u_r}{\partial t}+u_r\frac{\partial u_r}{\partial r}+u_z\frac{\partial u_r}{\partial z}\right)=-\frac{\partial p}{\partial r}+\mu\left[\frac{\partial^2 u_r}{\partial z^2}\right] \tag{C.27}$$

In line with the thin film assumption, the inertia of the flow can be neglected, reducing to the simple equation:

$$\frac{\partial p}{\partial r} = \mu \left[\frac{\partial^2 u_r}{\partial z^2} \right] \tag{C.28}$$

To solve this differential equation apply assumption 7, resulting in boundary conditions:

$$\begin{aligned} u_r\left(z = 0\right) &= 0 \\ u_r\left(z = h\right) &= 0 \end{aligned} \tag{C.29}$$

Integrate twice to obtain:

$$u_r = \frac{1}{2\mu}\frac{\partial p}{\partial r}\left(z^2 - hz\right) \tag{C.30}$$

Substitute the velocity profile in the continuity equation:

$$\frac{1}{r}\frac{\partial}{\partial r}\left(r\frac{1}{2\mu}\frac{\partial p}{\partial r}\left(z^2 - hz\right)\right) + \frac{\partial u_z}{\partial z} = 0 \tag{C.31}$$

Integrate with respect to z with boundary conditions:

$$\begin{aligned} u_z\left(z = 0\right) &= 0 \\ u_z\left(z = h\right) &= \frac{dh}{dt} \end{aligned} \tag{C.32}$$

To obtain:

$$\begin{aligned} &\int_0^h \frac{1}{r}\frac{\partial}{\partial r}\left(r\frac{1}{2\mu}\frac{\partial p}{\partial r}\left(z^2 - hz\right)\right) + \frac{\partial u_z}{\partial z} dz = 0 \\ &\int_0^h \frac{\partial}{\partial r}\left(r\frac{1}{2\mu}\frac{\partial p}{\partial r}\left(z^2 - hz\right)\right) dz = r\int_0^h \frac{\partial u_z}{\partial z} dz \\ &\frac{\partial}{\partial r}\left(r\frac{1}{2\mu}\frac{\partial p}{\partial r}\left(\frac{z^3}{3} - \frac{hz^2}{2}\right)\right)_0^h = r\frac{dh}{dt} \\ &\frac{\partial}{\partial r}\left(rh^3\frac{\partial p}{\partial r}\right) = 12\mu r\frac{dh}{dt} \end{aligned} \tag{C.33}$$

The boundary conditions on the pressure are:

$$\begin{aligned} p\left(r = R\right) &= 0 \\ \frac{\partial p}{\partial r}\left(r = 0\right) &= 0 \end{aligned} \tag{C.34}$$

Resulting in:

$$p = -\frac{3\mu\frac{dh}{dt}}{h^3}\left(R^2 - r^2\right) \tag{C.35}$$

The comparison with the numerical model is in this case not straightforward as the code works with rectangular grids, however a square with the same surface area should yield similar results. The parameters for the numerical model are:

- $r = 25mm$
- $B = \sqrt{\pi \cdot r^2}$
- $L = B$
- $h_0 = 0.2mm$
- $\eta = 1 \cdot 10^{-3}$
- $\frac{dh}{dt} = -7.84428 \frac{km}{h}$

With the following results:

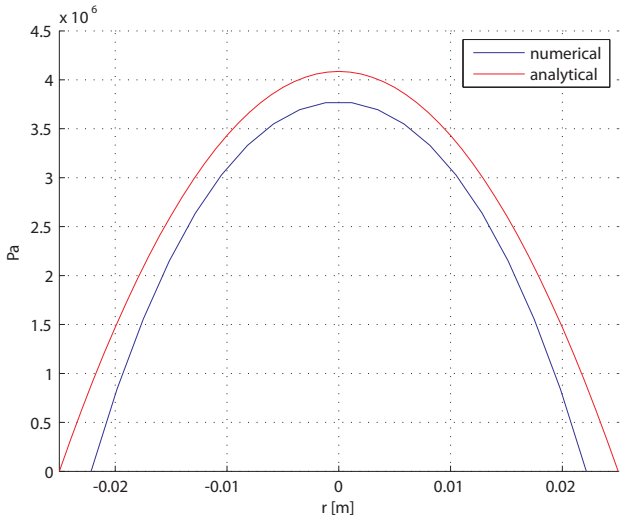

Figure C.10: Circular disc on flat, numerical and analytical

One can observe that the square plate gives a slightly lower pressure, but the order of magnitude is more or less the same.

Vertical tread block The next validation model is a vertical tread block of 50mm by 50mm with a V-shaped groove, at an inclination of 5 degrees. The groove is 5 mm deep and 2 mm wide. See figure:

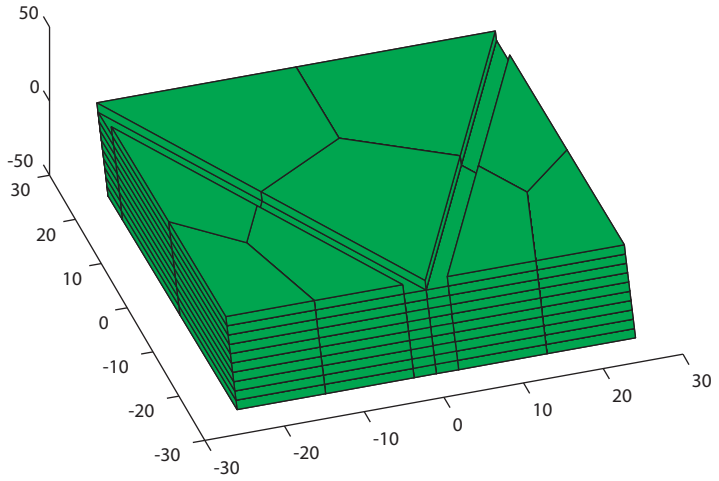

Figure C.11: Vertical tread block

The block is placed on a surface covered with 13.5 mm of water and is given a velocity of 7.8 km/h. The output of the CEL model is:

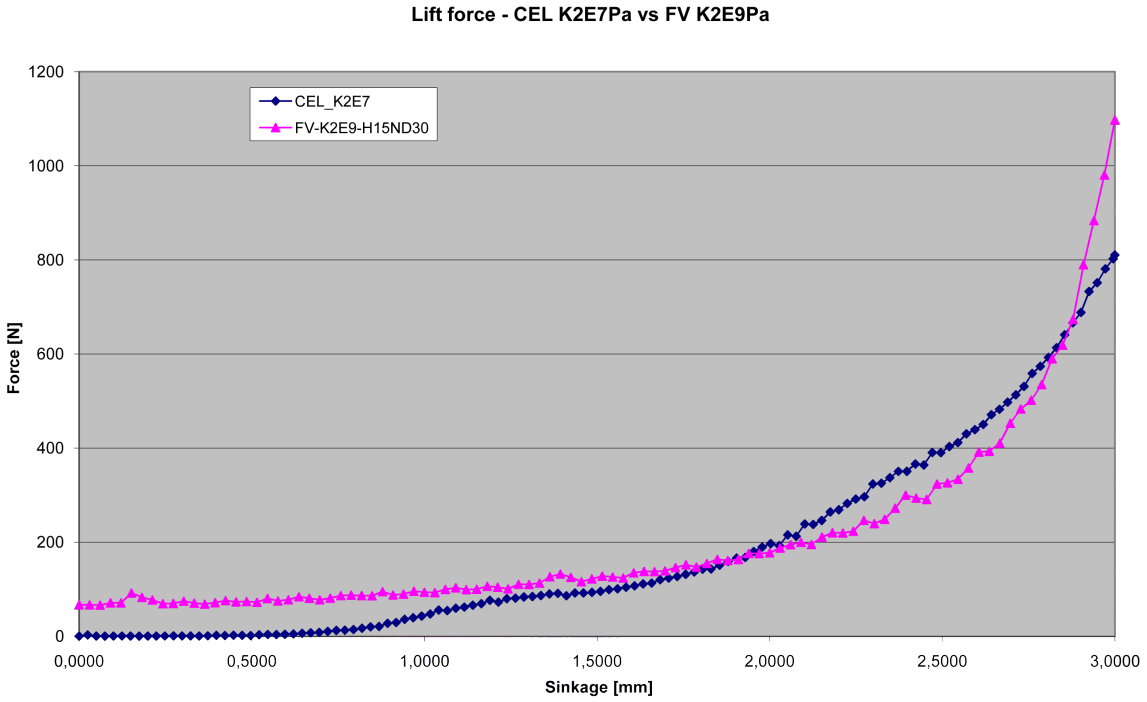

Figure C.12: Vertical tread block, CEL result in blue and FlowVision result in red

The output from the Reynolds model is:

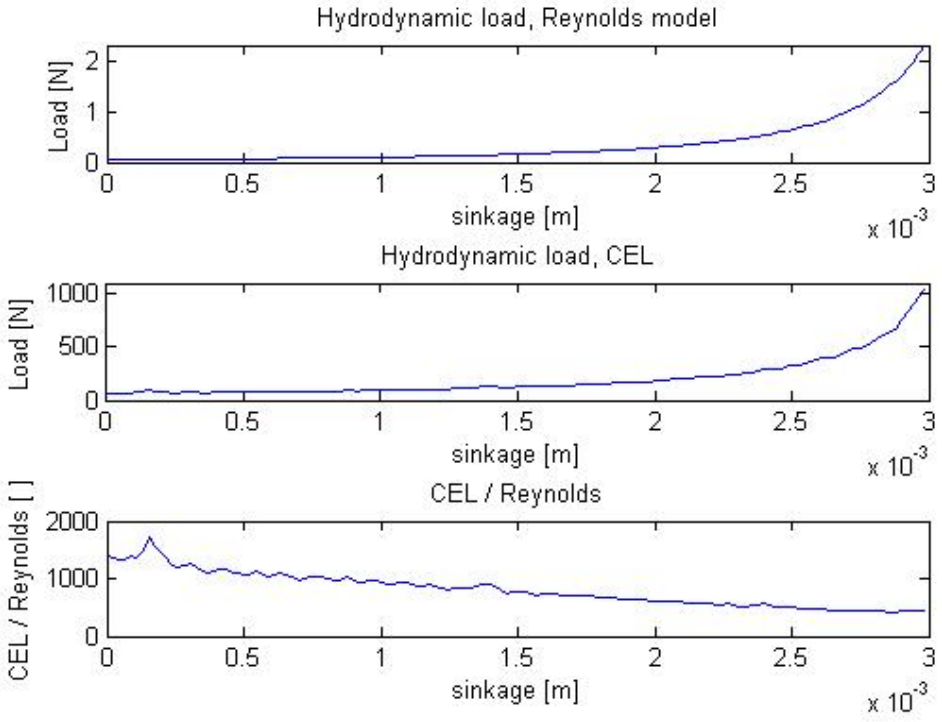

Figure C.13: Vertical tread block, CEL versus Reynolds equation result

One can see that the difference in both models ranges from 1500 to 500 over the sinkage domain. To explore further differences look at the pressure profile at different heights, the top image gives the Reynolds solution and the bottom image the solution obtained with FlowVision. Note the results from FlowVision are in MPa and the results from the Reynolds model are in Pa:

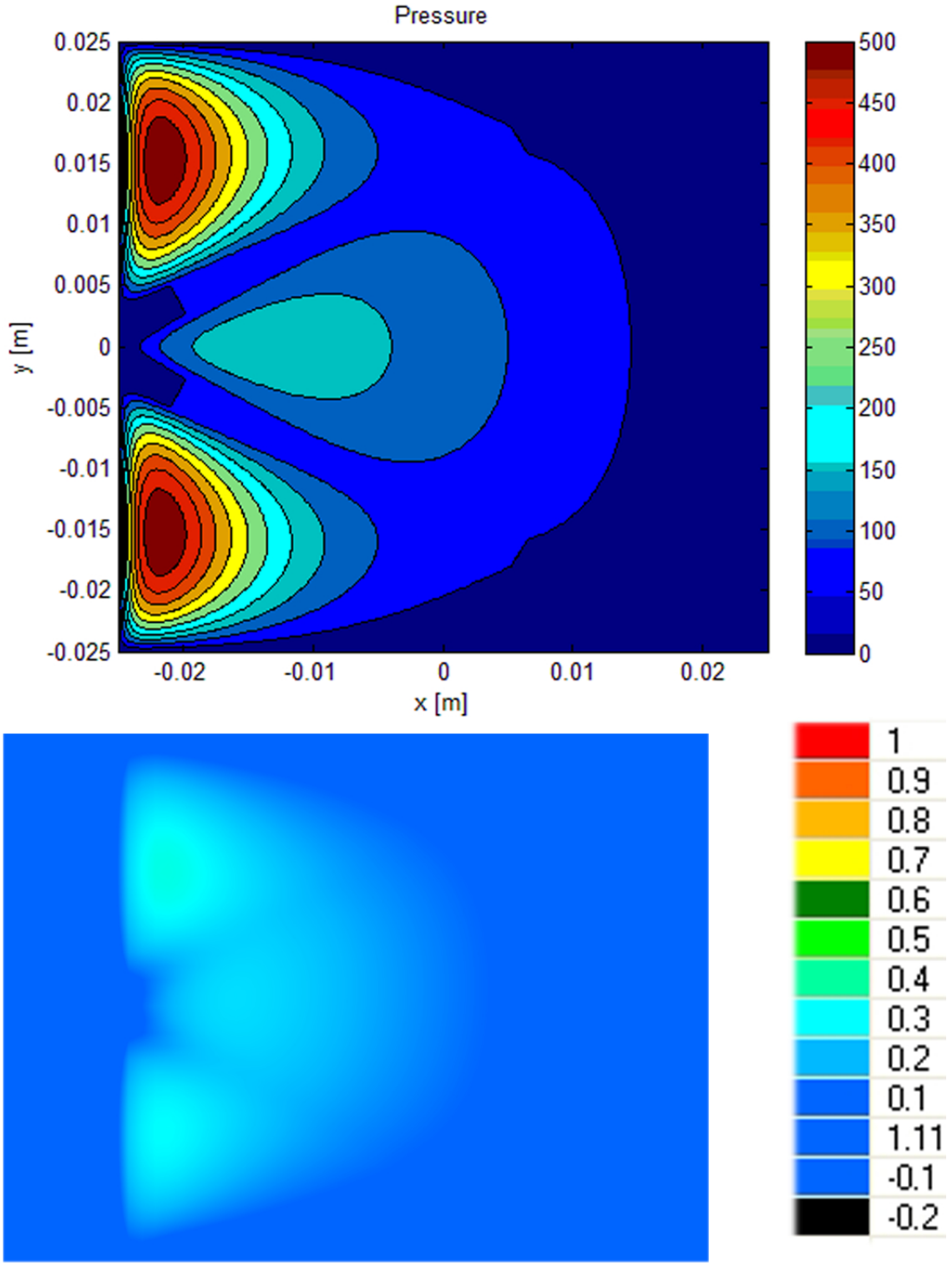

Figure C.14: Vertical tread block, $h = 0.54mm$

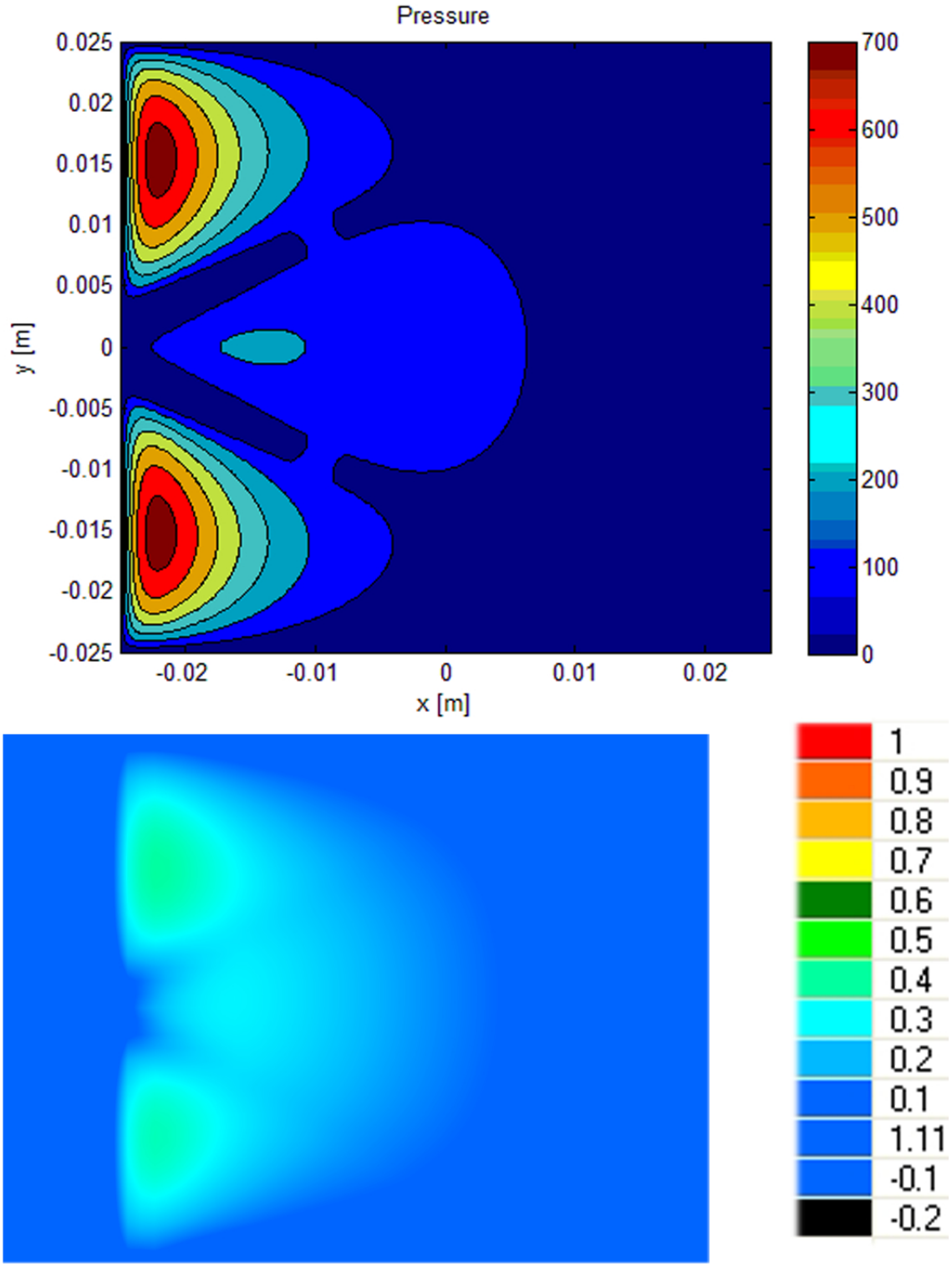

Figure C.15: Vertical tread block, $h = 0.45mm$

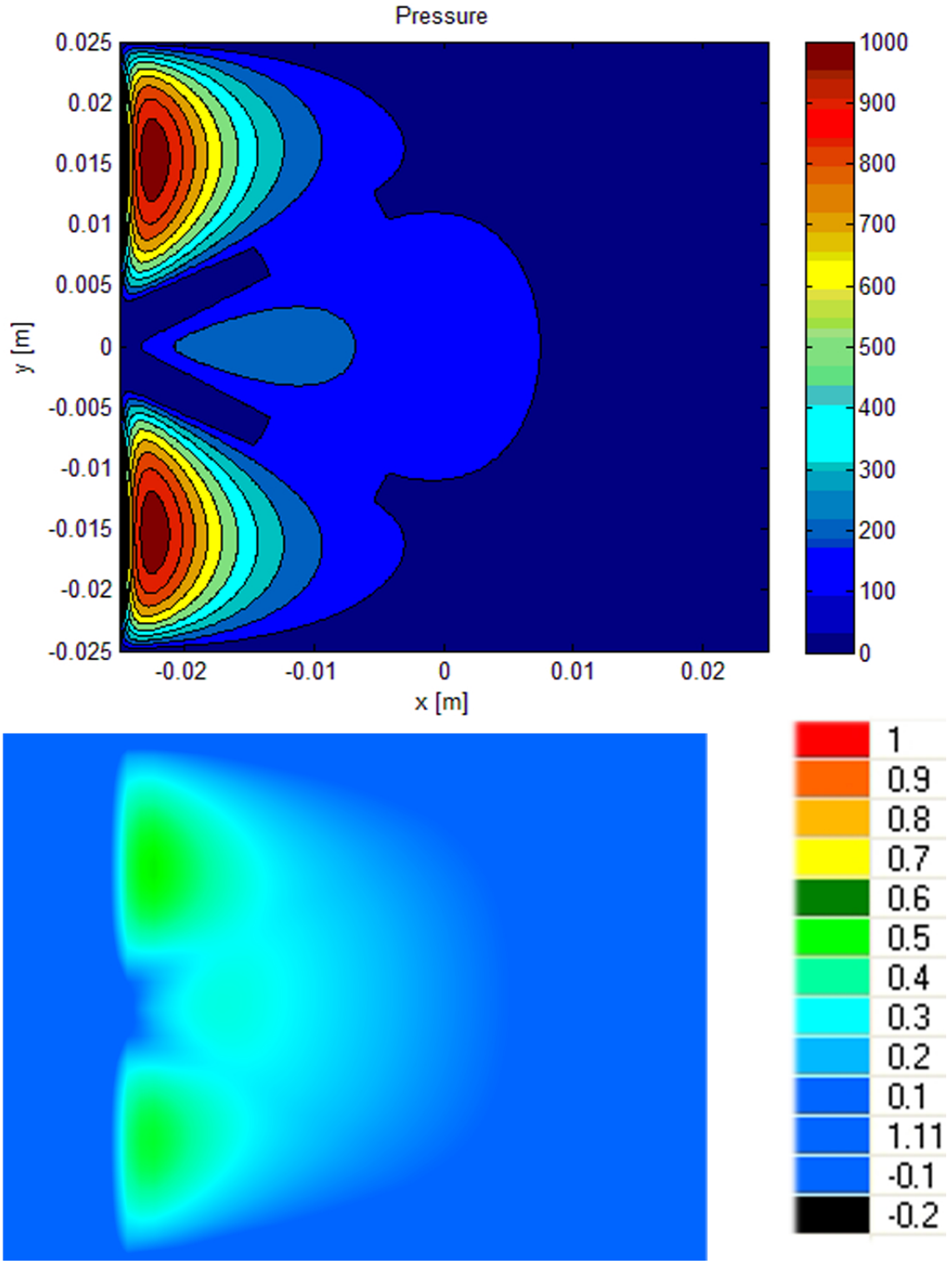

Figure C.16: Vertical tread block, $h = 0.40mm$

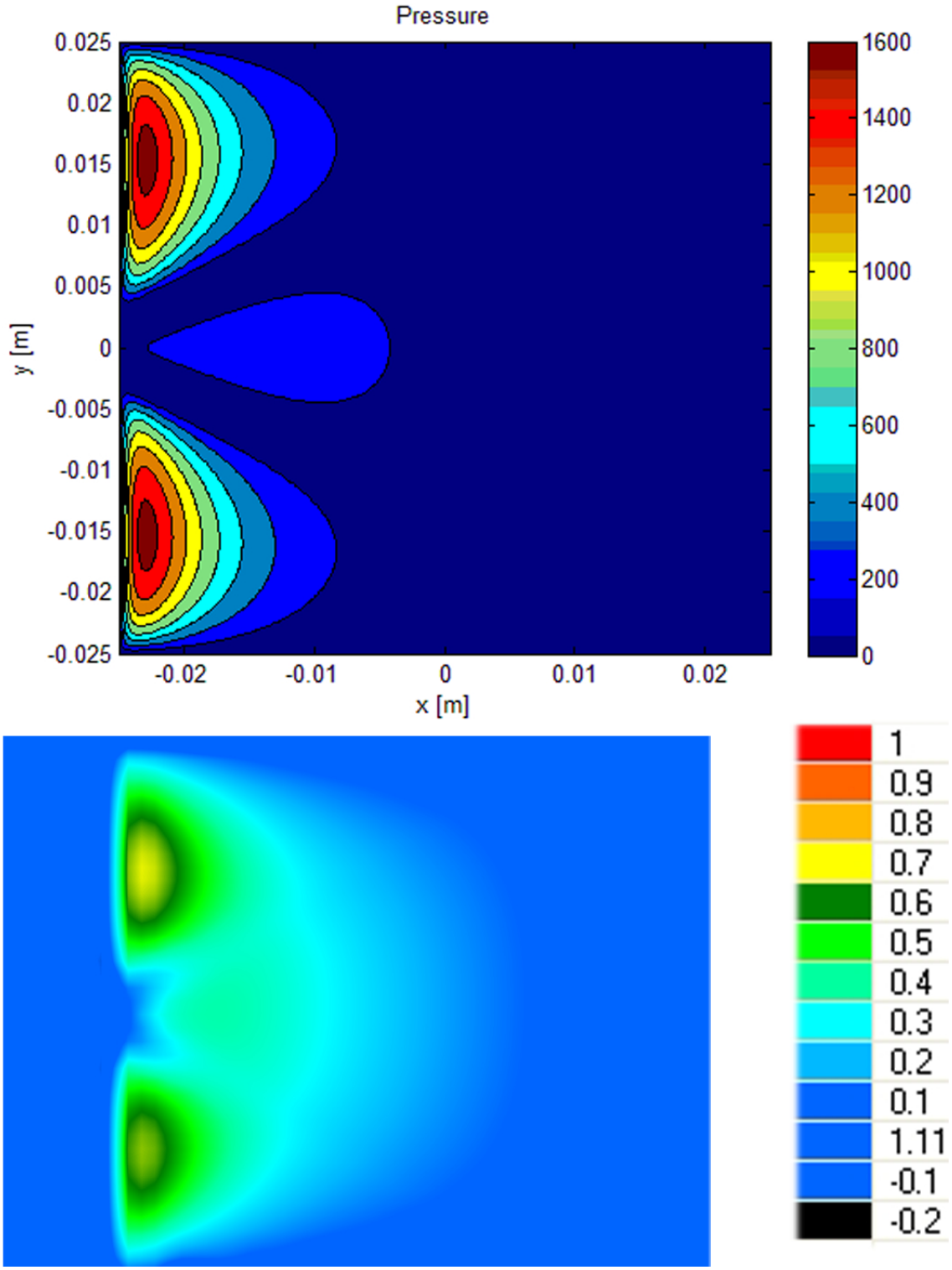

Figure C.17: Vertical tread block, $h = 0.30mm$

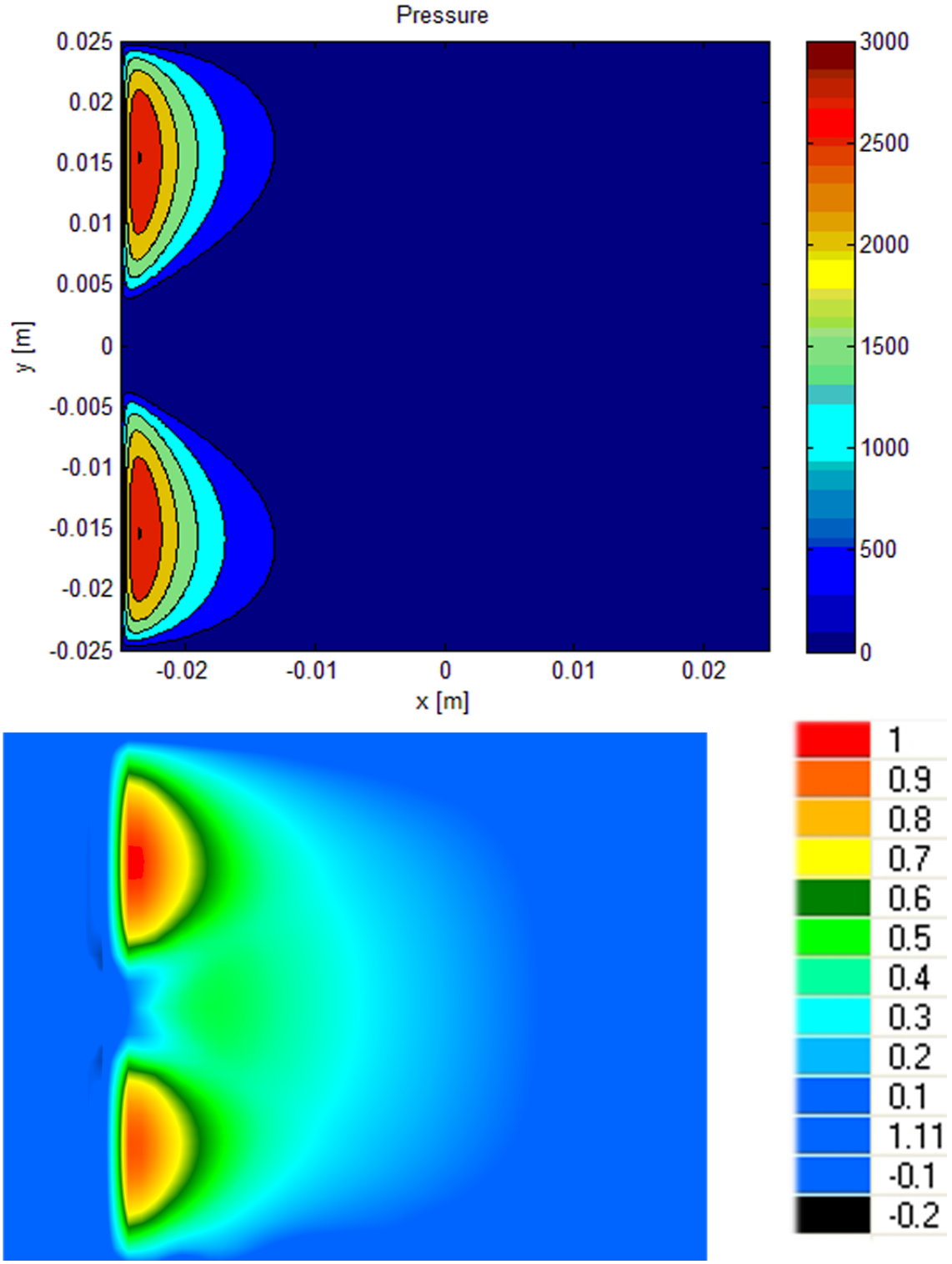

Figure C.18: Vertical tread block, $h = 0.18mm$

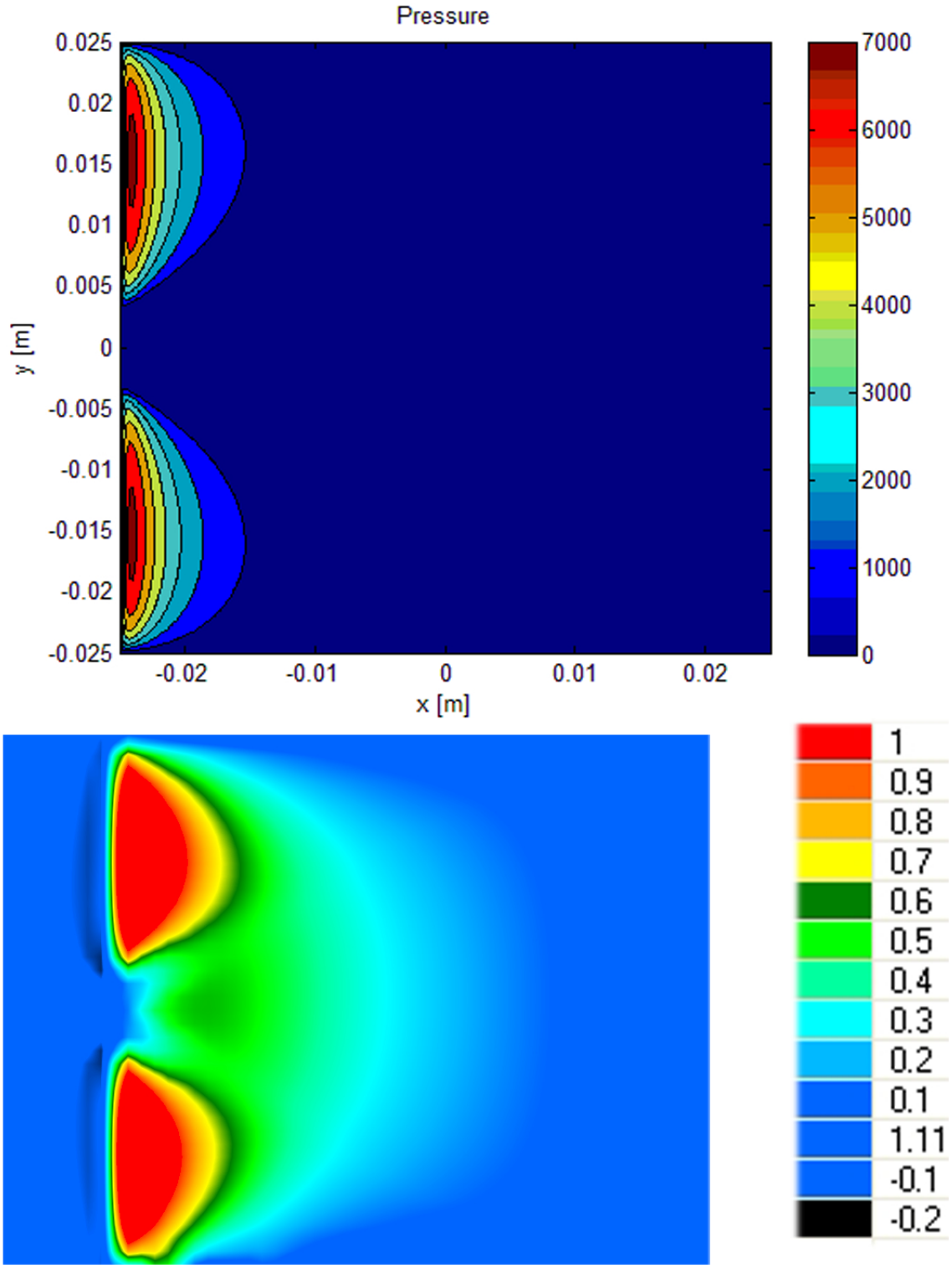

Figure C.19: Vertical tread block, $h = 0.09mm$

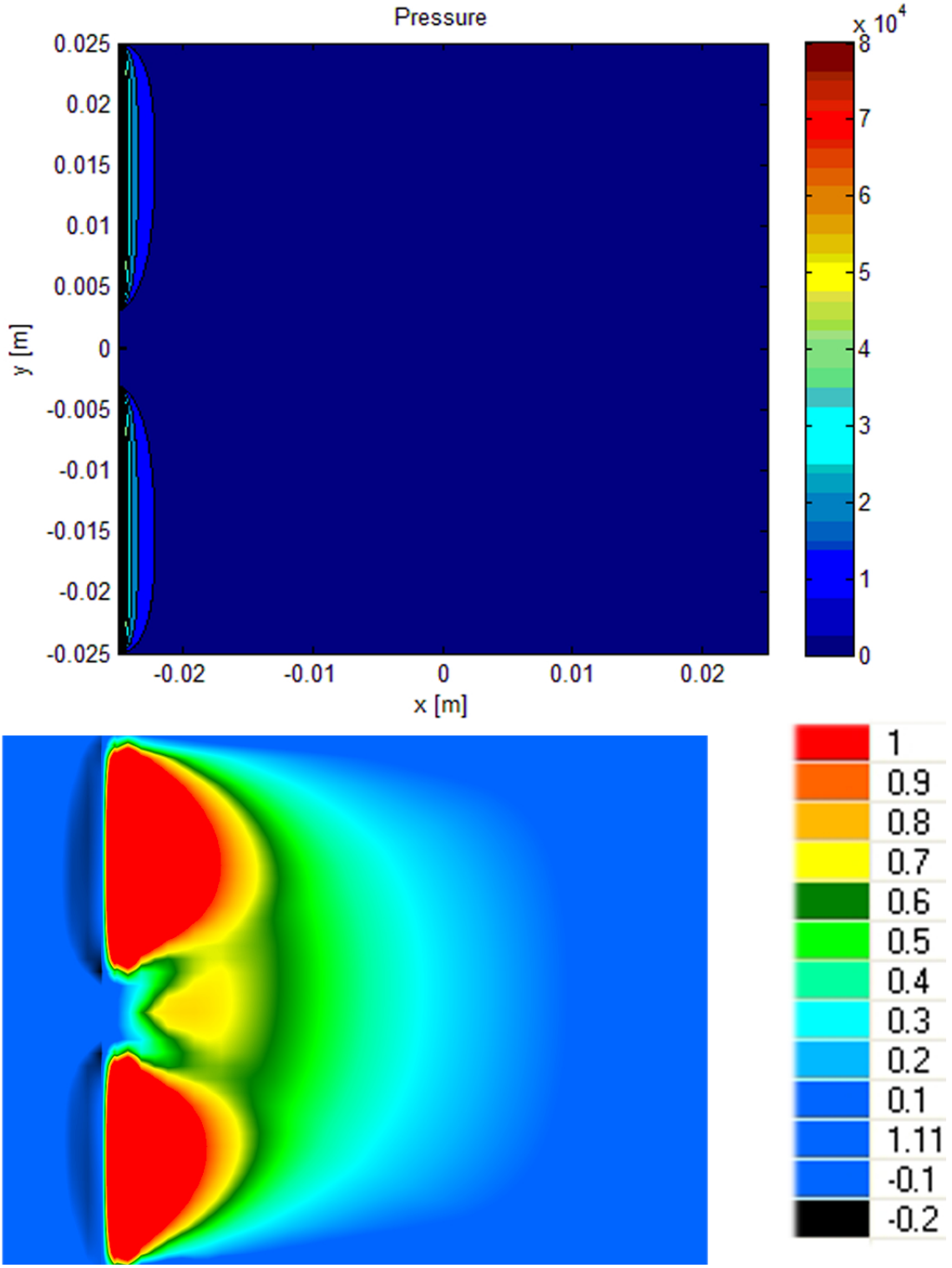

Figure C.20: Vertical tread block, $h = 0mm$

One can see the profiles do not only differ in order of magnitude but at lower film thicknesses the Reynolds profile gets a higher peak and gradient whereas the FlowVision model results in a more dispersed pressure profile.

C.1.3. CFD benchmark Grosch wheel

In addition to the half space model simulations with Fluent version 6.3.26 have been made using a multiphase laminar 3D model. The multiphase model was volume of fluid with an explicit scheme using Courant number of 0.25. The mesh has been generated with Gambit 2.3.16 using tetrahedral and hybrid elements of the TGrid type with interval size 1. The operating velocity is 50 km/h. The wheel is placed 0.1 mm above the road surface as Fluent is unable to deal with contact as in that case the volume of the elements goes to zero. Operating conditions include gravity. The solver used in Fluent uses the following settings:

- Pressure-Velocity coupling: SIMPLE, the standard Fluent algorithm
- Discretization:
  - Pressure: PRESTO! (Pressure Staggering Option)
  - Momentum: First order upwind
  - Volume fraction: Geo reconstruct
- Under relaxation factors
  - Pressure: 0.3
  - Density: 1
  - Body forces: 1
  - Momentum: 0.7

The solver is implicit pressure based, unsteady first order implicit in time with an absolute velocity formulation and the gradients calculated with Green-Gauss cell based. The time steps are chosen variable to let Fluent determine the faster scheme.

Although Fluent repeatedly reports convergence, some indications of unrealistic results are present. See the next figures:

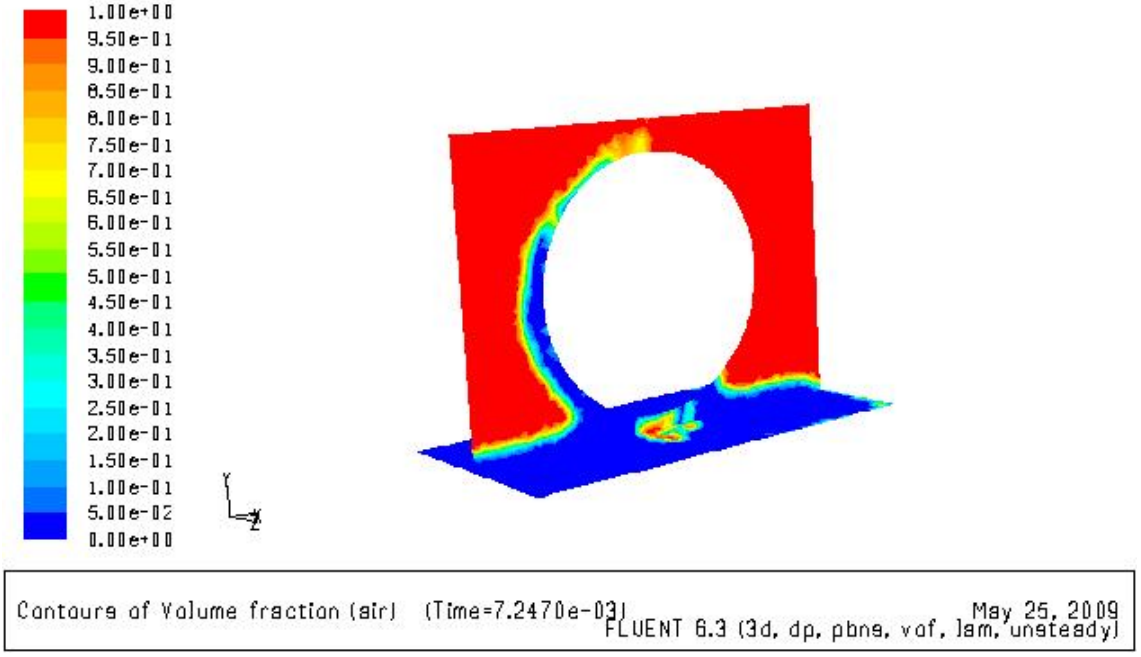

Figure C.21: Volume fraction air

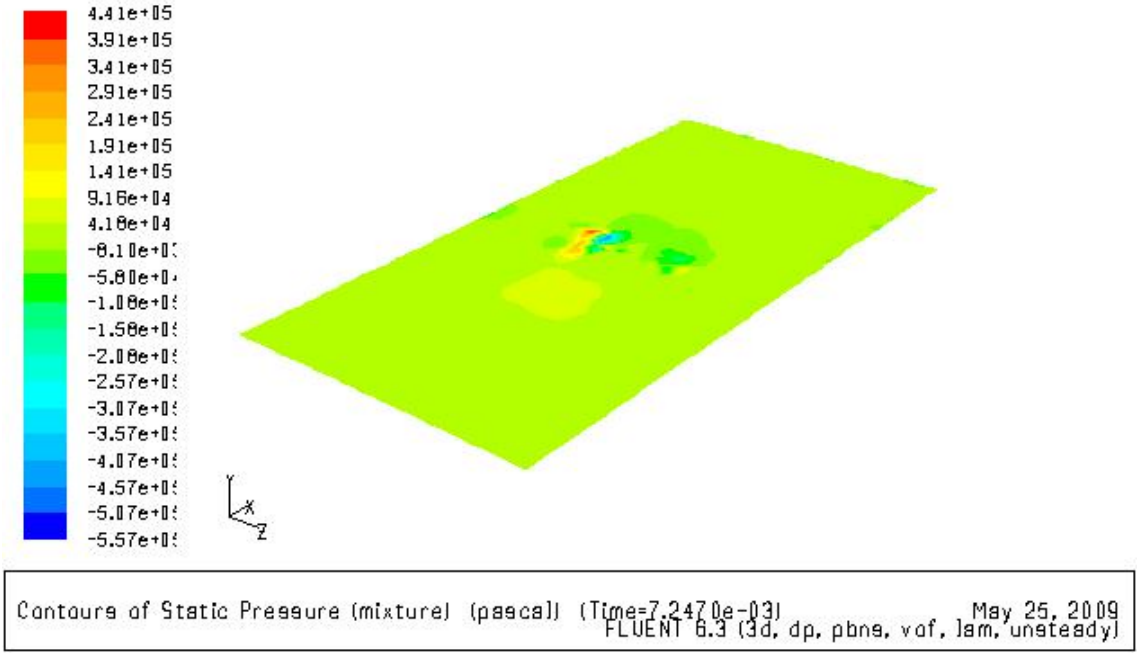

Figure C.22: Pressure on road surface

One can see that the water builds up unrealistically high in front of the wheel and that negative pressures occur which have no physical meaning. Therefore the results of Fluent are quite doubtful also because the (non-negative) pressure values are considerably lower than expected. Further work on this needs to be done.

The resulting pressure profiles of Fluent have been compared with the Matlab results with a stagnation pressure at the inlet:

The stagnation pressure at the inlet seems a reasonable approach. Comparing Fluent and Matlab:

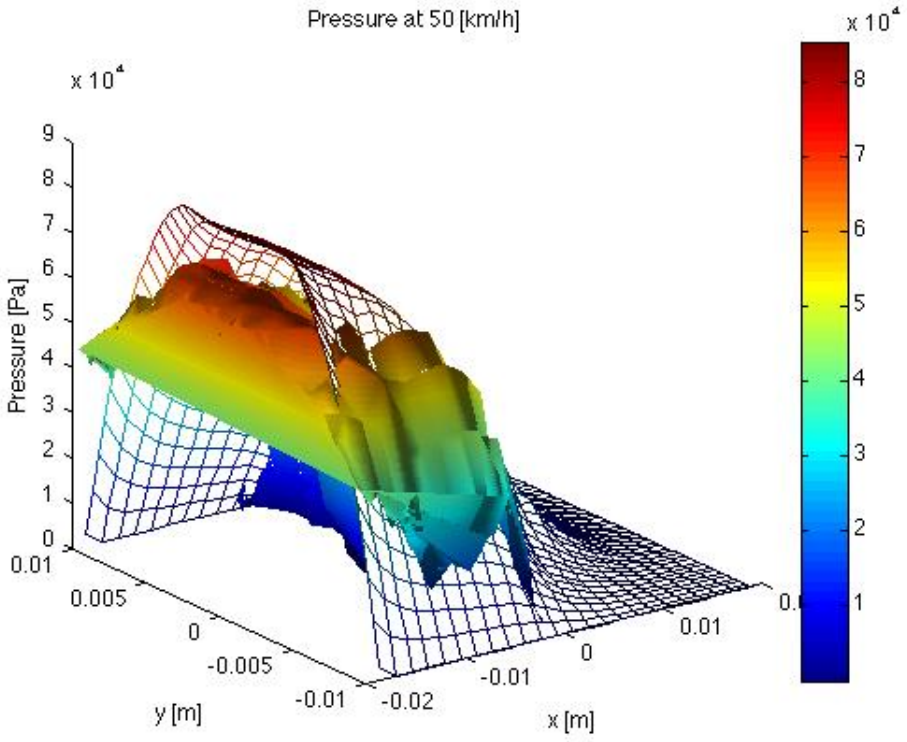

Figure C.23: Pressure distribution comparing Matlab and Fluent

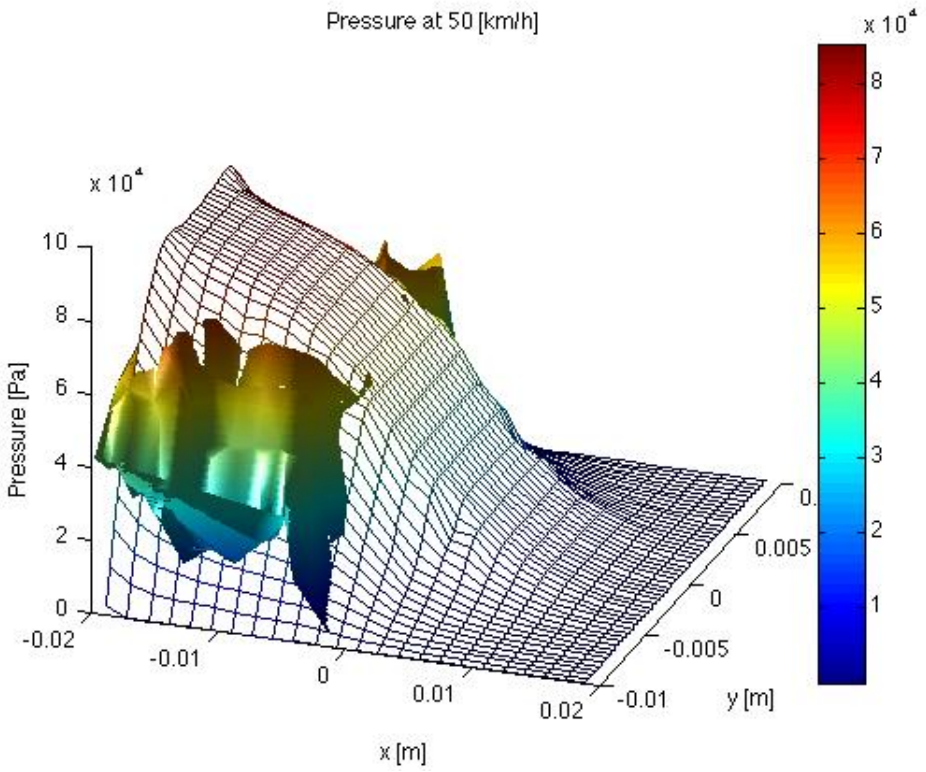

Figure C.24: Pressure distribution comparing Matlab and Fluent

Table 8: default

Speed	Reynolds	Reynolds + stagnation inlet	Fluent
50 km/h	3,14	25,56	23,14

Discussion and recommendations

- Matlab model
  - The Reynolds equation is limited to viscous and 2D flow and cannot deal with discontinuities and so the effect of the groove is not handled very adequate
  - also the inlet stagnation pressure is not taken into account in the Reynolds equation although imposing it as a boundary condition seems to give a reasonable approximation
  - The computational time of the Matlab model is a few seconds compared to approximately 40 hours for the Fluent model so the loss in accuracy is negligible compared to the computational gains
  - the thin film approximation which is underlying the Reynolds equation is a little challenging with this thick water layer, as the Fluent simulation shows some variation over the film height.

- Fluent model
  - The used grid could use some refinements, on the current machine this was not possible due to memory limitations
  - Some special attention should be given to the elements just below the wheel, more elements are needed to accurately take (possible) viscous effects into account
  - a higher order upwind scheme has been run with the same results
  - the Fluent simulations shows the stagnation point in the leading edge of the wheel as seen in the experiments
  - the stagnation pressure is dominant for the pressure field in the leading edge, in case of a deformable wheel a longer wedge shaped inlet will be formed and the viscous effects will be much more important but are not seen in this simulation due to the large height gradient
  - the "choice" for the tetrahedral / hybrid elements was made as this was the only one that I could get working without having a grid with negative volumes. I would recommend to further detail the flow regime to the bottom 5 mm and with that drastically reduce the size of the model and be able to improve the mesh around the leading edge. a grid refinement was not successful due to memory limitations but the size seems reasonable for most of the flow field as the solution is smooth except for the area at the edges of the groove where a refinement seems necessary.

D. Eigenmodes Grosch wheel

The eigenshapes of the Grosch wheel without groove are, leaving out the first 2 rigid body modes:

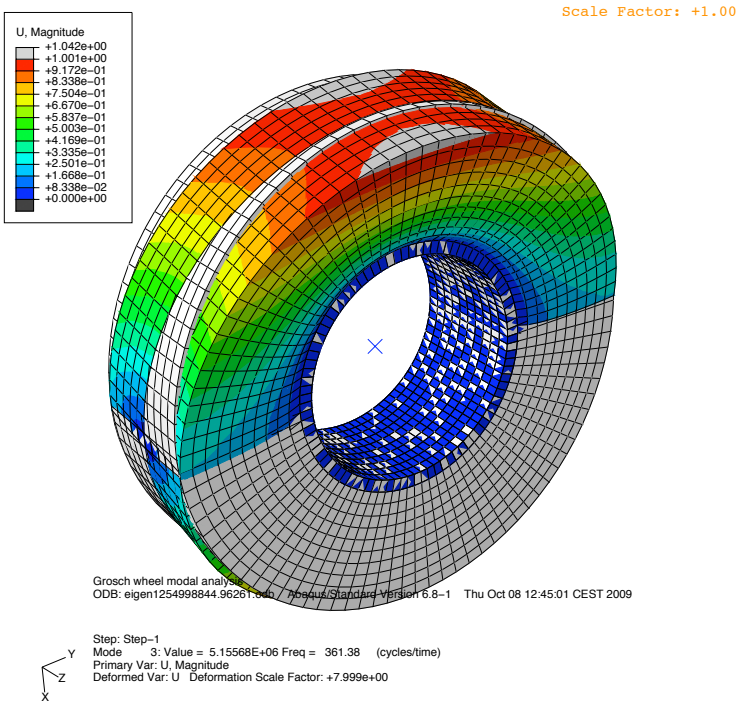

Figure D.1: Mode 3

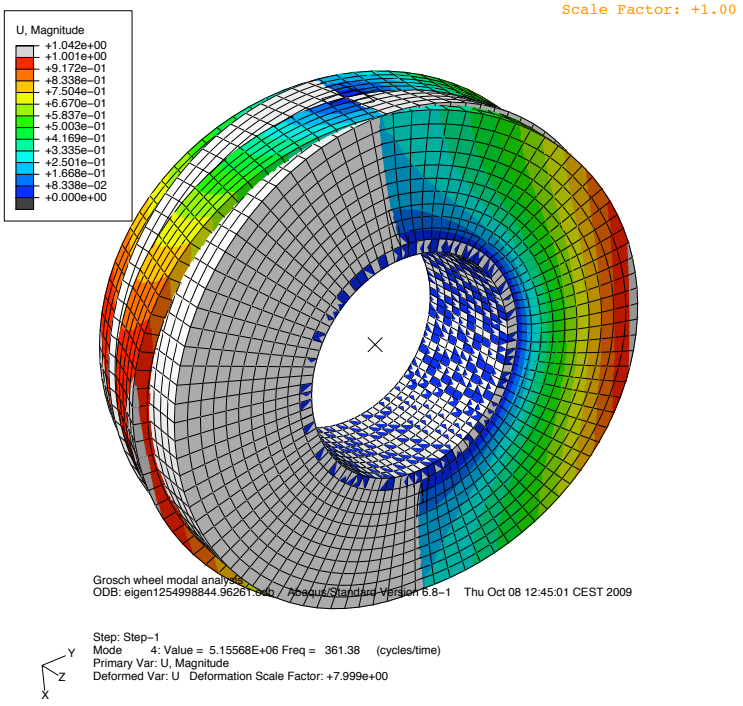

Figure D.2: Mode 4

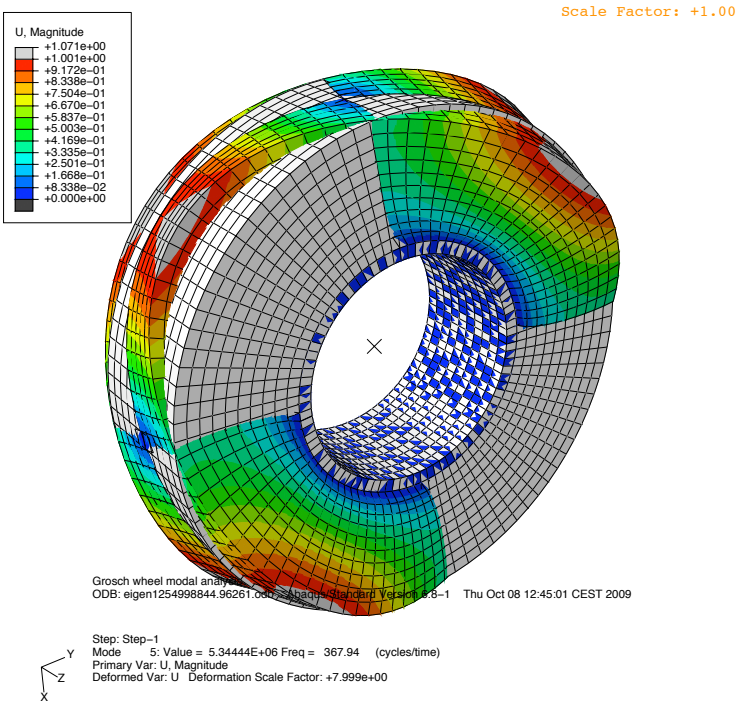

Figure D.3: Mode 5

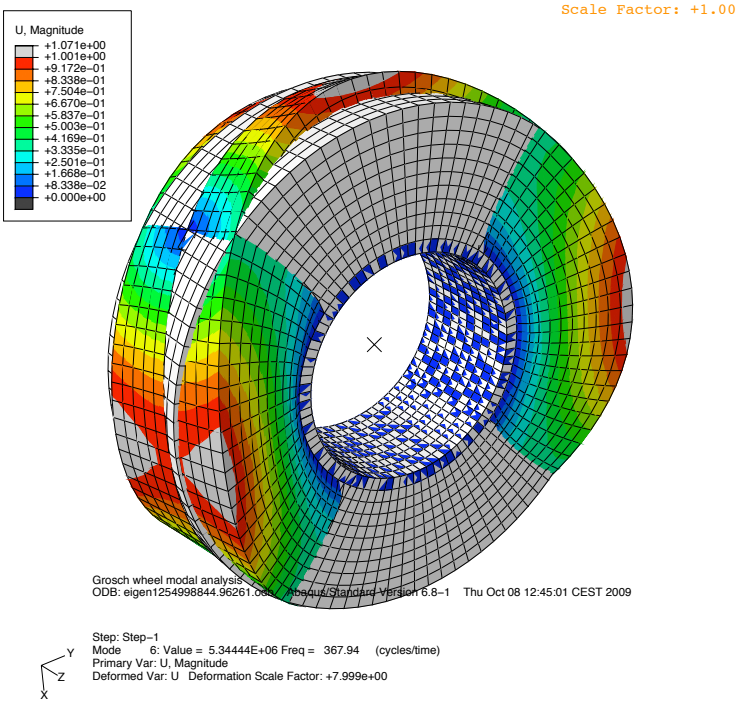

Figure D.4: Mode 6

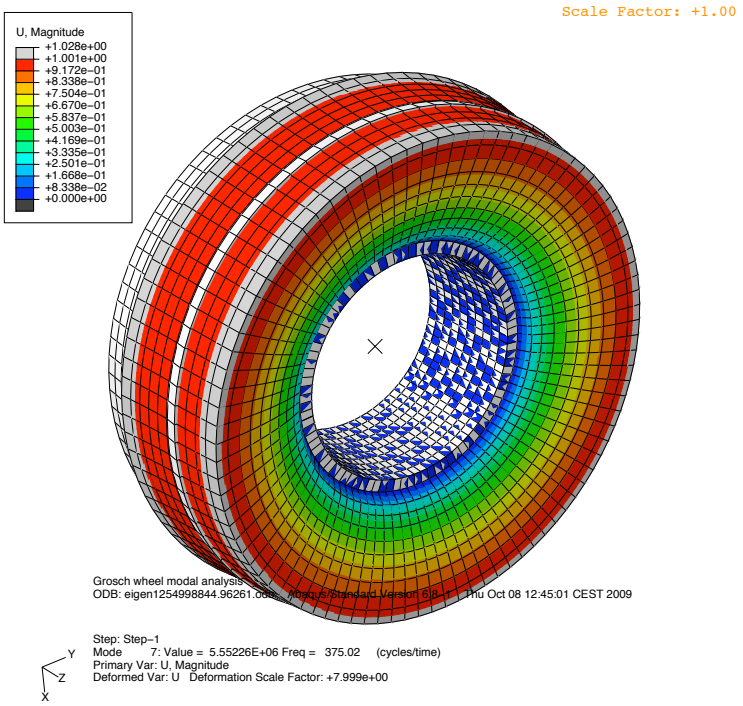

Figure D.5: Mode 7

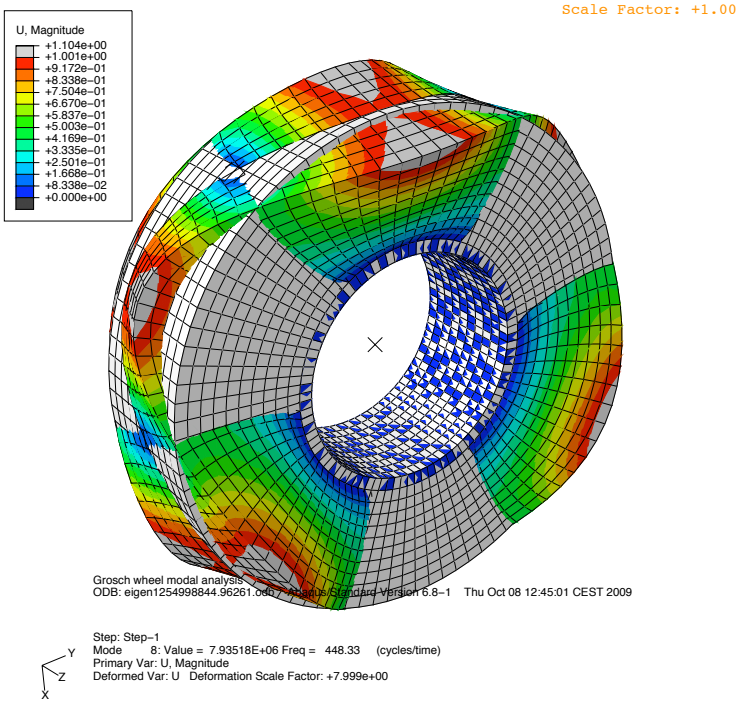

Figure D.6: Mode 8

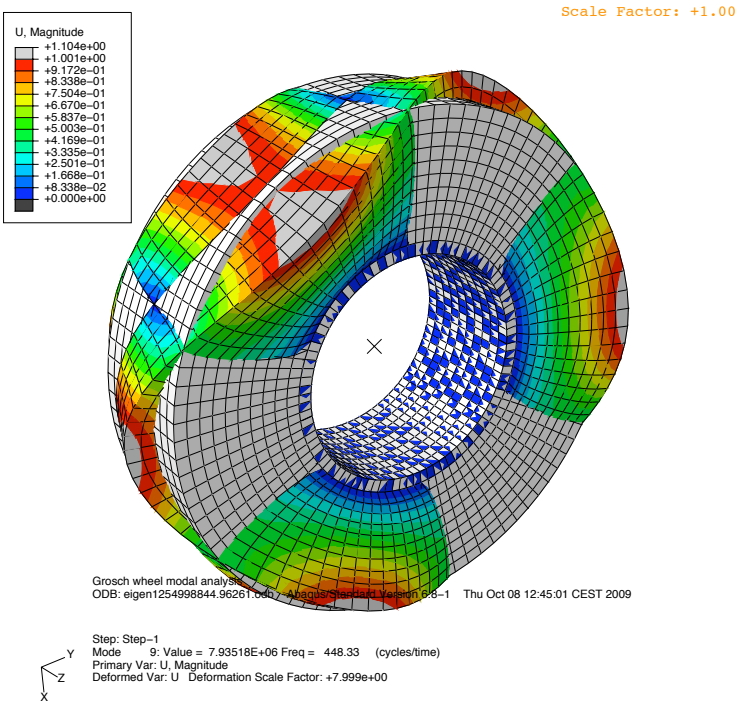

Figure D.7: Mode 9

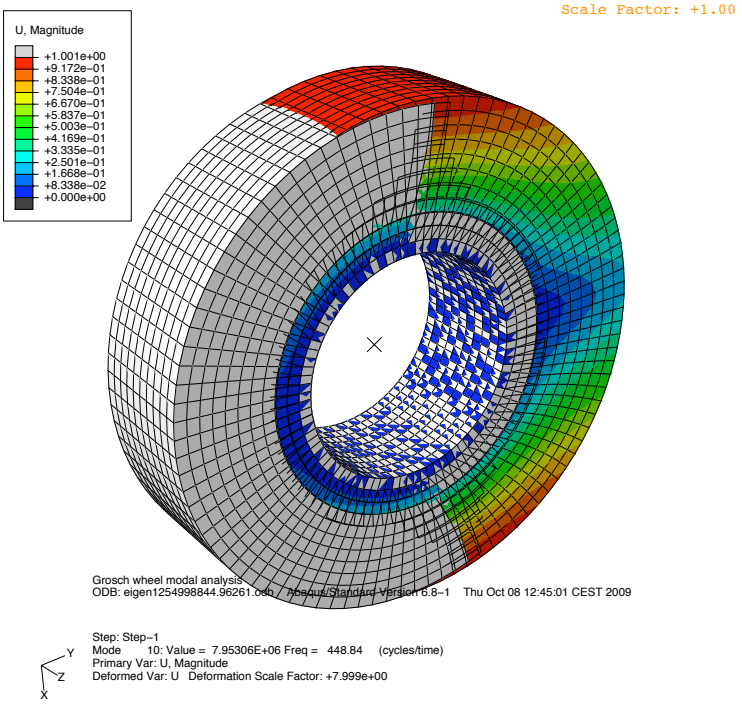

Figure D.8: Mode 10

E. ABAQUS user subroutines

Abaqus/Explicit offers the user the capability of defining custom loads, interactions etc via user subroutines written in Fortran. The following user subroutines are possible in Abaqus/Explicit 6.8.2:

Subroutine	function
VDISP	specify prescribed translational and rotational boundary conditions
VDLOAD	specify non-uniform distributed loads
VFABRIC	define fabric material behavior
VFRIC	define frictional behavior for contacting surfaces
VUAMP	specify amplitudes
VUANISOHYPER_INV	define anisotropic hyperelastic material behavior, invariant formulation
VUANISOHYPES_STRAIN	define anisotropic hyperelastic material behavior based on Green strain
VUEL	user defined element
VUFIELD	specify predefined field variables
VUHARD	define yield surface size and hardening parameters for isotropic plasticity or combined hardening models
VUINTER	define interaction between contact surfaces
VUMAT	define material behavior
VUSDFLD	redefine field variables at a material point
VUTRS	define a reduced time shift function for a viscoelastic material

For more information on the subroutines the reader is referred to the Abaqus/Explicit user manual.

F. Matlab engine

To call the Matlab engine is highly platform specific, here an outline will be given for running the Matlab engine on a 64-bit Unix architecture, on one single machine. The latter is a choice of the author but it is possible in Unix to start the Matlab engine on other machines on the network, possibly with another architecture. A first prerequisite to run the Matlab engine on a Unix machine is to have C shell installed at /bin/csh. Next, the following third party libraries must be installed:

- matlabroot/bin/glnxa64/libeng.so
- matlabroot/bin/glnxa64/libmx.so

The libeng library requires additional third-party library files. MATLAB uses these libraries to support Unicode character encoding and data compression in MAT-files. These library files must reside in the same directory as libmx. You can determine what most of these libraries are using the platform-specific command: ldd -d libeng.so. Furthermore the Unicode file is necessary, which can be found in: /matlabroot/bin/glnxa64/icudt32l.dat.

Next step is compiling the routine, standard compiler supported by Matlab is g95 version 0.90, with the options that can be found in /matlabroot/bin/engopts.sh. Most important for the Fortran subroutine is the C preprocessor as the file starts with a C header. From engops.sh one can see with library directories need to be included for linking and for compiling. The relevant section from engopts.sh:

```
#
# engopts.sh Shell script for configuring engine standalone applications.
# These options were tested with the specified compiler.
#
# usage: Do not call this file directly; it is sourced by the
# mbuild shell script. Modify only if you don't like the
# defaults after running mbuild. No spaces are allowed
# around the '=' in the variable assignment.
#
# Note: For the version of system compiler supported with this release,
# refer to Technical Note 1601 at:
# http://www.mathworks.com/support/tech-notes/1600/1601.html
#
#
# SELECTION_TAGs occur in template option files and are used by MATLAB
# tools, such as mex and mbuild, to determine the purpose of the contents
# of an option file. These tags are only interpreted when preceded by '#'
# and followed by ':'.
#
#SELECTION_TAG_SA_OPT: Template Options file for building standalone engine applications
#
# Copyright 1984-2006 The MathWorks, Inc.
# $Revision: 1.30.4.10 $ $Date: 2007/06/07 14:12:23 $
#----------------------------------------------------------------
#
if [ "$TMW_ROOT" = "" ]; then
TMW_ROOT="$MATLAB"
fi
MFLAGS="-I$TMW_ROOT/extern/include"
MLIBS="-L$TMW_ROOT/bin/$Arch -leng -lmx"
MCXXFLAGS="-I$TMW_ROOT/extern/include/cpp $MFLAGS"
MCXXLIBS="$MLIBS"
LDEXTENSION="
case "$Arch" in
Undetermined)
#----------------------------------------------------------------
# Change this line if you need to specify the location of the MATLAB
# root directory. The mex script needs to know where to find utility
# routines so that it can determine the architecture; therefore, this
# assignment needs to be done while the architecture is still
```

```
# undetermined.
#----------------------------------------------------------
#----------------------------------------------------------
;;
glnxa64)
#----------------------------------------------------------
RPATH="-Wl,-rpath-link,$TMW_ROOT/bin/$Arch"
CC='gcc'
CFLAGS='-ansi -D_GNU_SOURCE -fexceptions'
CFLAGS="$CFLAGS $MFLAGS"
CLIBS="$RPATH $MLIBS -lm -lstdc++"
COPTIMFLAGS='-O -DNDEBUG'
CDEBUGFLAGS='-g'
#
CXX='g++'
CXXFLAGS='-ansi -D_GNU_SOURCE'
CXXFLAGS="$CXXFLAGS $MCXXFLAGS -DGLNXA64 -DGCC"
CXXLIBS="$RPATH $MCXXLIBS -lm"
CXXOPTIMFLAGS='-O -DNDEBUG'
CXXDEBUGFLAGS='-g'
#
#
FC='g95'
FFLAGS='-fexceptions'
FFLAGS="$FFLAGS $MFLAGS"
FLIBS="$RPATH $MLIBS -lm"
FOPTIMFLAGS='-O'
FDEBUGFLAGS='-g'
#
LD="$COMPILER"
LDFLAGS=''
LDOPTIMFLAGS='-O'
LDDEBUGFLAGS='-g'
#
POSTLINK_CMDS=':'
```

Not officially supported by Matlab but also working on a 64-bit Unix architecture are:

- Intel Fortran compiler 9.1
- G95, version 0.91
- gfortran

Now, before the application can be run the runtime library path needs to be set, in the bash shell this is done in the following way:

export LD_LIBRARY_PATH = matlabroot/bin/glnxa64: matlabroot/sys/os/glnxa64:LD_LIBRARY_P

And, which is not mentioned in the Matlab help, one should also update the path so the engine can be run:

export PATH = matlabroot/bin/:PATH

Now the stand alone application can be run.

G. Matlab engine from ABAQUS subroutine

To couple the Matlab engine to the ABAQUS subroutine this first of all requires understanding of the ABAQUS make routine which is used by ABAQUS to compile the subroutine and link the shared libraries. Next to that the version with which the shared libraries of Matlab and Abaqus are compiled must be compatible.

The ABAQUS make routine uses the following syntax:

abaqus make job=job-name | library=source-file [user=source-file | object file] [directory=library-dir] [object_type=fortran | c | cpp]

And it takes the flags for the compiler from the abaqus_v6.env file, the relevant section for the compiler is:

```
#
# Linux (Opteron/EM64T) Settings:
#
# Compile and Link command for user subroutines.
# Compile_cpp and link_exe for Abaqus make utility.
#
import os, re, glob, driverUtils

   # Always use the newest version
fortDefPath = '/'
ccDefPath = '/'

   dirLst = glob.glob('/opt/intel/fce/*')
if dirLst:
dirLst.sort()
fortDefPath = dirLst[-1] + '/bin'

   dirLst = glob.glob('/opt/intel/cce/*')
if dirLst:
dirLst.sort()
ccDefPath = dirLst[-1] + '/bin'

   fortCompiler = "ifort"
cppCompiler = "icpc"

   if os.path.exists(os.path.join(fortDefPath, fortCompiler)):
fortCmd = os.path.join(fortDefPath, fortCompiler)
else:
```

```
fortCmd = fortCompiler

   if os.path.exists(os.path.join(ccDefPath, cppCompiler)):
cppCmd = os.path.join(ccDefPath, cppCompiler)
else:
cppCmd = cppCompiler

   # Avoid signal trapping by the Fortran RTE
os.environ["FOR_IGNORE_EXCEPTIONS"] = "T"
# Disable messages from the Fotran RTE
os.environ["FOR_DISABLE_DIAGNOSTIC_DISPLAY"] = "T"

   # Turn off use of ACML on AMD Opteron architecture if ABQ_USE_ACML is
# uncommented and the variable is set to 0
# os.environ["ABQ_USE_ACML"] = "0"

   # The following code can be used to set the gcc version information for the
# Intel compiler accoring to the version which is on the system. By default
# we set this information to teh gcc version setting with which Abaqus was
# compiled
verId = 330 # default
# Pattern to determine the gcc version on the systen
p = re.compile(r' b[0-9][0-9]|[0-9] b')
verStr = '3.3.1'
#try:
# verStr = p.findall(os.popen('gcc –version').readlines()[0])[0]
# verId = eval(verStr[0]) * 100 + eval(verStr[2]) * 10
#except:
# verId = 330 # default

   # Add the flag "-free" to the compile_fortran command below to use free-
# format FORTRAN 90 syntax.
compile_fortran = (fortCmd + " -cpp -c -fPIC -auto -extend_source -w90 -w95 " +
"-WB -I%I -I/apps/share/matlab/v142/x86_64/extern/include")

   compile_cpp = (cppCmd +
" -c -cxxlib-gcc -gcc-version=%i -Kc++eh -fPIC "%verId +
"-Krtti -Kc++ -pc64 -restrict -DABQ_LINUX -DABQ_LNX86_64 " +
"-DFOR_TRAIL -DHAS_BOOL -DASSERT_ENABLED -D_BSD_TYPES " +
"-D_BSD_SOURCE -D_GNU_SOURCE -D_POSIX_SOURCE " +
"-D_XOPEN_SOURCE_EXTENDED -D_XOPEN_SOURCE -DHAVE_OPENGL " +
"-DHKS_OPEN_GL -DTYPENAME=typename -DGL_GLEXT_PROTOTYPES " +
"-D_LARGEFILE64_SOURCE -D_FILE_OFFSET_BITS=64 -we1011 -we120 "+
"-we117 -we556 -we144 -we268 -we1224 -we167 -we880 -O0 -I%I" )

   link_sl = (fortCmd +
```

```
" -cxxlib-gcc -gcc-version=%i -fPIC -threads -shared " %verId +
" %E -Wl,-soname,%U -o %U %F %A -L /apps/share/matlab/v142/x86_64/bin/glnxa64
%L %B " +
" -parallel -Wl,-Bdynamic " +
" -i-dynamic -leng -lmx -lm -lifport -lifcoremt ")

   link_exe = (cppCmd + " -cxxlib-gcc -gcc-version=%i -fPIC " %verId +
"-Wl,-Bdynamic -i-dynamic -o %J %F %M %L %B %O -lpthread")
```

One can see that for the operation of the Matlab engine in the subroutine requires the inclusion of the right include directories and libraries, which are platform specific. For the 64 bit Linux workstation the /"matlabroot"/x86_64/include and /"matlabroot"/x86_64/bin/glnxa64 are needed.

As mentioned before, it is of critical importance that the version with which the Abaqus libraries and the Matlab libraries are made are compatible, again this is highly platform specific. For Matlab this information can be found at:

http://www.mathworks.com/support/compilers/current_release/mlcompilers.html.
An example is, for release 2009a:

Architecture	Compiler version
Windows (32-bit)	Microsoft Visual C++ 2005 SP1 (8.0) Professional Edition
Windows (64-bit)	Microsoft Visual C++ 2005 SP1 (8.0) Professional Edition
Linux (32-bit)	GNU gcc/g++ version 4.2.3
Linux (64-bit)	GNU gcc/g++ version 4.2.3
Solaris (64-bit)	Sun Studio 12 cc/CC 5.9
Mac Apple	Xcode 3.1 with gcc/g++ version 4.0.1 (Apple Computer, Inc. build 5488)

Which clearly exemplifies the platform dependency. For Abaqus the information can be found at:

http://www.simulia.com/support/v68/v68_sysRqmts.html.
For release 6.8 the compilers are:

Architecture	Compiler version
Windows x86-32	Microsoft Visual C++ 2005 SP1
Windows x86-64	Microsoft Visual C++ 2005 SP1
Linux x86-32	Intel C++ 9.1
Linux x86-64	Intel C++ 9.1
Linux Itanium	Intel C++ 9.1
HP UX	HP aC++ A.06.12
AIX Power	IBM xlC 9

This would make it seem like Windows is the only platform with matching libraries, however as seen before the Abaqus make routine uses the gcc libraries to link the user subroutines, actually in the abaqus_v6.env file one can see:
The following code can be used to set the gcc version information for the

# Intel compiler accoring to the version which is on the system. By default
# we set this information to teh gcc version setting with which Abaqus was
# compiled
verId = 330 # default

Therefore a Matlab version compiled with a GCC compiler version 3.3.0 should be compatible, and in fact the following compatible versions of Matlab and Abaqus have been tested.

Compatibility				
Matlab version	Abaqus version			
	6.8-1	6.8-2	6.8-5	6.9-1
R14SP2	ok	ok	ok	ok
R14SP3	ok	ok	ok	ok
2006b	-	-	-	-
2007a	-	-	-	-
2008a	-	-	-	-
2009a	-	-	-	-

H. Matlab engine and domain decomposition

For running the Matlab engine on the Goodyear cluster one is limited to Matlab R14SP3 as the older version SP2 is not running on these machines. Also, when using the LSF submission script one will not be able to update the LD_LIBRARY_PATH, a simple workaround is to copy the Matlab shared libraries to the directory in which the user subroutine shared library will be compiled, found in the abaqus_v6.env file, specified by usub_lib_dir. By default this is /'jobname'.shared_dir. Furthermore when using the LSF submission script one has to copy the abaqus_v6.env file to the $HOME directory as the script will not take the file from the working directory.

I. Benchmark problems FSI

To test an a benchmark slider has been made, using abaqus 6.8-5 the following geometry was made:

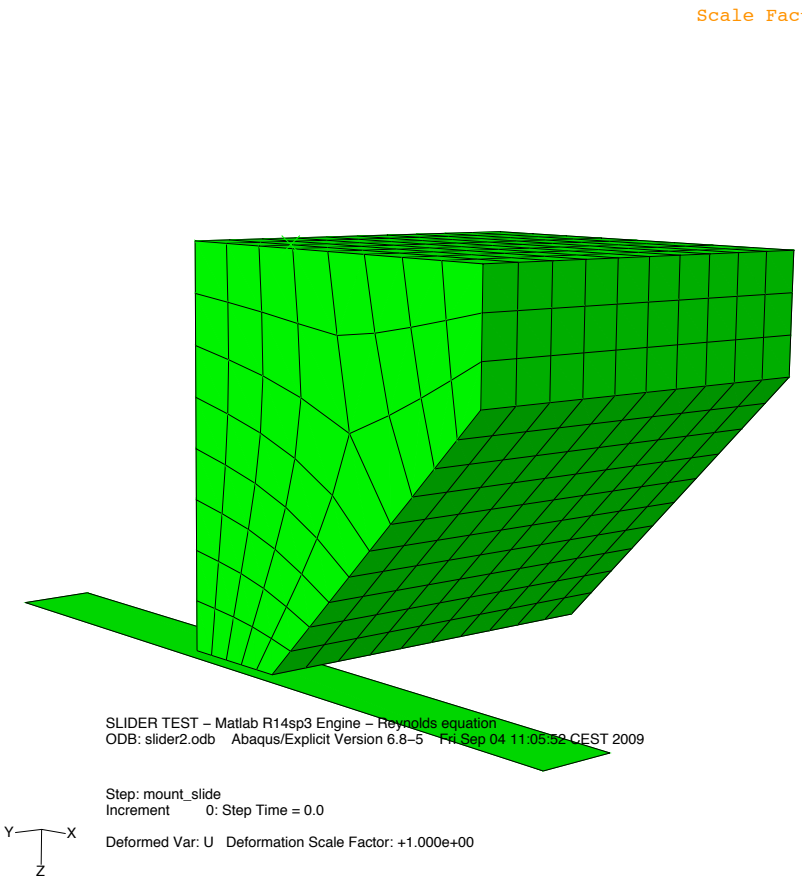

The Matlab engine calculated the following pressure field:

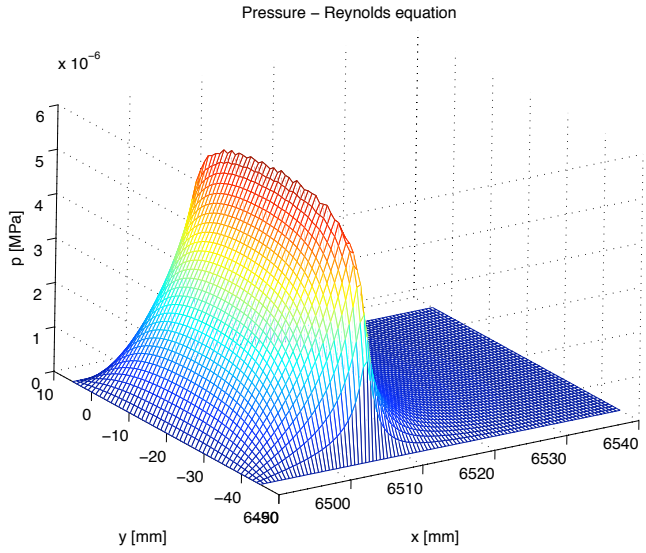

One can verify analytically that this pressure profile is correct.

I.1. Grosch wheel

The Grosch wheel has been modelled with Abaqus CEL and with FlowVision with the following results.

Speed [km/h]	CEL
50	33
60	48
70	64

With FlowVision the following results were obtained:

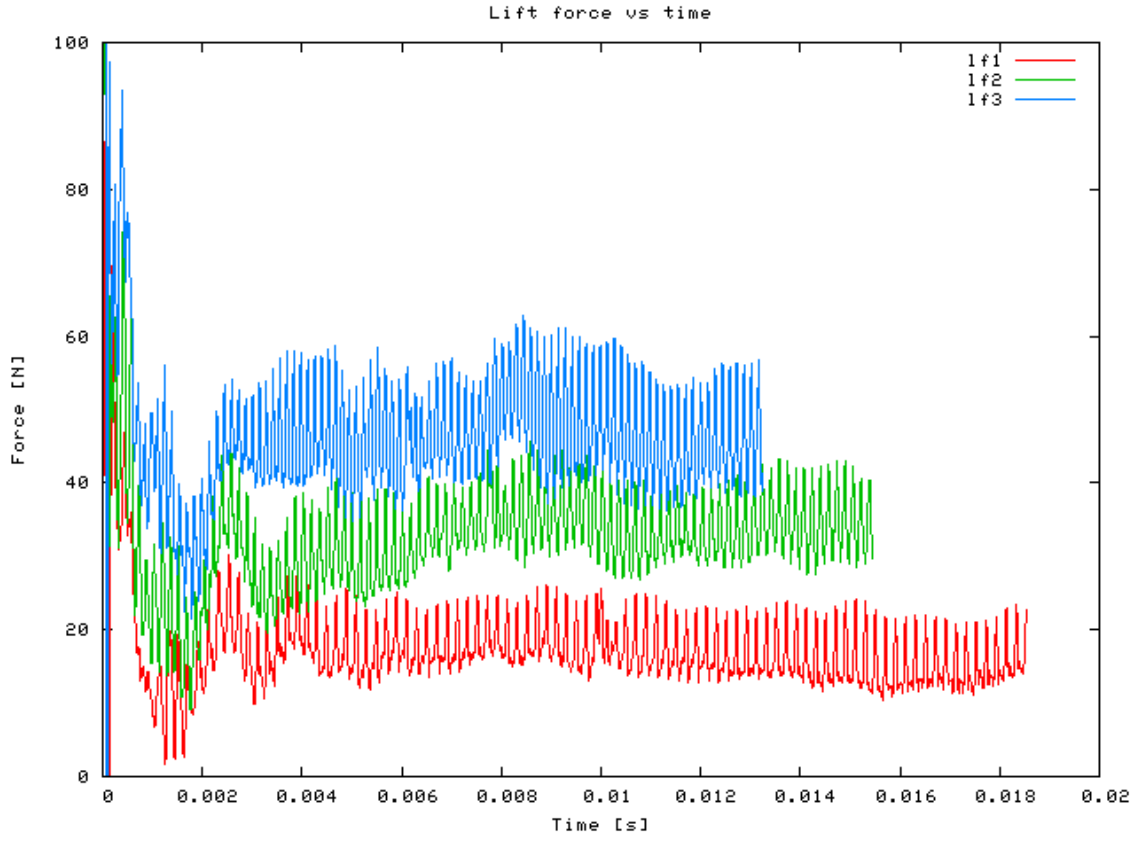

Figure I.1: Lift Force

The average values of the lift forces are:

Speed [km/h]	FlowVision
50	16,36
60	33,93
70	46,66